ROBUST WIRELESS COMMUNICATIONS UNDER CO-CHANNEL INTERFERENCE AND JAMMING

A Dissertation
Presented to
The Academic Faculty

By

Galib Asadullah M.M.

In Partial Fulfillment
of the Requirements for the Degree
Doctor of Philosophy
in
Electrical and Computer Engineering

School of Electrical and Computer Engineering
Georgia Institute of Technology
May 2008

ROBUST WIRELESS COMMUNICATIONS UNDER CO-CHANNEL INTERFERENCE AND JAMMING

Approved by:

Professor Gordon L. Stüber, Advisor
School of Electrical & Computer Engineering
Georgia Institute of Technology

Professor John A. Buck
School of Electrical & Computer Engineering
Georgia Institute of Technology

Professor Steven W. McLaughlin
School of Electrical & Computer Engineering
Georgia Institute of Technology

Professor Alfred D. Andrew
School of Mathematics
Georgia Institute of Technology

Professor Ye (Geoffrey) Li
School of Electrical & Computer Engineering
Georgia Institute of Technology

Date Approved: March 28, 2008

To

my parents, Monowara Khatun and Ali Akbar

and

my wife, Suraiya Tulip.

ACKNOWLEDGMENTS

This dissertation would not have been completed without the encouragement and support of many individuals. On this occasion, I extend my heartiest gratitude to all of them.

First, I am fortunate to have Prof. Gordon L. Stüber as my dissertation advisor. I thank him for providing me the opportunity to be a part his group. I could not be thankful enough for his support, motivation, guidance, and insightful suggestions that nurtured me and my research work throughout these years. I also appreciate the freedom he provided me to choose various research topics.

I am grateful to the thesis committee members, Prof. Steven W. McLaughlin, Prof. Ye (Geoffrey) Li, and Prof. John A. Buck for their efforts and time spent on my thesis. I am thankful to Prof. Alfred D. Andrew of the School of Mathematics for serving in the dissertation defense committee. I am also indebted to all the professors at Georgia Tech who taught me courses, which have been a source of many fundamentals.

I would like to thank all my friends who made my graduate life at Georgia Tech a memorable one. To mention a few, I am grateful to Arshad, Nova, Khalid bhai, Koli bhabi, Moin bhai, Farzana bhabi, Uttam, and Banani.

I would like to express thanks and appreciation to my current and previous lab-mates at the Wireless System Lab at Georgia Tech, Dr. Wajih Abu-Al-Saud, Dr. Jun Tan, Dr. Kihong Kim, Dr. Husang Kim, Dr. Apuva Mody, Dr. Qing Zhao, Dr. JoonBeon Kim, Dr. Chirag Patel, Dr. Heewon Kang, Alenka Zajic, Sami Almalfouh, and Nauman Kiyani for the wonderful times we shared together while taking a break from work and enjoying each other's company.

Finally, I would like to thank my dear wife, Tulip, our parents, and families for their unconditional love and support all these years. Without their love and understanding, it would have been difficult to complete this dissertation.

TABLE OF CONTENTS

LIST OF TABLES

LIST OF FIGURES

SUMMARY

Interference and jamming severely disrupt our ability to communicate by decreasing the effective signal-to-noise ratio and by making parameter estimation difficult at the receiver. The objective of this research work is to design robust wireless systems and algorithms to suppress the adverse effects of non-intentional co-channel interference (CCI) or intentional jamming. In particular, we develop chip-combining schemes with timing, channel, and noise-power estimation techniques, all of which mitigate CCI or jamming. We also exploit the spatial diversity and iterative receiver techniques for this purpose.

Most of the existing timing estimation algorithms are robust against either large frequency offsets or CCI, but not against both at the same time. Hence, we develop a new frame boundary estimation method that is robust in the presence of severe co-channel interference and large carrier-frequency offsets.

To solve the high peak-to-average-power ratio problem of a multicarrier code division multiple access (MC-CDMA) system and enhance its robustness against fading and jamming, we propose a constant-envelope MC-CDMA system employing cyclic delay diversity (CDD) as transmit diversity. We analyze the diversity order, coding gain, and bit-error rate (BER) upper bound for a quasi-static Rayleigh-flat-fading channel. We also propose a blind, accurate, and computationally efficient signal-to-noise ratio (SNR) estimator for the constant-envelope MC-CDMA-CDD system.

A robust anti-jam receiver must be able to suppress partial-band noise jamming and pulse jamming. We propose a configurable receiver that estimates the frequency- or time-domain jammer state information (JSI) and use it for chip combining in the corresponding domain. A soft-JSI-based chip-combining technique is proposed that outperforms conventional hard-JSI-based chip combining. We also derive a chip combiner that provides sufficient statistics to the decoder.

Channel estimation is necessary for coherent signal detection and JSI estimation. Conversely, knowledge of the jamming signal power and JSI of different subcarriers can improve the accuracy of the channel estimates. Hence, we propose joint iterative estimation of the multiple-input multiple-output (MIMO) channel coefficients, jamming power, and JSI for a coded MC-CDMA MIMO system operating under jamming and a time-varying frequency-selective channel. Finally, we reduce the computational complexity of the JSI-based anti-jam receivers by introducing an expectation-maximization (EM)-based joint channel and noise-covariance estimator that does not need either the subcarrier JSI or the individual powers of the AWGN and jamming signal.

CHAPTER 1

INTRODUCTION

1.1 Motivation

Wireless communication is one of the fastest growing technologies in recent times that has impacted our daily lives. The explosive demand to accommodate a higher number of users, high data rates, and high mobility has spurred the introduction of new services, products, and standards like wideband code division multiple access (W-CDMA), evolution-data optimized (EVDO), worldwide interoperability for microwave access (WiMax), and high speed packet access (HSPA). To improve efficiency further, lower costs, make use of new spectrum opportunities, and to make better integration with other open standards, the development of several other standards are in progress now. These standards include long term evolution (LTE) and ultra mobile broadband (UMB). Multipath-induced fading has been the main technical issue that dominates wireless communication. The key technologies enabling the recent developments in wireless communication are orthogonal frequency division multiplexing (OFDM) [1, 2] and multiple-input multiple-output (MIMO) wireless communication [3].

Interference and jamming can severely disrupt the ability to communicate in a military or commercial communication system. To accurately detect the intended signal, the receiver must typically be able to characterize the jamming signal or interference. The presence of jamming or interference also makes it difficult for the receiver to estimate many of the unknown parameters necessary for signal detection.

Frame boundary or timing is one of the crucial parameters that has to be acquired before any communication begins. Timing estimation is performed in burst-mode cellular data transmission during the initial cell search and in the idle and active modes. Because most carrier-frequency and phase estimation methods [4, 5] are very sensitive to timing errors, the receiver must perform the timing estimation before the carrier-frequency and

phase estimation. Hence, during the timing estimation, carrier-frequency and phase offsets between the transmitter and the receiver are unknown [6]. Moreover, the presence of CCI in cellular frequency-reuse systems further impairs the timing estimation. If multiple antennas are employed at the receiver, the additional spatial degrees of freedom can be used to mitigate the adverse effects of CCI during timing estimation and data detection. In any case, a synchronization method that is robust to frequency and phase offsets and CCI is highly desirable.

Multicarrier code division multiple access (MC-CDMA) [7, 8] combines OFDM and code division multiple access (CDMA) and bears the hallmarks of both OFDM and CDMA. Thus, MC-CDMA is robust against frequency-selective channels, jamming, and multiuser interference (MUI) [9]. However, MC-CDMA is typically characterized by a high peak-to-average-power ratio (PAPR). In [10], an MC-CDMA system that uses quadratic spreading sequences having a constant envelope (uplink only) in both the time and frequency domains was introduced as a solution to this high PAPR problem. These sequences, also known as poly-phase sequences proposed by Chu [11], have incidently been chosen as training sequences in the IEEE 802.16 standard because of their excellent PAPR properties.

MIMO techniques can be combined with MC-CDMA systems to further increase the robustness against fading and jamming or interference. The randomness of wireless channels resulting from fading can be exploited to enhance performance through diversity, where diversity is the method of conveying information through multiple independent transmit/receive antennas. A crucial design rule for a MIMO system is full spatial diversity, that is, every transmit and receive antenna should contribute its own diversity gain to system performance. In receive diversity, the signals from multiple receive antennas are combined, and performance gains, in terms of better link budget and tolerance to interference or jamming, are obtained as a result of the independence of the fading paths corresponding to the different receive antennas. Full receive diversity can be achieved with maximal-ratio combining (MRC) [12].

For full transmit diversity, special processing of the transmitting signal is essential, which is known as space-time coding (STC). Signal processing at the receiver is required to decode the superimposed signals coming from different transmit antennas. Delay diversity [13] is the simplest transmit diversity scheme [14]. Full diversity achieving, full rate, space-time block code (STBC) was proposed by Alamouti [15] for two transmit antennas. Later the concept was generalized to three and four transmit antennas [16], but the corresponding STBCs do not attain full rate. Space-time trellis codes (STTC) can also provide full diversity. However, the decoding complexity increases exponentially with the number of transmit antennas [17]. It is desirable that space-time codes be easily scalable or configurable for an arbitrary number of transmit antennas. Therefore, the design of an MC-CDMA system having a scalable full-diversity space-time code and low PAPR at the same time is an interesting research topic.

Signal-to-noise ratio (SNR), defined as the ratio of the desired signal power to the noise power, is widely used in wireless communication to describe the effect of noise on the received signal. SNR estimation is essential at the receivers for various purposes; e.g., in the calculation of *a posteriori* probabilities, in chip combining, and in power control. The sensitivity of a turbo decoder to mis-estimation of the SNR is investigated in [18], and a scheme that estimates the unknown SNR from each code block with adequate accuracy is presented. The SNR of different subcarriers can be used for calculating the chip-combining weights to suppress the adverse effect of jamming or unintentional interference for an MC-CDMA system. A modified maximal-ratio combining (MRC) scheme using the SNR of different RAKE fingers is proposed in [19] for WCDMA systems.

SNR estimation has been studied by several researchers [20, 21]. Data-aided signal-space projection-based signal-to-interference-plus-noise ratio (SINR) estimators [22–24] have been previously proposed for time division multiple access (TDMA) cellular systems and are well known for their excellent performance. However, these SNR estimators require training sequences or data decisions. In our research, we are interested in a

blind and computationally efficient, but accurate, SNR estimator for the constant-envelope MC-CDMA system that uses cyclic delay diversity and operates under a time-varying frequency-selective-fading channel.

Chip combining with appropriate weights at the despreader can mitigate jamming or interference in an MC-CDMA system, where each symbol is typically spread in the frequency domain. Maximal-ratio combining (MRC) [25, 26] has been used to combine different diversity branch signals with unequal Gaussian-noise power, where each combining weight is inversely proportional to the noise power of the associated diversity branch. There are two common types of jamming threat: partial-band noise jamming (PBNJ) and pulse jamming (PJ) [27]. To suppress PBNJ or PJ effectively, the system model must be configurable such that the chips can be combined in either the frequency or time domain, respectively. This is because the discrete Fourier transform (DFT) in an MC-CDMA receiver converts any PJ signal into a full-band jamming signal, which is difficult to suppress by a frequency-domain (FD) chip combiner. On the other hand, any PBNJ signal is transformed into a continuous PJ signal, which is difficult to suppress by a time-domain (TD) chip combiner. Hence, an MC-CDMA receiver that is capable of combining the chips in both the frequency and time domains is robust against different types of jamming.

For MC-CDMA anti-jam systems employing chip combining, jammer state information (JSI), which indicates the presence of a jamming signal in a sub-band or time-domain chip, is essential for determining the chip-combining weights [27, 28]. If the system employs turbo or convolutional coding, JSI can be iteratively estimated and exploited to perform the appropriate chip combining so as to enhance the input SINR to the decoder [29]. Another interesting idea is to apply the soft JSI (S-JSI) for chip combining.

Channel estimation is essential for achieving reliable information transmission in all modern wireless communication systems. Channel estimates are used for coherent signal detection, combining different receive antenna signals, and frequency-domain equalization

in multicarrier systems. The problem of channel estimation for MC-CDMA systems has received great attention in the last few years, and several solutions already exist [30–37]. The presence of jamming signals makes channel estimation difficult. In [38], Da silva and Milstein analyze the performance of ultra-wideband (UWB) systems under channel-estimation error and narrowband interference. They have shown that the effect of narrowband interference is exacerbated by channel-estimation errors. In an anti-jam receiver, channel estimation is also necessary for noise power and JSI estimation. Conversely, knowledge of the jamming-signal power and JSI can improve the accuracy of the channel estimation. For systems using multiple transmit antennas, any received signal is the superposition of the signals from multiple transmit antennas, which makes channel estimation even more challenging [39]. Therefore, for a coded MC-CDMA system employing transmit diversity, joint iterative estimation of MIMO time-varying fading-channel coefficients, jamming signal power, and JSI with soft chip combining is an important research matter.

Although the JSI-assisted channel-estimation and chip-combining techniques efficiently suppress the jamming signals, they require knowledge of the individual additive white Gaussian noise (AWGN) and jamming-signal variances in addition to the JSI. However, estimation of the JSI increases computational complexity of the receiver. Besides, the AWGN and jamming signal are perceived as a single-compound entity, and obtaining an accurate estimate of the AWGN variance in the presence of a jamming signal, or vice versa, is difficult. Hence, it is desirable to design an anti-jam receiver that does not require knowledge of the JSI and individual variances of AWGN and the jamming signal on each subcarrier.

1.2 Contributions

The key contributions of this dissertation are

- A new timing estimator is derived that is robust in the presence of severe co-channel interference and different carrier-frequency offsets [40]. The estimation metric is

obtained by considering double correlation in the elements of the spatio-temporal cross-correlation between the signals from multiple receive antennas and a known training sequence.

- A constant-envelope multicarrier code division multiple access (MC-CDMA) system employing highly configurable cyclic delay diversity (CDD) is introduced. The space-time coding aspects and bit-error rate (BER) of the MC-CDMA-CDD system are analyzed for quasi-static Rayleigh-flat-fading channel [41].

- A blind signal-projection (SP)-based SNR estimator is derived for the constant-envelope MC-CDMA-CDD system that operates under time-varying frequency-selective-fading channel. Because the orthogonal spreading sequences form the basis of the signal space, training sequences or data decisions are not needed, and orthonormalization is not required. Thus, the proposed SNR estimator is computationally efficient, and very accurate estimates are achieved without sacrificing power and bandwidth [42].

- Anti-jam receivers that iteratively estimate the JSI and use them for chip combining in the frequency and time domains to suppress partial-band noise jamming (PBNJ) and pulse jamming (PJ), respectively, are designed for a turbo-coded constant-envelope MC-CDMA-CDD system [43]. The proposed soft-JSI (S-JSI)-based chip-combining technique outperforms the conventional hard-JSI (H-JSI)-based chip combining by at least 1.75 dB at BER of 10^{-4} under both types of jamming. It is also shown that without pilot-assisted *a priori* JSI and with perfect channel estimates, iterative despreading (includes JSI estimation and chip combining), demapping, and decoding (IDDD) has almost similar performance as one-shot despreading followed by iterative demapping and decoding (IDD).

- Anti-jam receivers are introduced where the MIMO channel coefficients, jamming power, and JSI are jointly estimated to suppress the adverse effects of PBNJ [44, 45]. For PBNJ, weighted least square error (LSE) and linear minimum mean square error

(MMSE) channel estimators (CE) are derived. The constraints on the cyclic delays are also identified. The JSI for the pilot symbols is estimated to assist estimation of the time-varying frequency-selective channel coefficients by updating the noise covariance matrix. An optimum (sufficient statistics) chip combiner is derived that guarantees no loss of information in the soft output generated by the demapper. The optimum chip-combining weights for the data symbols require the JSI; hence, the JSI for the data symbols is iteratively estimated using the decoder output. The proposed iterative despreading, demapping, and decoding (IDDD) receiver with soft-JSI (S-JSI)-assisted channel estimation and chip combining enhances the receiver's robustness against PBNJ.

- An expectation-maximization (EM) joint channel and covariance estimator is derived for the generic MC-CDMA system operating under PBNJ [46, 47]. In the proposed receiver, the channel estimator or the chip combiner requires only the AWGN-plus-PBNJ power of each subcarrier to suppress jamming. Therefore, a significant complexity reduction is achieved because the receiver does not need to estimate the JSI and individual variances of the AWGN and PBNJ on each subcarrier for channel estimation and chip combining [44]. Simulation results show that the sufficient-statistic chip combiner always offers a smaller BER than the minimum mean square error (MMSE) chip combiner provided that reliable estimates of the channel and AWGN-plus-PBNJ-covariance are available.

1.3 Thesis Outline

The thesis is organized as follows. Chapter 2 provides a review of the related topics including wireless channels, CCI, jamming, space-time coding, multicarrier modulation, and parameter estimation. Chapter 3 presents the new frame boundary estimation technique. The constant-envelope MC-CDMA system employing CDD is introduced in Chapter 4, and its space-time coding aspects and bit-error rate (BER) are analyzed. Chapter 5 presents

the blind signal-projection (SP)-based SNR estimator. The IDDD-anti-jam receivers with iterative JSI estimation and soft chip combining in the frequency-domain and time-domain to suppress PBNJ and PJ, respectively, are discussed in Chapter 6. The next two chapters present joint channel and jamming-parameter estimation techniques proposed for anti-jam MC-CDMA systems. Chapter 7 presents the joint channel-coefficients, JSI, and jamming-power estimation techniques with iterative soft chip combining for the constant-envelope MC-CDMA-CDD system. The sufficient-statistic-based optimum chip combiner is also derived in this chapter. The expectation-maximization joint channel and noise-covariance estimator that does not require the JSI estimates and individual AWGN and PBNJ power estimates is presented in Chapter 8 for a generic MC-CDMA anti-jam system. Finally, Chapter 9 concludes the dissertation with future research interests.

CHAPTER 2

BACKGROUND

Wireless communication presents numerous challenges for designers that arise as a result of the demanding nature of the physical medium and the complexities of the dynamics of the underlying network. The main technical issues dominating wireless communication are fading of wireless channels, multiuser interference, co-channel interference, and jamming. Technologies like OFDM and MIMO have brought breakthroughs in wireless communication. To detect the transmitted signal in an efficient manner, the receiver must characterize the jamming or interference and estimate the parameters necessary for signal detection in the presence of interference and/or jamming. These parameters include timing/frame boundary, channel coefficients, SNR, and JSI.

2.1 Wireless Channels

Wireless channels place fundamental limitations on the performance of wireless communication systems because they introduce several forms of distortion to the transmitted signal. Fading is the random fluctuations in the channel gain and phase that arise as a result of the reflection, diffraction, and scattering of transmitted signals by intervening objects between the transmitter and receiver [12, 48]. Different wireless channel modeling techniques [49] are usually applied for different scenarios to simplify the design of communication systems.

2.1.1 Flat-Fading Channels

The simplest fading-channel model is the flat-fading channel. If x_n and y_n are the transmitted and received signal at discrete time n, then flat fading can be represented by a single-tap channel as

$$y_n = h_n x_n + w_n \ , \tag{1}$$

where h_n is the complex channel coefficient, and w_n is the additive white Gaussian noise (AWGN). The fading gain usually has Rayleigh, Ricean, or Nakagami distributions to model isotropic scattering or line-of-sight (LOS) propagation [48].

2.1.2 Frequency-Selective-Fading Channels

In this case, the signal bandwidth is larger than the coherence bandwidth of the fading channel, i.e., the channel excess delay is longer than the symbol interval causing intersymbol interference (ISI) at the receive antennas. Frequency-selective-fading channels are usually modeled as a delay-tapped filter as

$$y_n = h_n * x_n + w_n \ , \tag{2}$$

where h_n is the discrete time channel coefficients and $*$ denotes convolution operation. The fading gain of each channel tap h_n may be a Rayleigh or Ricean distribute random variable. The taps, h_n may be independent or correlated. The sum of sinusoids method is widely used to generate multiple independent fading coefficients for frequency-selective-fading channels [50, 51].

2.1.3 Time-Varying Channels

If the channel coefficient changes over time, the channel is known as a time-varying channel. When h_n is constant over a period of time or block, i.e., $h_n = h$, the channel is called a quasi-static or block-faded channel. The rate at which the channel tap changes depends on the relative velocity between the transmitter and receiver. This rate is known as Doppler rate or frequency and is defined as

$$f_d = \frac{v f_c}{c} \ , \tag{3}$$

where v is the relative velocity, f_c is the carrier frequency, and $c = 3 \times 10^8$ m/s is the light speed. The channel taps, h_n at different n, are correlated, where the correlation depends on the Doppler rate and the distance in time. To make the channel taps at different n

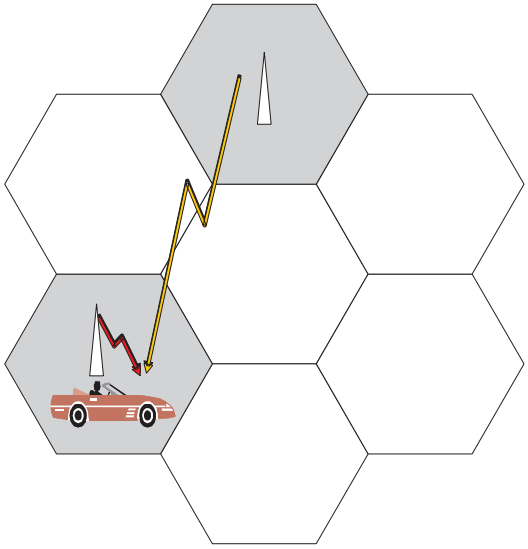

Figure 1. Co-channel interference in a frequency-reuse system.

statistically independent, interleavers are widely used. Both frequency-selective and flat-fading channels can be time varying or static over a block.

2.2 Co-Channel Interference (CCI)

Co-channel interference (CCI) is the crosstalk between two different transmitters sharing the same frequency channel. In wireless communication, spectrum is a very scarce resource. The explosive growth of wireless services in recent years illustrates the huge and growing demand for the spectrum, the reuse of which in cellular networks causes CCI. The aim of frequency reuse is to increase spectrum efficiency. Therefore, characterization of CCI, performance analysis [52–54], and estimation of the receiver parameters [55] on fading channels in the presence of CCI are of considerable interest.

Because system capacity is often limited by co-channel interference, receiver algorithms for cancelling CCI have recently attracted much interest. A low-complexity single-antenna interference-cancellation algorithm is introduced in [56]. Co-channel interference may be controlled by various radio resource management schemes. Cognitive radio technology allows spectrum reuse in various dimensions, including space, frequency, and time,

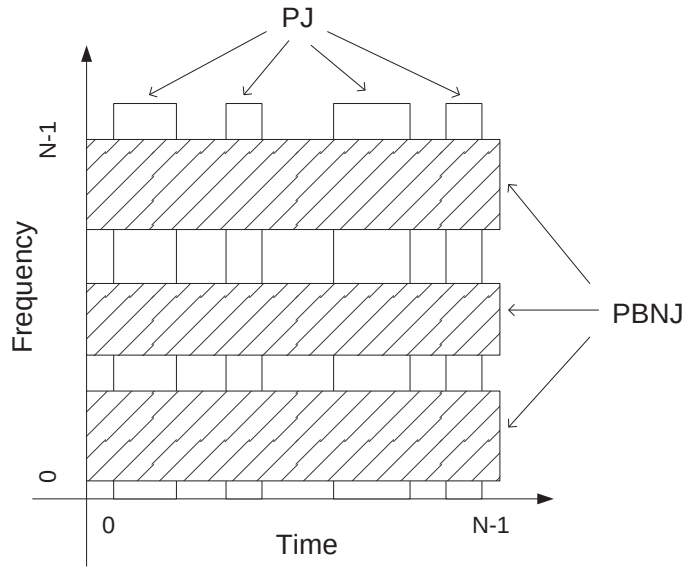

Figure 2. Partial-band noise jamming (PBNJ) and pulse jamming (PJ).

so as to obliterate the spectrum and bandwidth limitations. However, cognitive radio systems need to sense the environment and then alter transmission power, occupied frequency, modulation, and other parameters to dynamically reuse the available spectrum.

Nonuniform CCI may be generated by other systems operating in the same frequency band. For example, in hybrid in-band on-channel (HIBOC) DAB systems, analog and digital signals are transmitted simultaneously within the same license band [57–59]. Therefore, these systems require a solution to combine the received signals on different subcarriers so that the interference can be suppressed.

2.3 Jamming

Jamming is usually a deliberate transmission of radio signals that disrupts wireless communication by decreasing the effective SNR. A variety of jamming waveforms have been suggested in the literature, including partial-band noise jamming (PBNJ) and pulse jamming (PJ) [27]. A partial-band noise jammer is one that jams a contiguous or noncontiguous fraction of the signal bandwidth. On the other hand, a pulse jammer, or partial-time jammer, intermittently jams the whole transmission bandwidth [12, 60]. When the entire

signal bandwidth is continuously jammed, we refer to this type of jamming as full-band noise jamming (FBNJ). The jamming signal is usually modeled as a Gaussian distributed noise to a channel [60] as

$$y_n = x_n + j_n + w_n \ , \tag{4}$$

where x_n and y_n are the transmitted and received signals, respectively, and j_n and w_n are the jamming noise and AWGN, respectively, during discrete time or frequency n. Techniques used to mitigate the adverse effects of jamming are known as anti-jam techniques. Jammer state information (JSI) is a parameter that indicates the presence of a jamming signal in a subchannel (subcarrier or chip duration). When the jammer state is available at the receiver, the worst jammer is forced to continuously jam the entire bandwidth [10].

It is well known that effective anti-jamming performance can be achieved despite these threats by using either direct sequence spread spectrum (DS/SS) or frequency hopping spread spectrum (FH/SS) along with channel coding and interleaving techniques. Most previous work on hostile jamming focuses on FHSS systems [61, 62]. In an FHSS system, the most effective jamming strategy for many channels [63] is for the jammer to concentrate its power in some portions of the system's total spectrum, which is the same as PBNJ. After dehopping, the partial-band interference appears as PJ at the input to the decoder.

Typically, error-control coding is used both to provide coding gain against the jamming and to aid in the JSI estimation (discrimination between jammed and unjammed symbols or chips). The use of error-control coding with jamming detection has been considered for FHSS systems in [64–66]. In most of these works, the receiver is assumed either to use non-coherent detection and hard-decision decoding [61, 62, 66] or to have perfect knowledge of the amplitude and phase of the arriving signal [64, 67]. The latter assumption requires that the receiver have some sufficiently accurate method to acquire at least the phase of the received signal if coherent detection and soft-decision decoding are used. In [65], the authors propose the use of pilot symbols to aid in this phase acquisition in the presence of jamming. In [66], they further consider a fading-channel scenario in an FHSS system, in

which the fading-channel coefficient is estimated in each dwell interval. In both papers, the detection and estimation problems are simplified by the assumption that the jamming is constant over each dwell interval.

In [28], a constant-envelope multicarrier frequency-diversity spread spectrum (MC-SS) is proposed to combat PJ and PBNJ. When subjected to PJ, the proposed MC-SS system can obtain JSI by processing the received signal in the time domain. Likewise, by processing the received signal in the frequency domain, JSI can be obtained in the presence of PBNJ. The performance of the system is analyzed for both types of jamming. For the proposed MC-SS system with JSI estimation, the worst case partial-band jammer is the full-band jammer and the worst pulse jammer is the continuous jammer. In either case, the worst case jammer is forced to distribute its jamming power continuously in time over the entire signal bandwidth [10]. A simple JSI-estimation scheme for both partial-band and pulse jamming is also proposed.

2.4 Multicarrier Modulation

2.4.1 OFDM

OFDM is very a popular multicarrier modulation scheme suitable for block transmission systems. In OFDM [1, 2], each block of symbols is modulated with an inverse discrete Fourier transform (I-DFT) and transmitted on a set of subcarriers to form parallel overlapping but orthogonal subchannels. This is equivalent to saying that the symbol block is precoded by an IDFT matrix. When a cyclic prefix longer than the channel delay spread is used, a simple representation for the receiving symbol in the frequency domain can be obtained through circular convolution. Thus, in the frequency domain, OFDM converts a time-dispersive frequency-selective channel into a set of flat-fading channels, which are easy to equalize. In addition, OFDM allows adaptive bit loading, which can utilize the channel in an efficient manner.

The combination of forward-error correction (FEC) and OFDM introduces further robustness against frequency-selective fading. In a coded OFDM system, if the number of

subchannels with high attenuation is less than the number of bits the decoder can correct, the system is robust against frequency selectivity even without knowing which are the most attenuated subchannels. As the name implies, the orthogonality of OFDM is key to separating the symbols on different subcarriers. Therefore, OFDM is very sensitive to synchronization errors.

Because of its ease of implementation and robustness against frequency-selective fading, OFDM has been chosen for most high-speed wireless communication systems. The success of OFDM in wireless communication has been justified by wireless local area networks (WLAN), digital audio broadcasting (DAB) [87], digital video broadcasting (DVB) [88], and wireless metropolitan area networks (MAN). OFDM has also been chosen for most of the fourth-generation high-data-rate cellular systems.

2.4.2 MC-CDMA

Code division multiple access (CDMA) is the core wireless access technology for third-generation wireless systems. The performance of CDMA is limited by channel dispersion causing intersymbol interference (ISI), and complex detection algorithms are required to remove ISI. The combination of OFDM and CDMA (also known as spread spectrum techniques) has drawn a lot of attention because of its simple receiver implementation, robustness to channel dispersion, and ability to accommodate a higher number of users compared to CDMA alone. Several multicarrier (MC) spread spectrum techniques have been proposed that include MC-CDMA, MC direct-sequence CDMA, and multitone CDMA [8].

In an MC-CDMA system, one or more symbols are spread in the frequency domain using a spreading sequence, i.e., the spread chips are transmitted over all or a subset of the subcarriers. Multiuser access is possible through orthogonal spreading codes. For frequency-selective channels, MC-CDMA can use a cyclic guard interval to remove ISI

similar to OFDM. In [68, 69], it is shown that MC-CDMA systems outperform a conventional direct sequence spread spectrum (DS/SS) system in partial-band jamming. Despite having all these benefits, the MC-CDMA systems suffer from a high peak-to-average-power ratio (PAPR). The complex envelope of an MC-CDMA signal is not constant, even with BPSK or QPSK signaling. This property is due to the IDFT applied at the transmitter and causes distortion when the signal is passed through a high-efficiency nonlinear power amplifier. In [28], an MC-CDMA system that uses quadratic spreading sequences [11] having a constant envelope in both the time and frequency domains was introduced as a solution to this high PAPR problem.

2.5 Space-Time Coding

MIMO technology, which uses multiple transmit and multiple receive antennas, constitutes a breakthrough in the field of wireless communication. Several key ideas developed in the mid-1990s prompted a tremendous amount of research and development in this field. Multipath scattering is commonly known for causing impairments to wireless signals. However, it also provides an opportunity to improve channel capacity and communication reliability. MIMO wireless communication can exploit the rich scattering channel to either increase the data rate by spatial multiplexing or improve the reliability through increased spatial diversity. In MIMO systems, interference may also be mitigated by exploiting the spatial dimensions to increase separation between users, which improves the signal-to-interference-plus-noise ratio (SINR) [70].

In MIMO wireless communication, space-time coding (STC) is a method of improving the reliability of data transmission by using multiple transmit antennas as opposed to increasing the data rate by spatial multiplexing. In STC, by using special signal processing, spatial and temporal correlation is introduced into the signals transmitted from different antennas without increasing the total power. It is assumed that the redundant copies of a data signal are conveyed through multiple independent instantiations of the random fades.

The idea is to exploit the randomness of fading to enhance performance through diversity. The goal of STC is to achieve full transmit diversity and good STC gain without requiring multiple receive antennas. The receiver needs signal processing to decode the space-time codes.

There have been extensive works on the design of STC. The main STC schemes are described in the following sections.

2.5.1 Delay Diversity (DD)

Delay diversity is the simplest and earliest form of spatial transmit diversity proposed by [13, 71]. In delay diversity, a signal is transmitted from one antenna and then delayed one or multiple time slots before transmitting from another antenna. In [14], Winters showed that delay diversity using M transmit antennas provides a diversity gain within 0.1 dB of that with M receive antennas for any number of antennas.

2.5.2 Space-Time Block Code (STBC)

The first STBC was proposed by Alamouti [15]. The goal was to replace the receive diversity with transmit diversity without performance degradation. Alamouti code transmits two symbols at different times with two transmit antennas and achieves full rate in addition to achieving full diversity. The STBCs as originally introduced, and as usually studied, are orthogonal; i.e., the vectors representing any pair of columns taken from the coding matrix are orthogonal. This code design results in simple, linear, and optimal decoding at the receiver. The same concept was generalized to three and four transmit antennas [16], but the corresponding STBCs do not attain full rate.

2.5.3 Space-Time Trellis Code (STTC)

A space-time trellis code (STTC) encoder maps the information bits into symbols simultaneously transmitted from multiple transmit antennas. Delay diversity is a special form of STTC. The STTC design criteria are based on minimizing the codeword pairwise-error

probability (PEP), which involves two criteria; the first one is the full spatial diversity criterion, and the second one is the coding gain criterion. The STTCs can also provide full diversity. STTC design criteria for single-carrier transmission over frequency-selective-fading channels are presented in [72].

The initial STC research focused on narrowband flat-fading channels [15, 16, 73]. Successful implementation of STC for multiuser broadband frequency-selective channels requires the development of novel and high-performance signal processing algorithms for channel estimation, joint equalization/decoding, and interference/jamming suppression. However, such algorithms for broadband wireless channels promise more significant performance gains than those reported for narrowband channels [15, 16, 73] because of available multipath gain in addition to STC gain. In [73, 74], it is shown that STCs are robust aginst non-ideal operating conditions such as antenna correlation, channel-estimation error, and Doppler effects.

Both STBC and STTC have some technical issues like lack of scalability for transmit antennas. That is, when the number of transmit antennas is changed, different space-time codes are needed to ensure full diversity. Besides, the complexity of STTC increases exponentially with the number of transmit antennas [17].

2.6 Time Synchronization under CCI and Frequency Offset

Time synchronization is a process of locating the start of the frame from the received complex baseband samples. A receiver operating in the acquisition mode must perform time synchronization before transmitting any data. Time synchronization is normally divided into coarse time synchronization and fine time synchronization. Coarse time synchronization consists of estimating the approximate range of samples over which a frame is likely to start, whereas fine time synchronization consists of locking the receiver onto the most dominant component of the received signal.

Time synchronization, also known as frame boundary estimation, is necessary in burst

mode cellular data transmission during initial cell search and the idle and active modes. Because most carrier-frequency and phase estimation methods [4, 5] are very sensitive to timing errors, the receiver must perform timing estimation before carrier-frequency and phase estimation. Hence, during timing estimation, carrier-frequency and phase offsets between the transmitter and the receiver are unknown [6]. Moreover, the performance of timing synchronization schemes in digital mobile communication systems, such as global system for mobile communications (GSM) [75, 76] and digital European cordless telecommunications (DECT), is severely degraded when CCI is present.

Typically, correlation methods and maximum-likelihood (ML) methods are used for timing estimation [77–80]. Data-aided and non-data-aided ML frame synchronization methods for unknown frequency-selective channels are proposed in [81]. The ML methods proposed in [79, 82, 83] outperform the correlation methods, but they are intolerant to frequency offsets and/or CCI. The ML algorithm proposed in [84] is tolerant to frequency offset. Choi and Lee [85] introduced a double-correlation (DC) method that is robust against frequency offsets, but is vulnerable to CCI. A timing estimation method using array antennas is presented in [86] that is robust against CCI because of increased receive diversity.

2.7 SNR Estimation

Signal-to-noise ratio (SNR) is widely used in digital communication. Many receiver algorithms need the SNR information. For example, knowledge of SNR is required in power control [89], rate adaptation [90], and calculation of the maximal-ratio combining (MRC) weights [25]. SNR is also used in the calculation of the log-likelihood ratio (LLR) that goes into decoder.

Numerous applications justify the motivation behind investigating SNR estimation techniques. In [91], a maximum-likelihood SNR estimator for pulse-code modulated signals in a real AWGN channel is derived and shown to be asymptotically optimal in minimum variance sense. Later, the same technique was extended for M-ary phase shift keying (MPSK)

modulated signals in complex AWGN [92]. However, these estimators have fairly large biases when the true value of SNR is small. In [20], four SNR estimators are proposed based on the receiver statistics related to SNR and its inverse. A maximum-likelihood SNR estimator is introduced in [21] for slow-Ricean-fading channels. A subspace-based technique is proposed in [22] to estimate the signal-to-interference-plus-noise ratio (SINR) for time division multiple access (TDMA) cellular systems. In [23], the interference plus AWGN variance is estimated for the same system by projecting the received signal onto a single vector of the left-null space of the matrix formed by the known training sequence or estimated data symbols. The signal projection (SP)-based SNR estimator [24] introduced for a TDMA system has less complexity, shorter estimation time, and smaller estimation error than the previous two methods. In [93], the noise power estimation for a turbo decoder has been improved by utilizing hard-decision output from the decoders to obtain an extended number of symbol samples.

2.8 Channel Estimation

Wireless channels introduce various impairments such as time-varying attenuation and phase changes that distort the transmitted data. A receiver mitigates these distortions for reliable demodulation of the transmitted data. This reception strategy is called coherent detection [12]. In non-coherent detection, compensation for the channel distortions is not required, but the performance of this reception scheme is inferior compared to that of the coherent detection in terms of the bit-error rate (BER) achieved for a given amount of transmit power [48]. Therefore, most modern communication systems employ coherent detection.

The wireless radio channel is widely parameterized by a combination of paths, each characterized by a delay and a complex amplitude, also known as channel coefficient. The channel coefficients show temporal variations resulting from the mobility of terminals, while the delays are usually almost constant over a large number of symbols.

In general, pilot symbols or training sequences multiplexed with data symbols are used for channel estimation. For multicarrier applications like OFDM and MC-CDMA, the known symbols are inserted in both the frequency and time dimensions [94]. Once the initial channel coefficients are acquired, the estimates may be used for channel tracking (e.g. least mean square (LMS) tracking) or interpolation (e.g., Wiener or optimal minimum mean square error (MMSE) filtering).

An enormous amount of research has been done in the field of channel estimation. Most of the existing literature assumes that time and frequency synchronization has been achieved prior to channel estimation. Some of the work on channel estimation for MIMO-OFDM systems can be found in [95–98]. In [95], least square (LS) channel estimation using pilot tones followed by noise reduction in the time domain is performed. In [97], the initial channel estimates are obtained using the LS approach, followed by mean squared error (MSE) reduction using the frequency-domain channel-correlation matrix and the noise variance. Raleigh and Jones [99] have suggested channel estimation for MIMO-OFDM system using a training structure consisting of independent and orthogonal training sequences from various transmit antennas. The structure is composed such that no two transmit antennas send a training symbol on the same subcarrier. Yang [98] suggested the use of windowing in the frequency domain before processing the channel estimates in the time domain to reduce the spectral leakage. In [96, 100], Li has derived channel estimators for an OFDM system with transmitter diversity based on the minimum MSE (MMSE) principle using both the time- and frequency-domain correlations of the channel. A significant tap catching (STC) approach is suggested to reduce the computational complexity of this estimator. Li has made further contributions with simplified channel estimation for OFDM systems using transmit diversity in [39, 101].

Channel estimation for MC-CDMA systems has also received attention in the last few years, and several solutions are proposed in [30–37]. Zemen [36] has applied Slepian basis expansion [102] to estimate the time-varying channel for an MC-CDMA system, where the

complete knowledge of the second-order channel statistics is not required. A maximum-likelihood channel acquisition and least mean square (LMS) channel tracking for a single-transmit-antenna MC-CDMA system are presented in [37]. In [38], the authors propose an analytical formulation that allows the analysis of channel estimation in the presence of narrowband interference or jamming for ultra-wideband (UWB) systems. They conclude that the effect of narrowband interference is deteriorated by channel-estimation errors.

CHAPTER 3

FRAME BOUNDARY ESTIMATION UNDER CO-CHANNEL INTERFERENCE AND FREQUENCY OFFSET

3.1 Overview

The objective of this thesis is to design robust wireless systems and receiver algorithms to alleviate the adverse effects of co-channel interference (CCI) or intentional jamming. To achieve our goal, first, we consider the problem of frame synchronization under CCI and other parameter uncertainties. These parameters include phase and frequency offsets.

Timing or frame boundary defines the beginning of a frame at the receiver. Frame boundary is estimated in almost all communication systems. Typically, frame boundary is estimated using training sequences (TS), which are periodically inserted into the data stream. In burst mode cellular data transmission, timing estimation is performed during the initial cell search and in the idle and active modes. Because most carrier-frequency and phase estimation methods [4, 5] are very sensitive to timing errors, the receiver must perform timing estimation before carrier-frequency and phase estimation. Hence, during timing estimation, carrier-frequency and phase offsets between the transmitter and the receiver are unknown [6]. Moreover, the presence of co-channel interference (CCI) in cellular frequency-reuse systems further impairs timing estimation. However, if multiple antennas are employed at the receiver, then the additional spatial degrees of freedom can be used to mitigate the adverse effects of CCI during timing estimation and data detection. In any case, a synchronization method that is robust to frequency and phase offsets, and CCI is highly desirable.

Correlation methods and maximum-likelihood (ML) methods are typically used for timing estimation [77–80]. Some of the ML methods [79,82,83] outperform the correlation methods but they are intolerant to frequency offsets and/or CCI. Most existing algorithms are robust against either large frequency offsets or CCI, but not against both at the same

time. The ML algorithm in [84] is tolerant to frequency offset. In [85], a double-correlation (DC) method is introduced that improves the performance in [84]. The method is robust against frequency offsets, but is vulnerable to CCI. The timing estimation method using array antennas in [86] is very sensitive to frequency and phase errors.

In this chapter, a new timing (frame boundary) estimation method is proposed that is robust in the presence of severe co-channel interference and large carrier-frequency offsets. We apply the concept of double correlation [85] to the array antenna method of [86]. To be more specific, the estimation metric is obtained by considering double correlation in the elements of the spatio-temporal cross-correlation between the signals from multiple receiver antennas and a known training sequence. The method is applied to GSM and results show that the spatial freedom of the signals from multiple receiver antennas along with a double correlation in the cross-correlation terms yields a robust timing estimator. Under large frequency offsets and CCI, it works much better than the estimators of [86] and moderately better than the estimator in [85].

The remainder of this chapter is organized as follows. Section 3.2 introduces the system and channel models. The proposed method for timing estimation is derived in section 3.3. Simulation results are presented in section 3.4 followed by some concluding remarks in section 3.5.

Figure 3. Synchronization burst bearing the extended training sequence in GSM

3.2 System Model

Each transmitter periodically transmits a training sequence of length N_{TS} symbols as shown in Fig. 3. The overall system model under consideration is shown in Fig. 4. The desired

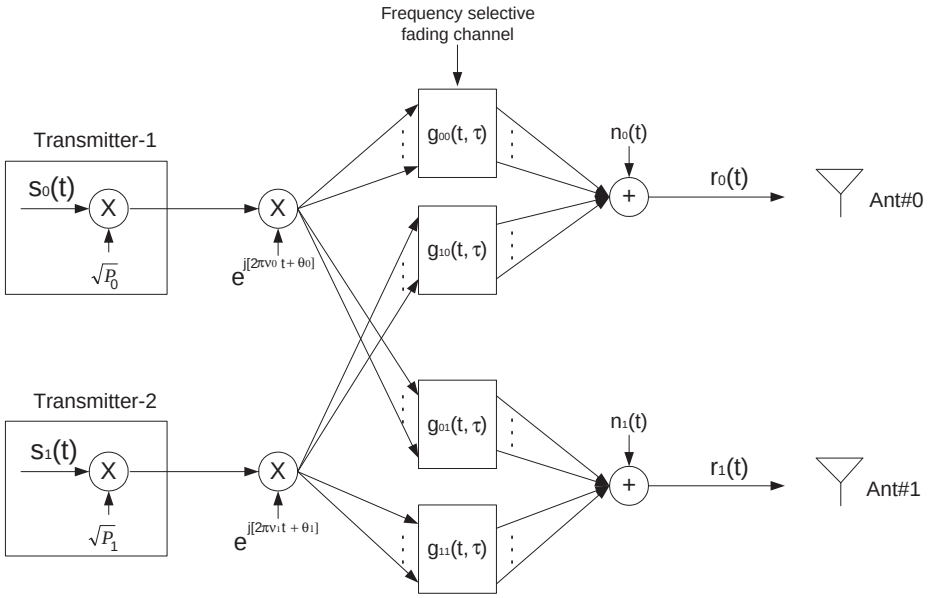

Figure 4. System model

and co-channel signals have power P_0 and P_1, respectively, while the additive white Gaussian noise (AWGN) has power P_N. Therefore, the signal-to-interference ratio (SIR), and signal to noise ratio (SNR) can be expressed as $\frac{P_0}{P_1}$ and $\frac{P_0}{P_N}$, respectively. The term $e^{j2\pi\nu_0 t+\theta_0}$ models the frequency offset, ν_0, and phase offset, θ_0, between the desired transmitter and the receiver. The phase offset θ_0 is uniformly distributed over $[0, 2\pi]$. Similarly, the term $e^{j2\pi\nu_1 t+\theta_1}$ is used to model the frequency and phase offsets for the interfering co-channel signal. The desired and co-channel signals are passed through a time-varying frequency-selective-fading channel with impulse response

$$g_{ij}(t,\tau) = \sum_{l=0}^{N_l-1} g_{ij,l}(t)\delta(\tau - \tilde{\tau}_{ij,l}(t)) \ , \tag{5}$$

where $g_{ij,l}(t)$ and $\tilde{\tau}_{ij,l}$ are the complex channel gain and delay, respectively between transmitter i and receiver antenna j, and N_l is the number of rays.

For the Gaussian Minimum Shift Keying (GMSK) modulated signals, the complex envelope of the ith GMSK modulated signal is

$$s_i(t) = e^{j\psi(t;\alpha_\mathbf{i})} \ , \tag{6}$$

where the $\alpha_\mathbf{i} = \{\alpha_{m,i}\}$ is a sequence of independent, differentially encoded, data symbols

with $\alpha_{m,i} \in \{\pm 1\}$. The phase term $\psi(t, \alpha_{\mathbf{i}})$ is

$$\psi(t, \alpha_i) = \pi \sum_m \alpha_{m,i} q(t - mT) \ , \tag{7}$$

where $q(t)$ is the GMSK phase pulse, characterized by the normalized filter bandwidth BT equal to 0.3 for GSM.

3.3 Derivation of Timing Estimators

In this study, the spatial dimension of the receiver is exploited to improve the synchronization performance. Assume the receiver has M antennas. The received signal at the jth antenna is

$$\begin{aligned} r_j(t) \ &= \ \sqrt{2P_0} \sum_{l=0}^{N_l-1} g_{0j,l}(t) e^{j(2\pi\nu_0(t-\tau_{0j,l})+\theta_0)} s_0(t - \tau_{0j,l}) \\ &\quad + \ \sqrt{2P_1} \sum_{l=0}^{N_l-1} g_{1j,l}(t) e^{j(2\pi\nu_1(t-\tau_{1j,l})+\theta_1)} s_1(t - \tau_{1j,l}) \ + \ n_j(t) \ , \end{aligned} \tag{8}$$

where θ_0 and θ_1 are random phase offsets corresponding to the desired and interfering transmitters, respectively. ν_0 and ν_1 are frequency offsets between the receiver and desired transmitter, and the receiver and interferer, respectively, and $n_j(t)$ is the AWGN at the jth antenna. The first and second terms on the RHS of (8) are the contributions to $r_j(t)$ from the desired and co-channel signal, respectively. We consider a single dominant co-channel interferer.

The received baseband signals is over-sampled by a factor J. The channel is modeled as a length-L FIR filter, where L is a design parameter that is chosen *a priori* to handle the maximum expected time dispersion. The sampled sequences are arranged [103] as

$$\mathbf{y}(k) = \ \mathbf{H}\, \mathbf{a_L}(k - n) + \mathbf{w}(k) \ , \tag{9}$$

where $\mathbf{y}(k) = [r_0(kT_s), \ r_1(kT_s), \ \ldots, \ r_{M-1}(kT_s)]^T$ is a $M \times 1$ column vector, $T_s = T/J$ is the sampling period, and $r_j(kT_s)$ is the received baseband sample at the jth antenna. The $M \times (L+1)$ matrix, $\mathbf{H}$ represents the single-input-multiple-output (SIMO) channel and the

$(L+1)\times 1$ column vector $\mathbf{a_L}$ contains samples from the transmitted training sequence (TS). These are expressed as

$$\begin{aligned} \mathbf{H} &= [\mathbf{h_0},\ \mathbf{h_1},\ ...,\ \mathbf{h_L}]\ , \\ \mathbf{a_L}(k) &= [a(k),\ a(k-1),\ \ldots,\ a(k-L)]^T\ , \end{aligned} \tag{10}$$

respectively. The $M \times 1$ column vector $\mathbf{w(k)}$ represents the CCI and noise. If $\mathbf{w(k)}$ is modeled as a wide-sense stationary random process then (9) can be rewritten as

$$\mathbf{y}(k+n) = \mathbf{H}\,\mathbf{a_L}(k) + \tilde{\mathbf{w}}(k)\ , \tag{11}$$

where $\tilde{\mathbf{w}}(k)$ is the time shifted process associated with $\mathbf{w}(k)$. The goal is to find the time index n where the training sequence starts.

The co-channel and desired signals have the same structure. The digital sequences transmitted by the interferers are in general unknown. So the optimum solution to the synchronization problem involves a joint exhaustive search over all possible sequences. Since this is computationally cumbersome, a suboptimal approach treats the CCI and the AWGN as *temporally* white complex Gaussian random process. However, the CCI can be modeled as being either *spatially* colored or white. Under the assumption that the AWGN and CCI are temporally white, and that the training sequence starts at index n, the negative log-likelihood function for $N = JN_{TS} - L$ consecutive observations of $y(n)$ can be expressed as

$$\Lambda(n, \mathbf{H}, \mathbf{Q}) = -\sum_{l=L}^{JN_{TS}-1} \log f(\mathbf{y(n+l)} - \mathbf{Ha_L(l)}; \mathbf{Q})\ , \tag{12}$$

where $f(\ \cdot\ ; \mathbf{Q})$ is the pdf of a zero-mean complex Gaussian vector with covariance $\mathbf{Q}$. The negative log-likelihood function in (12) is a function of unknown channel $\mathbf{H(n)}$ and unknown spatial covariance matrix $\mathbf{Q(n)}$, which must be estimated at every n. Thus, the timing estimate is

$$\hat{n} = \arg\min_n \Lambda(n)\ . \tag{13}$$

In [86] two metrics are derived for spatially colored and white CCI models. The first metric that considers the CCI as spatially colored [86] is obtained as

$$\Lambda_{color}(n) = \log|\hat{\mathbf{Q}}(\mathbf{n})| \ . \tag{14}$$

The second metric that ignores the spatial coloring and models CCI as spatially white [86] is

$$\Lambda_{white}(n) = \text{trace}\{\hat{\mathbf{Q}}(\mathbf{n})\} \ . \tag{15}$$

When deriving the above metrics, the ML estimates of the channel and the covariance matrix are obtained by minimizing the cost function in (12) as

$$\hat{\mathbf{H}}(n) = \hat{\mathbf{R}}_{\mathbf{ya}}\hat{\mathbf{R}}_{\mathbf{aa}}^{-\mathbf{1}} \ , \tag{16}$$

$$\hat{\mathbf{Q}}(n) = \hat{\mathbf{R}}_{\mathbf{yy}} - \hat{\mathbf{R}}_{\mathbf{ya}}\hat{\mathbf{R}}_{\mathbf{aa}}^{-1}\hat{\mathbf{R}}_{\mathbf{ya}}^{\mathbf{H}} \ , \tag{17}$$

where the ML channel estimate is a least-square (LS) fit to the received signal, and the ML spatial covariance matrix estimate is the sample covariance matrix of the residuals. The sample covariance matrices are calculated as

$$\hat{\mathbf{R}}_{\mathbf{yy}}(n) = \frac{1}{N}\sum_{l=L}^{JN_{TS}-1}\mathbf{y}(l+n)\mathbf{y}^{H}(l+n) \ , \tag{18}$$

$$\hat{\mathbf{R}}_{\mathbf{ya}}(n) = \frac{1}{N}\sum_{l=L}^{JN_{TS}-1}\mathbf{y}(l+n)\mathbf{a}_{\mathbf{L}}{}^{H}(l) \ , \tag{19}$$

$$\hat{\mathbf{R}}_{\mathbf{aa}} = \frac{1}{N}\sum_{l=L}^{JN_{TS}-1}\mathbf{a}_{\mathbf{L}}(l)\mathbf{a}_{\mathbf{L}}{}^{H}(l) \tag{20}$$

for a correlation window of length $N = (JN_{TS} - L)$ samples.

The frequency offset causes phase rotation in the received signal at each antenna with respect to the reference training sequence, $a(k)$. Therefore, the elements of the spatio-temporal cross-correlation matrix

$$\left[\hat{\mathbf{R}}_{\mathbf{ya}}(n)\right]_{ij} = \frac{1}{N}\sum_{l=L}^{JN_{TS}-1} r_i(l+n)a^{*}(l-j); \quad i = 0,..,M-1; \ \ j = 0,..,L \tag{21}$$

are affected by the frequency offset. However, the phase rotations due to frequency offset are cancelled out in the elements of the auto-correlation matrix $\hat{\mathbf{R}}_{\mathbf{yy}}(n)$.

In the case of GMSK, the received signal in (8) can be expressed as

$$\begin{aligned} r_j(t) &= \sqrt{2P_0}\sum_{l=0}^{N_l-1} g_{0j,l}(t)e^{j(2\pi v_0(t-\tau_{0j,l})+\theta_0)}s_0(t-\tau_{0j,l}) + w_j(t) \\ &= \sqrt{2P_0}\left[\sum_{l=0}^{N_l-1} g_{0j,l}(t)e^{j(-2\pi v_0\tau_{0j,l}+\theta_0+\theta'_{0j,l})}\right] \\ &\quad \cdot\ e^{j[\psi(t;\alpha_\mathbf{0})+2\pi v_0 t]} + w_j(t)\ , \end{aligned} \tag{22}$$

where $w_j(l)$ is the CCI and noise at the jth antenna, and desired signal received by the jth antenna and the lth path is $s_0(t-\tau_{0j,l}) = e^{j\psi(t-\tau_{0j,l};\alpha_\mathbf{0})} = e^{j\theta'_{0j,l}}\, e^{j\psi(t;\alpha_\mathbf{0})}$. Assuming that the channel remains constant over the training sequence, the effect of the channel on the desired signal received by the jth antenna can be approximated as

$$\sum_{l=0}^{N_l-1} g_{0j,l}(t)e^{j(2\pi v_0(t-\tau_{0j,l})+\theta_0+\theta'_{0j,l})} \approx G_0 e^{j\phi_0}\ , \tag{23}$$

where G_0 is a real number and ϕ_0 is a random variable uniformly distributed on $[0, 2\pi]$. Therefore, the sampled received signal at the jth antenna is approximately

$$r_j(n) \approx \sqrt{2P_0}G_0\, e^{j[\psi(nT_s;\alpha_\mathbf{0})+2\pi v_0 nT_s+\phi_0]} + w_j(n)\ . \tag{24}$$

Following the methodology in [85], the cross-correlation between the training sequence and the received signal at each antenna can be measured to mitigate frequency offset. The idea is to replace each of the spatio-temporal cross-correlation elements of $\hat{\mathbf{R}}_{\mathbf{ya}}(n)$ by the corresponding double cross-correlation (DC) term. In [85], several metrics L_0, L_1 and L_2 are introduced for the DC. Applying the balanced DC metric L_1 to (21) yields the following new spatio-temporal cross-correlation

$$\begin{aligned} \left[\hat{\mathbf{R}}^{(\mathbf{DC})}_{\mathbf{ya}}(n)\right]_{ij} = \frac{1}{N'}\sum_{m=1}^{JN_{TS}-1}\Bigg\{\Bigg|\sum_{l=L+m}^{JN_{TS}-1} r_i^*(l+n)\, a(l-j)\, r_i(l+n-m) \\ \cdot\ a^*(l-m-j)| - \sum_{l=L+m}^{JN_{TS}-1} |r_i(l+n)|\,|r_i(l+n-m)|\Bigg\}\ , \end{aligned} \tag{25}$$

where $i = 0, \cdots, M-1$, $j = 0, \cdots, L$, and $N' = \frac{1}{2}(JN_{TS} - 1)(JN_{TS} - 2L)$.

Using this new cross-correlation matrix $\hat{\mathbf{R}}_{\mathbf{ya}}^{(\mathbf{DC})}(n)$ in (17), a new estimate of the covariance matrix is obtained as

$$\hat{\mathbf{Q}}^{(\mathbf{DC})}(\mathbf{n}) \;=\; \hat{\mathbf{R}}_{\mathbf{yy}}(\mathbf{n}) - \hat{\mathbf{R}}_{\mathbf{ya}}^{(\mathbf{DC})}(\mathbf{n})\hat{\mathbf{R}}_{\mathbf{aa}}^{-1}(n)\hat{\mathbf{R}}_{\mathbf{ya}}^{(\mathbf{DC})^{\mathbf{H}}}(\mathbf{n}) \;. \tag{26}$$

Replacing $\hat{\mathbf{Q}}(\mathbf{n})$ in (14) and (15) by $\hat{\mathbf{Q}}^{(\mathbf{DC})}(\mathbf{n})$ gives two new DC timing estimation metrics for colored and white CCI-plus-noise models, respectively, as

$$\Lambda_{color}^{(DC)}(n) = \log|\hat{\mathbf{Q}}^{(\mathbf{DC})}(\mathbf{n})| \;, \tag{27}$$

$$\Lambda_{white}^{(DC)}(n) = \text{trace}\{\hat{\mathbf{Q}}^{(\mathbf{DC})}(\mathbf{n})\} \;. \tag{28}$$

3.4 Numerical Results and Discussions

During initial cell search, the receiver exploits the extended training sequence of the synchronization burst. The desired transmitter periodically transmits the training sequence of length, $N_{TS} = 64$ symbols whereas the co-channel interferer transmits a random data sequence. The receiver uses a two-element antenna (i.e. $M = 2$) and over-samples the received signal by a factor $J = 4$. The channels considered are COST207 typical-urban (TU) and rural-area-non-hilly (RANH) channels [104].

Figures 5 and 6 show the timing estimation error rate with different frequency offsets for typical-urban and rural-area-non-hilly channel models when the SIR is fixed at -2 dB and SNR= 20 dB, and the maximum Doppler frequency is 5 Hz and 100 Hz, respectively. A synchronization error occurs when the estimated frame boundary is more than half a symbol away from the true frame boundary [6]. The solid and dotted lines correspond to the rural-area-non-hilly and typical-urban channels, respectively. For comparison purposes, results using the correlation method [6], the double-correlation method of [85] with metric L_1, and the colored and white CCI-plus-noise models of [86] are also plotted. The results illustrate that the proposed metric in (27) outperforms the other methods. Such performance

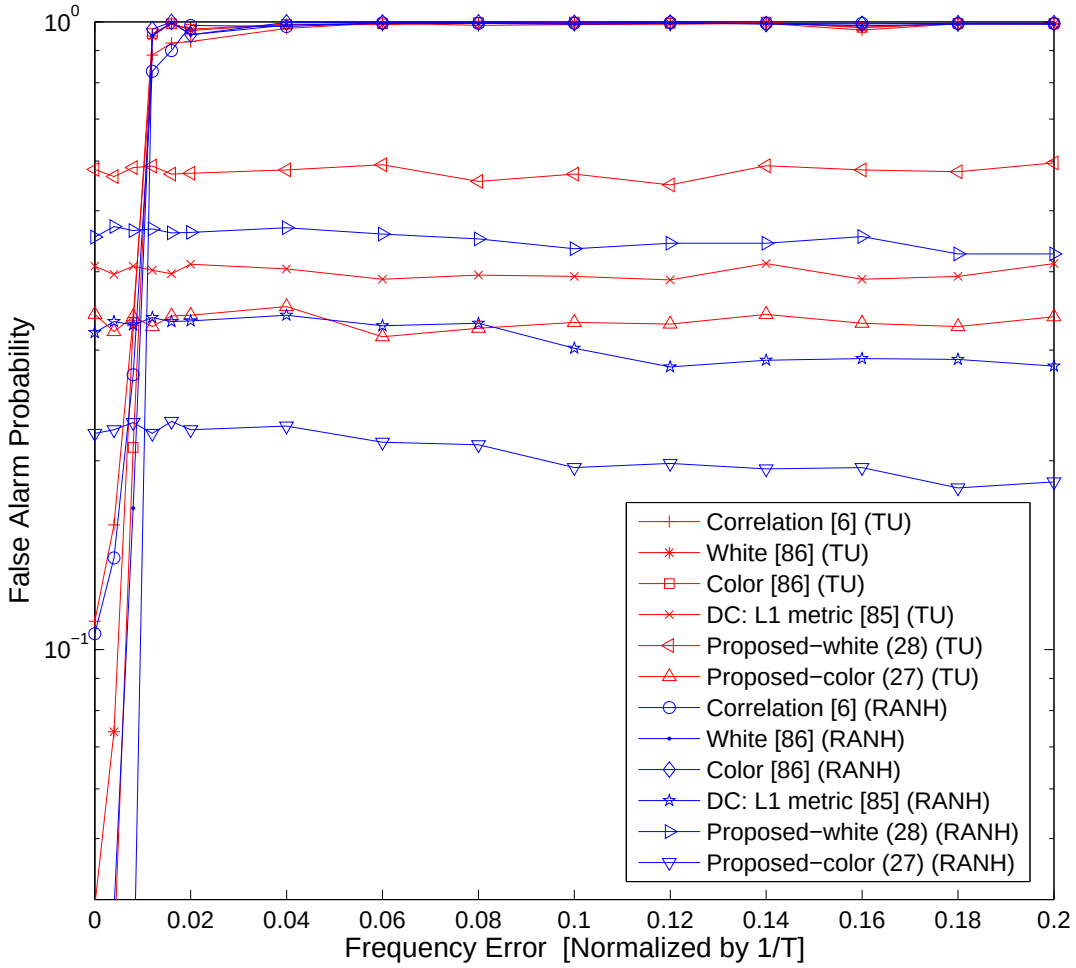

Figure 5. Timing estimation error rate against frequency offset for TU and RANH channel models ($SIR = -2\ dB, M = 2, f_m = 5\ Hz$**)**

improvement could be valuable in applications where the receiver implements co-channel interference cancellation schemes and must synchronize at low SIR. Finally, it should be noticed that the performance is fairly insensitive to Doppler frequency.

The proposed DC color method (27) outperforms the DC white method (28) at SIR= −2 dB. However they perform almost the same at higher SIR. In fact, at very high SIR values, the white DC metric (28) slightly outperforms the color DC metric (27). This is because the covariance matrix, $\mathbf{Q}^{\mathbf{DC}}(\mathbf{n})$ contains M^2 real parameters that are jointly estimated. For the color DC method, all M^2 elements of the covariance matrix are used, while only

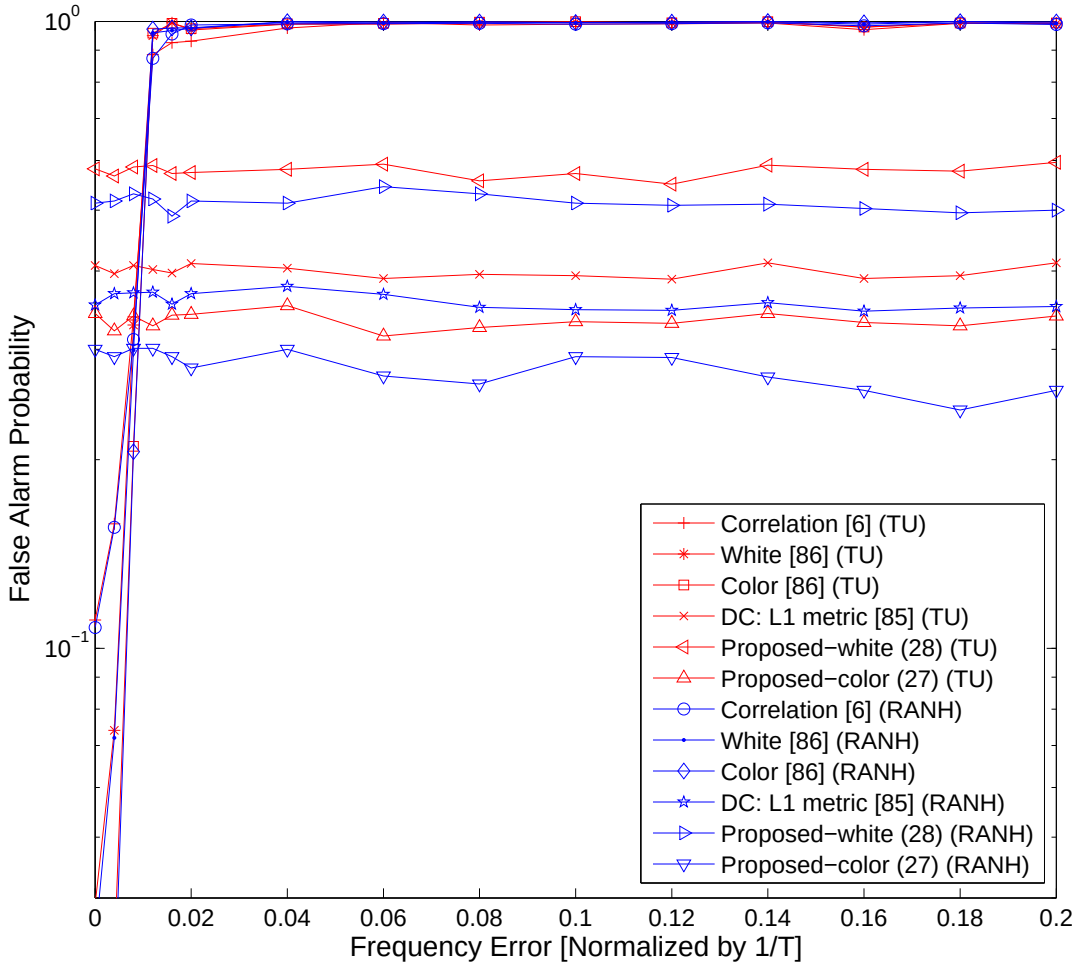

Figure 6. Timing estimation error rate against frequency offset for TU and RANH channel models ($SIR = -2\ dB, M = 2, f_m = 100\ Hz$**)**

the M diagonal elements are used in the white DC method. Ideally, the channels corresponding to the different receiver antennas are uncorrelated, but in practice there will exist some cross-correlation. At low SIR, even a small amount of cross-correlation improves the synchronization performance of the DC color method. However, as the SIR increases the diagonal elements of the covariance matrix dominate the off-diagonal elements. So the white DC method (28), which only considers diagonal elements of the covariance matrix performs somewhat better at high SIR. However, at low SIR the color DC method outperforms the white DC method, since it exploits the off diagonal elements as well in the

covariance matrix.

3.5 Summary

Two new timing estimators have been derived by applying the concept of double correlation to the spatio-temporal cross-correlation matrix elements of the colored and white CCI-plus-noise models. Simulation results demonstrate that the proposed timing estimator given by (27) performs better than the correlation method of [6] and the two estimators of [86] using white- or color-CCI-noise models, respectively. It also moderately outperforms the double-correlation method [85], which is known to be robust to large frequency offsets. The improved performance of the estimator (27) at low SIR values can be attributed to the fact that the spatially colored model helps to boost the effective SIR by considering all the elements of the covariance matrix at low SIR, while the phase offset due to frequency error that exists in the cross-correlation is diminished by the double correlation that is applied to the spatio-temporal cross-correlation matrix.

CHAPTER 4

CONSTANT-ENVELOPE MC-CDMA SYSTEMS USING CYCLIC DELAY DIVERSITY

4.1 Overview

Orthogonal frequency division multiplexing (OFDM) systems have been proposed for high data rate wireless applications due to their robustness on frequency-selective-fading channels and simplicity of implementation. Multicarrier code division multiple access (MC-CDMA) [8] that combines orthogonal frequency division multiplexing (OFDM) and code division multiple access (CDMA) is robust against fading, jamming, and multiuser interference (MUI) [9]. However, MC-CDMA is typically characterized by a high peak-to-average-power ratio (PAPR). In [10, 11], an MC-CDMA system that uses quadratic spreading sequences having a constant envelope in both the time and frequency domains was introduced as a solution to this high PAPR problem. These sequences, also known as Chu sequences, have incidently been chosen as training sequences in the IEEE 802.16a standard due to their excellent PAPR properties.

Multiple-input multiple-output (MIMO) systems with suitable space-time coding (STC) can significantly improve power efficiency. Delay diversity [13] is the simplest transmit diversity scheme [14]. Full diversity achieving, full rate, space-time block code (STBC) was proposed by Alamouti [15] for two transmit antennas. Later the concept was generalized to three and four transmit antennas [16], but the corresponding STBCs do not attain full rate. Space-time trellis codes (STTC) can also provide full diversity. However, the decoding complexity increases exponentially with the number of transmit antennas [17].

It is desirable that space-time codes be easily scalable or configurable for an arbitrary number of transmit antennas. Although STBCs and STTCs provide full diversity, they require different space-time codes for different numbers of transmit antennas. Cyclic delay diversity (CDD) with OFDM is easily scalable to an arbitrary number of transmit antennas

compared to STBC and STTC. When OFDM is used with CDD, an error-correction code having minimum distance greater than or equal to the number of transmit antennas will achieve full diversity, and suitable block interleaving will yield good coding gain [105].

In the pursuit of a robust wireless system, in this chapter, we study a constant-envelope MC-CDMA system using CDD (CE-MC-CDMA-CDD). The constant envelope provides a low probability of intercept (LPI) for the transmitted waveform. A simple receiver implementation that is independent of the number of transmit antennas is possible [106–108]. The proposed system does not need additional error-correction coding beyond multicarrier spreading to guarantee full diversity and, thus, there is no additional loss in data rate. Moreover, interleaving is not needed to guarantee satisfactory coding gain. Potential applications of our proposed system include military communication links and the transmission of control channels (CCH) in commercial MC-CDMA systems where link reliability is of primary concern. The space-time coding performance is also analyzed for quasi-static Rayleigh-flat-fading channel. It is shown that full diversity is always achieved regardless of the modulation-type and modulation-order provided that the number of transmit antennas is less than or equal to the number of subcarriers. However, the minimum symbol distance determines the minimum coding gain. Pairwise symbol error probability is derived and utilized for calculating the bit-error rate (BER) upper bound (UB) for arbitrary modulation type, which is verified by simulation results.

The chapter is organized as follows. Section 4.2 describes the system and signal models of CE-MC-CDMA-CDD. The analysis of space-time coding diversity order and coding gain are presented in Sections 4.3.1 and 4.3.2, respectively. Bit-error rate (BER) upper bound (UB) utilizing the symbol pairwise error probability (PEP) is derived in Section 4.3.3. Numerical results are presented in Section 4.4 and Section 4.5 concludes the chapter.

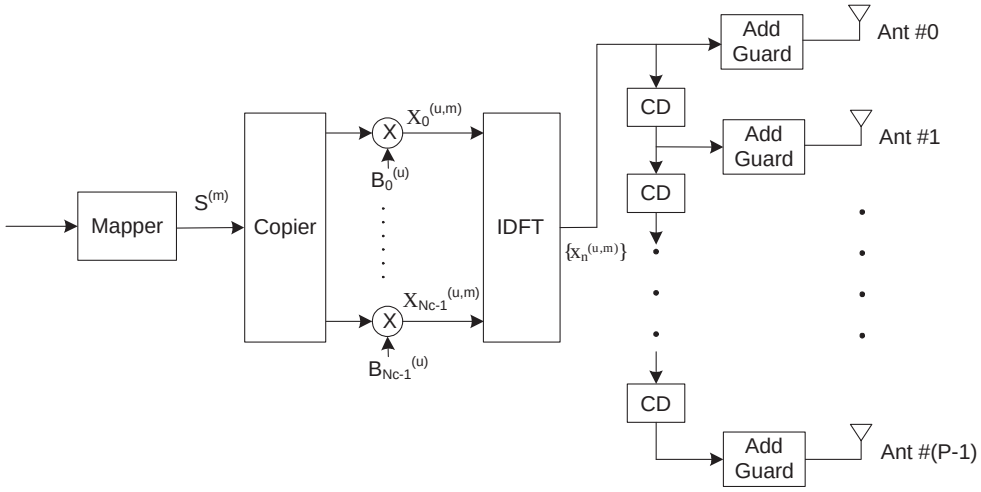

Figure 7. Constant-envelope MC-CDMA-CDD transmitter.

4.2 CE-MC-CDMA-CDD System

Fig. 7 shows a CE-MC-CDMA-CDD transmitter with $P \leq N_c$ transmit antennas, where N_c is the spreading factor (an even number). We consider M-ary phase shift keying (MPSK), since the MC-CDMA waveform with MPSK will have constant envelope. However, if other modulations are used, the envelope will still remain constant during every MC-CDMA symbol period. Each mapped symbol $s^{(m)} = e^{j\frac{2\pi m}{M}}$, $m \in \{0, 1, \cdots, M-1\}$ is multiplied by the u-th user's frequency-domain spreading sequence $\{B_k^{(u)}\}$, $k = 0, 1, \cdots, N_c - 1$ to generate the frequency-domain signal (normalized by $\sqrt{E_s}$) $X_k^{(u,m)} = s^{(m)} B_k^{(u)}$, where E_s is the average received symbol energy.

The time- and frequency-domain polyphase spreading sequences [10, 11] considered are defined as $b_n = e^{-j\frac{\pi}{8}}\, e^{j\frac{\pi n^2}{N_c}}$, $n = 0, 1, \cdots, N_c - 1$ and $B_k = e^{j\frac{\pi}{8}}\, e^{-j\frac{\pi k^2}{N_c}}$, $k = 0, 1, \cdots, N_c - 1$, respectively. The attractive features of the sequences $\{b_n\}$ and $\{B_k\}$ are: they are a discrete Fourier transform (DFT) pair, i.e., $b_n \underrightarrow{DFT} B_k$, $B_k \underrightarrow{IDFT} b_n$; they are auto-orthogonal, i.e. orthogonal to any non-zero cyclic shifts; and they have a constant envelope in both the time and frequency domains.

If $\{B_k\} = \{B_k^{(0)}\}$ is the frequency-domain spreading sequence assigned to the desired user

($u = 0$), the frequency-domain spreading sequence for the u-th user is [10]

$$B_k^{(u)} = e^{-j\frac{2\pi}{N_c}ku} B_k, \quad k = 0, 1, \cdots, N_c - 1. \tag{29}$$

The corresponding time-domain sequence of the u-th user's spreading sequence is $\{b_n^{(u)} = b_{(n-u)_{N_c}}\}$, which is a cyclicly shifted replica of the desired user's time-domain sequence $\{b_n^{(0)} = b_n\}$. Here, $(n)_{N_c}$ denotes the residue of n modulo-N_c. Since $\{b_n\}$ and $\{b_{(n-u)_{N_c}}\}$ are orthogonal for any $u \neq 0$, this method of allocating spreading codes does not generate any multiuser interference unless the transmitted signal experiences delay spread or is delayed by the transmitter for CDD. Hence, CDD with P transmit antennas will cause multiuser interference even with a flat-fading channel unless the total number of users, U, is constrained by $U \leq \lfloor \frac{N_c}{P} \rfloor$. To maintain orthogonality among the signals transmitted from all transmit antennas, the following multiuser spreading code assignment is used:

$$u \in \mathcal{U} = \left\{ 0, P, \cdots, \left(\left\lfloor \frac{N_c}{P} \right\rfloor - 1 \right) P \right\} \ , \tag{30}$$

where $\lfloor c \rfloor$ denotes the largest integer that is smaller than or equal to the real number c.

The frequency-domain signal is transformed by an IDFT to generate the time-domain signal, $x_n^{(u,m)} = \frac{1}{\sqrt{N_c}} \sum_{k=0}^{N_c-1} X_k^{(u,m)} e^{j2\pi kn/N_c} = s^{(m)} b_n^{(u)}, n = 0, \ldots, N_c$. Throughout the chapter, the number of subcarriers is assumed equal to the spreading factor N_c. Before transmission from the p-th transmit antenna, the sequence $\{x_n^{(u,m)}\}$ is cyclic delayed by p chip periods, $p \in \{0, 1, \cdots, P-1\}$ and a cyclic prefix or guard of length G is appended [108] to facilitate frequency-domain equalization at the receiver. The guard interval G is greater than or equal to the maximum channel delay. To compare fairly with the single-antenna case and to account for different spreading factors N_c, the signal power from each of the P transmit

antennas is reduced by the factor $\sqrt{1/(PN_c)}$. After removing the cyclic prefix, the space-time codeword generated by symbol m of user $u \in \mathcal{U}$ (normalized by $\sqrt{E_s}$) is

$$\begin{aligned}
\mathbf{C}(u,m) &= \sqrt{\frac{1}{PN_c}} \begin{bmatrix} x_0^{(u,m)} & x_1^{(u,m)} & \cdots & x_{N_c-1}^{(u,m)} \\ x_{N_c-1}^{(u,m)} & x_0^{(u,m)} & \cdots & x_{N_c-2}^{(u,m)} \\ \vdots & \vdots & \ddots & \vdots \\ x_{N_c-P+1}^{(u,m)} & x_{N_c-P+2}^{(u,m)} & \cdots & x_{N_c-P}^{(u,m)} \end{bmatrix}_{P\times N_c} \\
&= \sqrt{\frac{1}{PN_c}}\, s^{(m)} \begin{bmatrix} \mathbf{b_{n-u}} \\ \mathbf{b_{n-u-1}} \\ \vdots \\ \mathbf{b_{n-u-P+1}} \end{bmatrix}_{P\times N_c}, \qquad (31)
\end{aligned}$$

where row vector $\mathbf{b_n} = [b_0, b_1, \cdots, b_{N_c-1}]$ and row vector $\mathbf{b_{n-u}}$ is generated from u cyclic delays of $\mathbf{b_n}$.

Suppose the codeword $\mathbf{C} = \mathbf{C}(u,m)$ is transmitted, but the maximum-likelihood (ML) detector erroneously decides in favor of a different codeword $\tilde{\mathbf{C}} = \mathbf{C}(u,\tilde{m})$, where $\mathbf{C} \neq \tilde{\mathbf{C}}$, i.e., $m \neq \tilde{m}$. Then the conditional pairwise error probability averaged over the Rayleigh-fading channel gain is upper bounded by [17]

$$\begin{aligned}
P_{c|m,\tilde{m}} &= Pr\{\, \mathbf{C}(u,m) \rightarrow \mathbf{C}(u,\tilde{m}) \mid m, \tilde{m} \,\} \\
&\leq \prod_{q=0}^{Q-1} \prod_{p=0}^{r-1} \frac{1}{1 + \frac{E_s}{4N_0}\lambda_p(m,\tilde{m})} \\
&\leq \left(\frac{E_s}{4N_0}\, G_c(m,\tilde{m})\right)^{-rQ}, \qquad (32)
\end{aligned}$$

where $\lambda_l(m,\tilde{m})$s are the nonzero eigenvalues of the $P \times P$ matrix defined as $\mathbf{A}(m,\tilde{m}) = [\mathbf{C}(u,m) - \mathbf{C}(u,\tilde{m})]\,[\mathbf{C}(u,m) - \mathbf{C}(u,\tilde{m})]^H$, r is the minimum rank of $\mathbf{A}(m,\tilde{m})$, Q is the number of receive antennas, N_0 is the variance of the complex additive white gaussian noise (AWGN), and the coding gain is $G_c(m,\tilde{m}) = (\,\lambda_0(m,\tilde{m}) \ldots \lambda_{r-1}(m,\tilde{m})\,)^{1/r} = (\det[\mathbf{A}(m,\tilde{m})])^{1/r}$.

From the multiuser code allocation given by (10), it is obvious that the MUI in AWGN channel will be zero. In flat fading, $h_n^{(u,p,q)} = h^{(u,p,q)}\,\delta_n$, where $h^{(u,p,q)}$ are assumed i.i.d.

complex Gaussian random variables with zero mean and unit variance. Using (38) and (40), the equivalent frequency-domain channel coefficients are

$$H_k^{(u,q)} = \frac{1}{\sqrt{N_c}} \sum_{p=0}^{P-1} h^{(u,p,q)} e^{-j2\pi \frac{pk}{N_c}}. \tag{33}$$

If the symbols belonging to the interferers are denoted by m_u and mapped to $s^{(m_u)} = e^{j2\pi \frac{m_u}{M}}$, then the multiuser interference for flat fading becomes

$$\begin{aligned} I &= \frac{1}{N_c} \sqrt{\frac{E_s}{P}} \sum_{u \in \mathcal{U}'} \sum_{k=0}^{N_c-1} \sum_{q=0}^{Q-1} \sum_{p_1=0}^{P-1} \sum_{p_2=0}^{P-1} s^{(m_u)} \cdot \; h^{(0,p_1,q)^*} h^{(u,p_2,q)} e^{-j\frac{2\pi k}{N_c}(u-p_1+p_2)} \\ &= \sqrt{\frac{E_s}{P}} \sum_{u \in \mathcal{U}'} \sum_{q=0}^{Q-1} \sum_{p_1=0}^{P-1} \sum_{p_2=0}^{P-1} s^{(m_u)} \, h^{(0,p_1,q)^*} \cdot \; h^{(u,p_2,q)} \delta_{u-p_1+p_2} \\ &= 0. \end{aligned} \tag{34}$$

The above result of *zero* MUI is obtained by using the constant-envelope property ($|B_k|^2 = 1$) of the frequency-domain spreading sequences and the fact that $(u - p_1 + p_2) \neq 0$ for any $p_1, p_2 \in \{0, 1, \cdots, P-1\}$ and any interferer $u \in \mathcal{U}'$.

In uplink, the transmitters are usually located at different places. Therefore, $h^{(0,p,q)}$ and $h^{(u,p,q)}$ are i.i.d. in uplink; whereas, in downlink, $h^{(0,p,q)} = h^{(u,p,q)}$ for all $u \in \mathcal{U}'$. However, the MUI in both the uplink and downlink will be zero since the condition $(u - p_1 + p_2) \neq 0$ is satisfied in both cases.

4.3 Performance Analysis

4.3.1 Diversity Order

Full diversity is achieved if only if the matrix $\mathbf{A}(m, \tilde{m})$ has full rank for all possible codeword pairs $(\mathbf{C}(u, m), \mathbf{C}(u, \tilde{m}))$, $\mathbf{C}(u, m) \neq \mathbf{C}(u, \tilde{m})$. Because the signals from different users are orthogonal to each other, it suffices to consider the codewords of any user e.g. user u. The auto-orthogonal property of the time-domain spreading sequences ($\mathbf{b}_n \mathbf{b}_{n-d}^H = N_c \delta_d$, d any integer) can be used to simplify the matrix $\mathbf{A}(m, \tilde{m})$ as

$$\begin{aligned} \mathbf{A}(m, \tilde{m}) &= \frac{1}{P} \left| s^{(m)} - s^{(\tilde{m})} \right|^2 \mathbf{I}_P \\ &= \frac{1}{P} \, d_{m,\tilde{m}}^2 \, \mathbf{I}_P \;, \end{aligned} \tag{35}$$

where $\mathbf{I}_P$ denotes $P \times P$ identity matrix and $d_{m,\tilde{m}} = \left|s^{(m)} - s^{(\tilde{m})}\right|$ is the distance between the symbols m and $\tilde{m}$. Therefore, $rank\{\mathbf{A}(m, \tilde{m})\} = P$ and the diversity order of our CE-MC-CDMA-CDD scheme for $Q = 1$ is $r = P$, which is the maximum achievable minimum rank of the matrix $\mathbf{A}$ over all possible codeword pairs.

In [105], it has been shown for any OFDM system with cyclic delay diversity that the maximum possible number of transmit antennas achieving full diversity is determined by the minimum number of subcarrier coordinates where all possible frequency-domain sequence pairs, corresponding to the desired and erroneous codewords, are different. Let $\{X_k^{(u,m)} = s^{(m)} B_k^{(u)}\}$ and $\{X_k^{(u,\tilde{m})} = s^{(\tilde{m})} B_k^{(u)}\}$ be the frequency-domain sequences after spreading associated with the codewords $\mathbf{C}(u, m)$ and $\tilde{\mathbf{C}}(u, \tilde{m})$, respectively. The condition $m \neq \tilde{m}$ guarantees that $X_k^{(u,m)} \neq X_k^{(u,\tilde{m})}$ for all subcarrier coordinates $k \in \{0, 1, \cdots, N_c - 1\}$. Therefore, maximum N_c transmit antennas can be used while achieving full diversity. The above result is valid for any modulation-type of any order. From the above results, we can conclude this section with the following theorem:

Theorem 1 (Diversity Order): The CE-MC-CDMA-CDD with multiuser code assignment given by (10) always achieves full diversity in flat-fading channel for any number of transmit antennas $P \leq N_c$.

4.3.2 Coding Gain

For achieved full diversity, the corresponding coding gain is obtained using (35) as

$$G_c(m, \tilde{m}) \;=\; \frac{1}{P}\, d_{m,\tilde{m}}^2. \tag{36}$$

Thus the coding gain $G_c(m, \tilde{m})$ is proportional to the squared distance between the desired and erroneous data symbols, and inversely proportional to the number of transmit antennas. Therefore, the coding gain will diminish as the number of transmit antennas increases.

For MPSK modulation, $s^{(m)} = \exp(j2\pi m/M)$ and $s^{(\tilde{m})} = \exp(j2\pi\tilde{m}/M)$. So, the coding gain is simplified as $G_c(m, \tilde{m}) = \frac{2}{P}\left[1 - \cos\left(\frac{2\pi}{M}(m - \tilde{m})\right)\right]$, $m \neq \tilde{m}$. Thus the minimum coding gain decreases with the increase of the modulation order M. The maximum coding

gain $G_{c,max} = 4/P$ is achieved when $2(\tilde{m} - m)/M$ is an odd integer.

4.3.3 BER Upper Bound

To calculate the upper bound of the BER, we first consider the symbol pairwise error probability (PEP). The receiver of the CE-MC-CDMA-CDD system is a simple implementation in the frequency domain similar as MC-CDMA receivers. Fig. 8 shows the receiver for the CE-MC-CDMA-CDD system. It is assumed that the channel coefficients corresponding to the desired user ($u = 0$) are perfectly known at the receiver. The received signal at the q-th antenna, $q = 0, 1, 2, \cdots, Q-1$ can be expressed as

$$\begin{aligned} y_n^{(q)} &= \sqrt{\frac{E_s}{PN_c}} \sum_{p=0}^{P-1} h_n^{(0,p,q)} \circledast x_{n-p}^{(0,m)} + \\ &\sqrt{\frac{E_s}{PN_c}} \sum_{u \in \mathcal{U}'} \sum_{p=0}^{P-1} h_n^{(u,p,q)} \circledast x_{n-p}^{(u,m_u)} + w_n^{(q)} \quad , \end{aligned} \tag{37}$$

where $\circledast$ denotes convolution, and $h_n^{(u,p,q)}$ is the Rayleigh faded channel coefficient between the p-th transmit antenna of u-th user and the q-th receive antenna. The channel coefficients are assumed independent complex Gaussian random variables with zero mean. The second term on the right side of (11) is the multiuser interference contributed by users $u \in \mathcal{U}' = \left\{P, 2P, \cdots, \left(\left\lfloor \frac{N_c}{P} \right\rfloor - 1\right)P \right\}$ and $w_n^{(q)}$ is the AWGN at the q-th receive antenna having zero mean and variance N_0. If the DFT of the time-domain channel coefficients is

$$H_k^{(u,p,q)} = \frac{1}{\sqrt{N_c}} \sum_{n=0}^{N_c-1} h_n^{(u,p,q)} e^{-j2\pi \frac{nk}{N_c}} \quad , \tag{38}$$

then the received frequency-domain signal after applying DFT at each receive antenna becomes

$$\begin{aligned} Y_k^{(q)} &= \sqrt{\frac{E_s}{P}} \sum_{p=0}^{P-1} H_k^{(0,p,q)} X_k^{(0,m)} e^{-j\frac{2\pi pk}{N_c}} + I_k^{(q)} + W_k^{(q)} \\ &= \sqrt{\frac{E_s}{P}} H_k^{(0,q)} X_k^{(0,m)} + I_k^{(q)} + W_k^{(q)} \quad , \end{aligned} \tag{39}$$

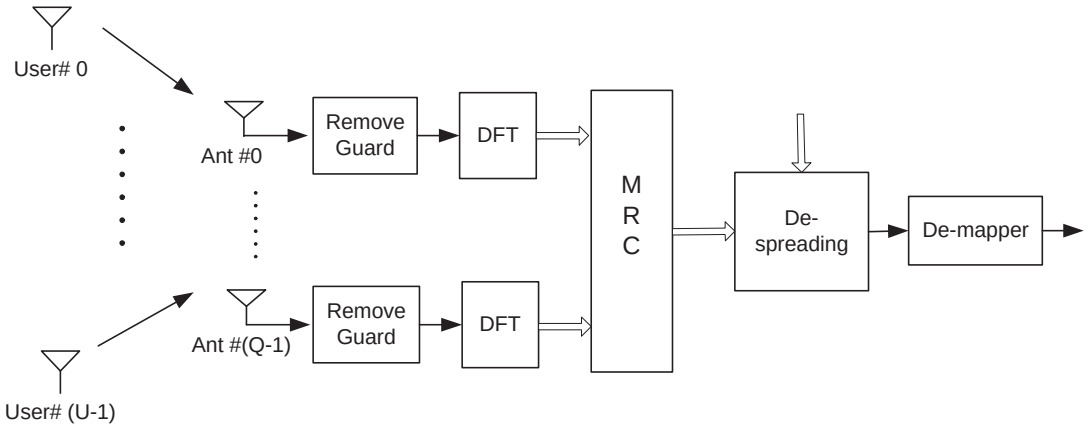

Figure 8. CE-MC-CDMA-CDD receiver.

where $w_n^{(q)} \xrightarrow{DFT} W_k^{(q)}$. The DFT of the interference at the q-th receive antenna is $I_k^{(q)} = \sqrt{\frac{E_s}{P}} \sum_{u \in \mathcal{U}'} H_k^{(u,q)} X_k^{(u,m_u)}$ and equivalent frequency-domain channel coefficients are defined as

$$H_k^{(u,q)} = \sum_{p=0}^{P-1} H_k^{(u,p,q)} e^{-j\frac{2\pi pk}{N_c}} \tag{40}$$

Therefore, the output after maximal-ratio combining (MRC) of different receive-antenna signals is

$$\begin{aligned} Y_k &= \sum_{q=0}^{Q-1} H_k^{(0,q)^*} Y_k^{(q)} \\ &= \sqrt{\frac{E_s}{P}}\, s^{(m)} \sum_{q=0}^{Q-1} \left|H_k^{(0,q)}\right|^2 B_k + \sum_{q=0}^{Q-1} H_k^{(0,q)^*} I_k^{(q)} + \sum_{q=0}^{Q-1} H_k^{(0,q)^*} W_k^{(q)}. \end{aligned} \tag{41}$$

Let the Rayleigh flat-fading channel coefficients be expressed as $h_n^{(u,p,q)} = h^{(u,p,q)}\delta_n$, where the channel coefficients, $h^{(u,p,q)}$, are i.i.d. complex Gaussian random variables with zero mean and unit variance. After despreading, the signal at the input to the demapper is expressed as

$$\begin{aligned} \hat{s} &= \sum_{k=0}^{N_c-1} B_k{}^* Y_k \\ &= \sqrt{\frac{E_s}{P}}\, \alpha\, s^{(m)} + I + \tilde{n}\ , \end{aligned} \tag{42}$$

where the contribution from AWGN is $\tilde{n} = \sum_{k=0}^{N_c-1} \sum_{q=0}^{Q-1} H_k^{(0,q)^*} B_k{}^* W_k^{(q)}$. The channel effect

is $\alpha = \sum_{k=0}^{N_c-1} \sum_{q=0}^{Q-1} \left|H_k^{(0,q)}\right|^2 = \sum_{p=0}^{P-1} \sum_{q=0}^{Q-1} \left|h^{(0,p,q)}\right|^2$ and multiuser interference (MUI) is $I = \sum_{k=0}^{N_c-1} \sum_{q=0}^{Q-1} H_k^{(0,q)^*} B_k{}^* I_k^{(q)}$.

Although multiple users ($u \in \mathcal{U}$) transmit signal simultaneously, the MUI in flat-fading channel is always zero (in both the uplink and downlink) for the multiuser code assignment of (10). This has been shown in Section 4.2. Therefore, the PEP conditioned on α is obtained as

$$\begin{aligned} P(m \to \tilde{m} \mid \alpha) &= Pr\{P(\hat{s}|s^{(\tilde{m})}, \alpha) \geq P(\hat{s}|s^{(m)}, \alpha)\} \\ &= Q\left(\sqrt{\frac{E_s}{2PN_0}\, d_{m,\tilde{m}}^2\, \alpha}\right), \end{aligned} \tag{43}$$

where $Q(.)$ denotes the Gaussian Q-function. The channel effect α has chi-square distribution with $2PQ$ degrees of freedom verifying again that the system achieves spatial diversity of order PQ. The symbol PEP is obtained by averaging the conditional PEP over α as [109]

$$\begin{aligned} P(m \to \tilde{m}) &= \beta^{PQ} \sum_{i=0}^{PQ-1} \binom{PQ-1+i}{i} [1-\beta]^i \\ \beta &= \frac{1}{2} - \frac{1}{2}\left(1 + \frac{1}{\frac{E_s}{4N_0P} d_{m,\tilde{m}}^2}\right). \end{aligned} \tag{44}$$

Assuming that the transmitted symbols are equally likely, the average BER upper bound can be calculated as [110]

$$\begin{aligned} P_b &= \frac{1}{M} \sum_{m=0}^{M-1} P_b(m) \\ &= \frac{1}{M \log_2 M} \sum_{m=0}^{M-1} \sum_{\tilde{m}=0}^{M-1} H(m,\tilde{m})\, P(\tilde{m}|m) \\ &\leq \frac{1}{M \log_2 M} \sum_{m=0}^{M-1} \sum_{\tilde{m}=0}^{M-1} H(m,\tilde{m}) P(m \to \tilde{m}). \end{aligned} \tag{45}$$

Here, the BER conditioned on transmitted symbol m is $P_b(m) = \frac{1}{\log_2 M} \sum_{\tilde{m}=0}^{M-1} H(m,\tilde{m}) \cdot P(\tilde{m}|m)$, where $H(m,\tilde{m})$ is the Hamming distance between the bits associated with symbols m and $\tilde{m}$, and $P(\tilde{m}|m)$ is the probability that the ML decoder detects the symbol $\tilde{m}$ when symbol m is transmitted.

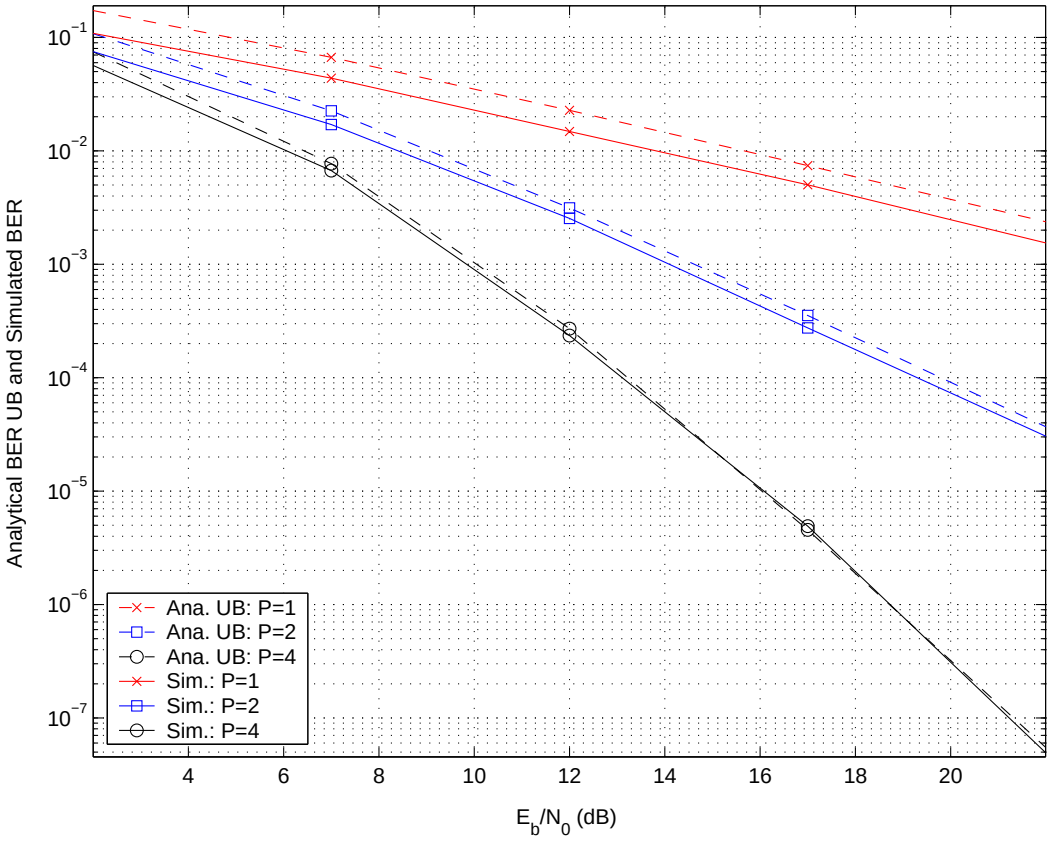

Figure 9. Analytical BER upper bound and simulated BER for QPSK ($Q = 1, N_c = 32$).

4.4 Numerical Results and Discussions

We consider an uncoded constant-envelope MC-CDMA system employing cyclic-delay diversity (CE-MC-CDMA-CDD). Figs. 9 and 10 show the analytical BER UB plotted with the simulated BER for QPSK and $N_c = 32$, when $Q = 1$ and 2, respectively. Figs. 11 and 12 show the analytical BER upper bounds plotted with the simulated BER for 8PSK and $N_c = 32$, when $Q = 1$ and 2, respectively. In each figure, $P = 1, 2$, and 4 transmit antennas have been used where the total number of users is $U = 32, 16$, and 8, respectively. The results demonstrate the full diversity achieved by the CE-MC-CDMA-CDD system. They also show that the analytical BER upper bound and simulated BER match very well. Similar results have been verified for other antenna configurations and PSK modulation orders.

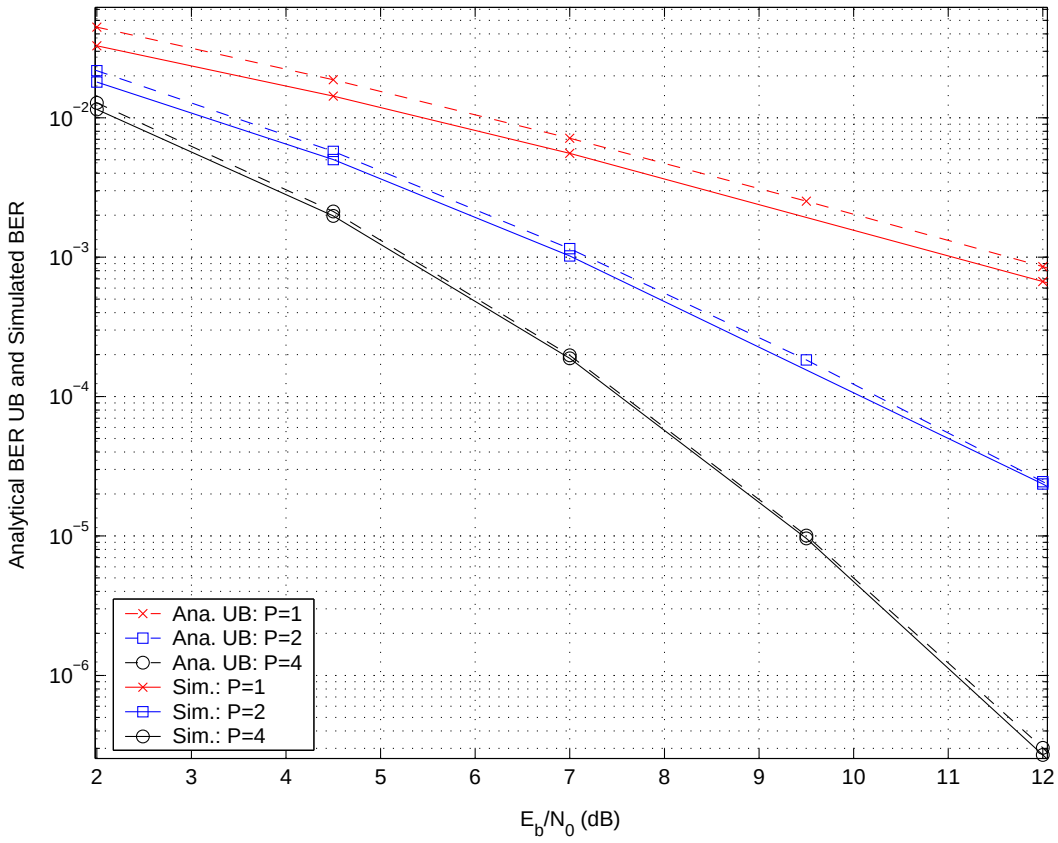

Figure 10. Analytical BER upper bound and simulated BER for QPSK ($Q = 2, N_c = 32$).

4.5 Summary

In this chapter, we have introduced a constant-envelope MC-CDMA system using cyclic delay diversity (CE-MC-CDMA-CDD) with PSK modulation. For uplink, the system maintains constant envelope both in the time and frequency domains. Thus, the system can exploit efficient, nonlinear power amplifiers. The space-time coding aspects of the system have been analyzed including the diversity order and coding gain. It is shown that full diversity is always achieved if the number of transmit antennas is less than or equal to the number of subcarriers, independent of the modulation type and alphabet size. The proposed MC-CDMA system does not require additional error-correction coding or interleaving to guarantee full spatial diversity. It has also been shown that the coding gain is determined by the squared symbol distance. Analytical and simulation results on BER are presented, which confirm the achieved full diversity.

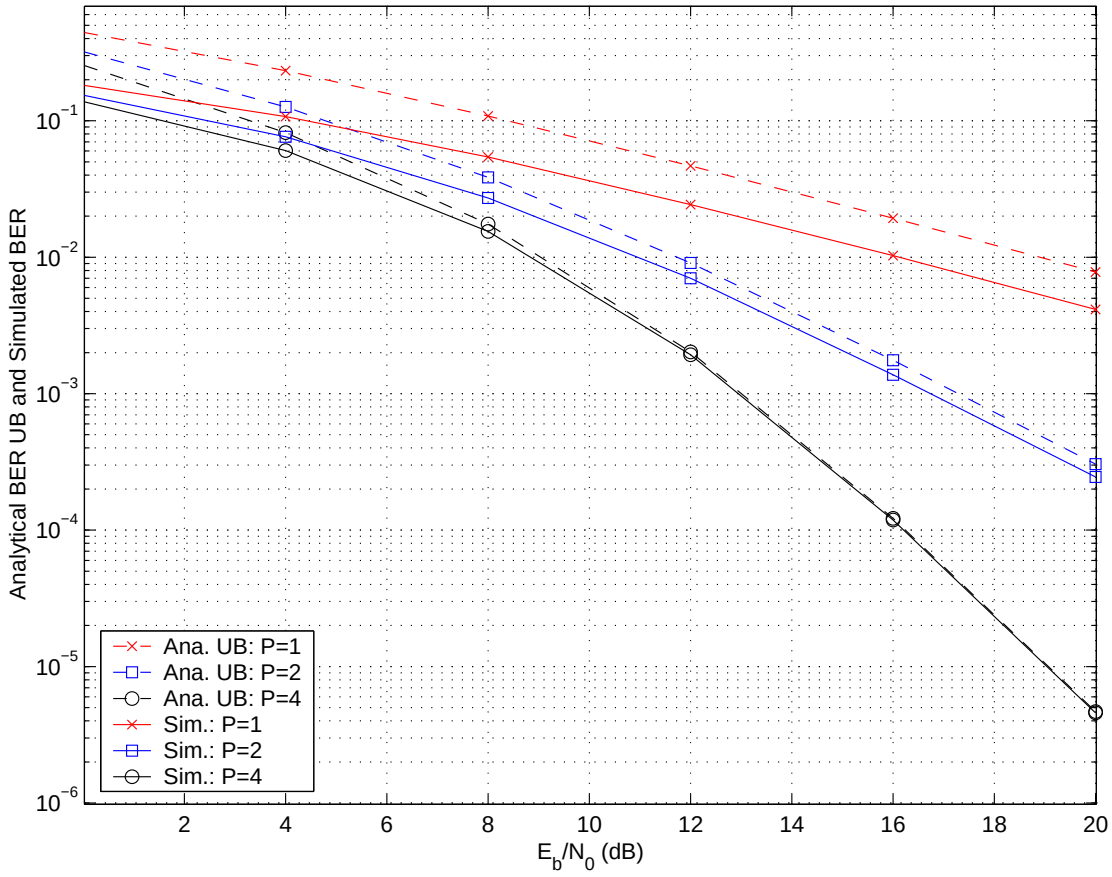

Figure 11. Analytical BER upper bound and simulated BER for 8PSK ($Q = 1, N_c = 32$).

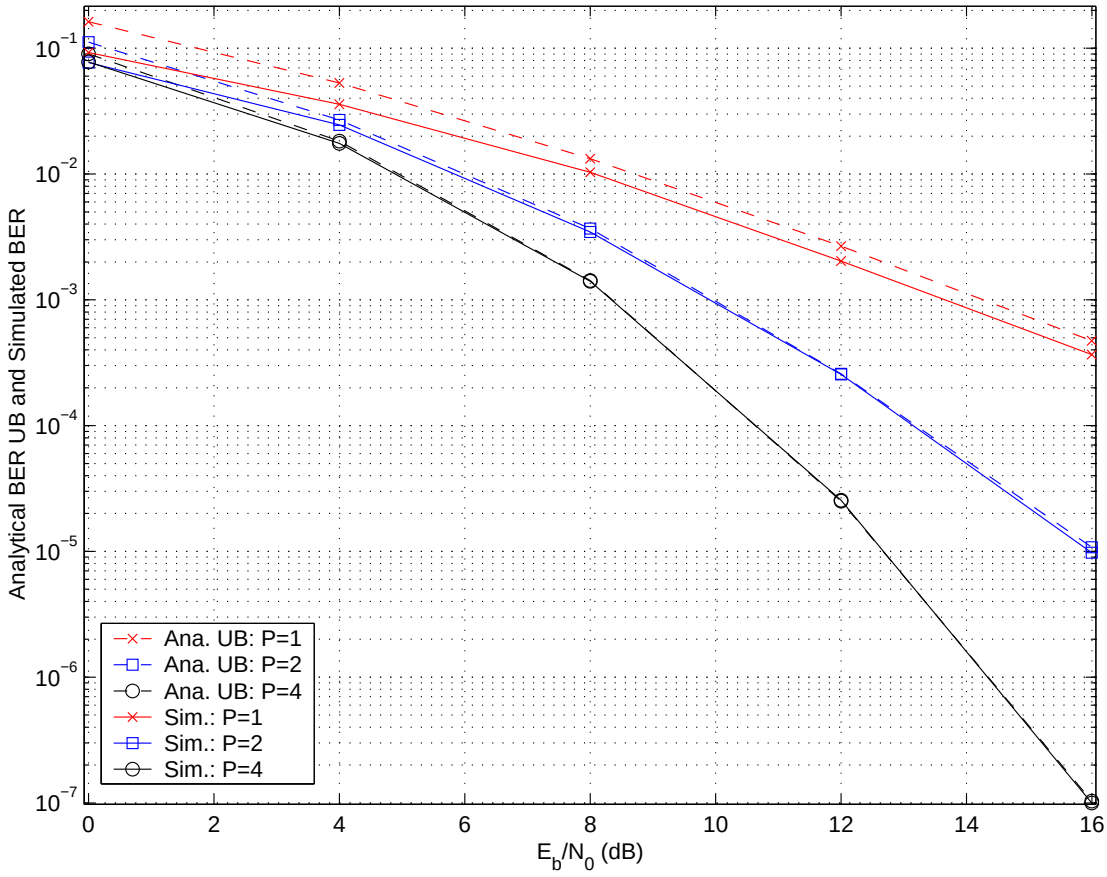

Figure 12. Analytical BER upper bound and simulated BER for 8PSK ($Q = 2, N_c = 32$).

CHAPTER 5

BLIND SNR ESTIMATION

5.1 Overview

In Chapter 4, we have introduced an uncoded multi-input multi-output (MIMO) constant-envelope MC-CDMA system employing cyclic delay diversity (CE-MC-CDMA-CDD [41]) as a solution to the high peak-to-average-power ratio (PAPR) problem prevalent in multicarrier systems. Beyond multicarrier spreading, the MC-CDMA-CDD system require neither error-correction coding to achieve full spatial diversity, nor chip interleaving to achieve a satisfactory space-time coding (STC) gain [105]. It also provides a simple STC implementation, which is independent of the number of transmit antennas [106, 108]. This chapter presents a blind signal-projection (SP)-based Signal-to-noise-ratio (SNR) estimator for the CE-MC-CDMA-CDD system that operates under time-varying frequency-selective-fading channel.

SNR, defined as the ratio of the desired signal power to the noise power, is widely used in communication to describe the effect of noise on the received signal. SNR estimation is essential at the receivers for various purposes, e.g., in the calculation of *a posteriori* probabilities, in chip combining, in power control so that the transmitter can decide the transmission power, etc. The sensitivity of a turbo decoder to mis-estimation of the SNR is investigated in [18] and a scheme that estimates the unknown SNR from each code block with adequate accuracy is presented. The SNR of different subcarriers can be used for calculating the chip-combining weights to suppress the adverse effect of jamming signal or unintentional interference for an MC-CDMA system. A modified maximal-ratio combining (MRC) scheme using the SNR of different RAKE fingers is proposed in [19] for wideband code division multiple access (WCDMA) systems.

Data aided signal-space projection-based signal-to-interference-plus-noise ratio (SINR)

estimators have been previously proposed for time division multiple access (TDMA) cellular systems and are well known for their excellent performance and computational simplicity. A subspace-based technique is proposed in [22] to estimate the SINR for TDMA cellular systems. In [23], the interference plus AWGN variance is estimated by projecting the received signal onto a single vector of the left-null space of the matrix formed by the known training sequence or estimated data symbols. In [24], the interference plus noise variance for TDMA systems is estimated by projecting the received signal onto the entire signal subspace. The signal-projection (SP) method [24] has less complexity, shorter estimation time, and smaller estimation error than the previous two methods. In this chapter, we apply the SP method to estimate SNR for the single-user constant-envelope (uplink only) MC-CDMA-CDD system. Because the orthogonal spreading sequences form the basis of the signal space, a training sequence or data decisions are not needed and orthonormalization is not required. Thus, the proposed SNR estimator is computationally efficient and very accurate estimates are achieved requiring training symbols or symbol decisions, i.e., without sacrificing power and bandwidth.

The remainder of this chapter is organized as follows. Section 5.2 illustrates the MC-CDMA-CDD transmitter. The channel model is discussed in Section 5.3. The SNR estimator is introduced in Section 5.4. Section 5.5 presents the simulation results and Section 5.6 concludes the chapter.

5.2 MC-CDMA-CDD Transmitter

Fig. 13 shows the constant-envelope MC-CDMA-CDD transmitter with $P(\leq N)$ transmit antennas, where N is the number of subcarriers, which is also equal to the spreading factor. The subcarriers are uniformly spread over the system bandwidth so that the frequency diversity of the channel can be well exploited. The transmitter is same as the one shown in Chapter 4 except that there is only one single user in this case. However, extending the techniques developed in this chapter for multiuser case is fairly straight forward. We

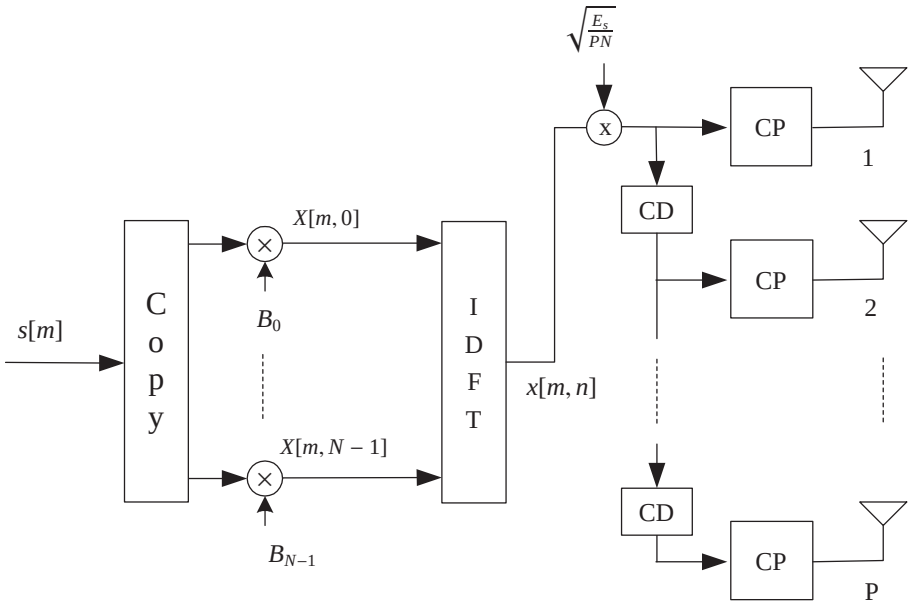

Figure 13. Constant-envelope MC-CDMA-CDD transmitter.

consider M-ary phase shift keying (MPSK). Throughout the chapter the following notations are used: $(\cdot)^T$, and $(\cdot)^H$ denote transpose and conjugate transpose, respectively.

The mth mapped symbol $s[m]$ is spread by the frequency-domain spreading sequence $\{B[k]\}$, $k = 0, 1, \cdots, N-1$, to generate the frequency-domain signal $X[m,k] = s[m]B[k]$. The time- and frequency-domain complex-quadratic or polyphase spreading sequences considered here are defined as $b[n] = e^{-j\frac{\pi}{8}}\, e^{j\frac{\pi n^2}{N}}$, $n = 0, 1, \cdots, N-1$ and $B[k] = e^{j\frac{\pi}{8}}\, e^{-j\frac{\pi k^2}{N}}$, $k = 0, 1, \cdots, N-1$, respectively. If the corresponding time- and frequency-domain chips without any cyclic shifts are arranged in vector form as $\mathbf{b}^{(0)} = [b[0], b[1], \cdots, b[N-1]]^T$ and $\mathbf{B}^{(0)} = [B[0], B[1], \cdots, B[N-1]]^T$, respectively, then $\mathbf{B}^{(0)} = \mathbb{F}\,\mathbf{b}^{(0)}$, where the elements of the discrete Fourier transform (DFT) matrix are $[\mathbb{F}]_{k,n} = e^{-j\frac{2\pi kn}{N}}$; $k, n = 0, 1, \cdots, N-1$. As mentioned in the previous chapter, the sequences $\{b[n]\}$ and $\{B[k]\}$ are a discrete Fourier transform (DFT) pair, i.e., $b[n] \xrightarrow{DFT} B[k]$, $B[k] \xrightarrow{IDFT} b[n]$; they are auto-orthogonal, i.e. orthogonal to any non-zero cyclic shifts; and they have a constant envelope in both the time and frequency domains.

The frequency-domain signal is transformed by an inverse DFT (IDFT) into the time-domain signal, $x[m,n] = \frac{1}{\sqrt{N}} \sum_{k=0}^{N-1} X[m,k]\, e^{j2\pi kn/N} = s[m]b[n]$, where $n = 0, 1, \ldots, N-1$ is the time-domain (TD) chip index. Before transmission from the p-th ($1 \leq p \leq P$) antenna, the sequence $\{x[m,n]\}_{n=0}^{N-1}$ is cyclic delayed (CD) by $d_p T_c$ so that the transmitted signal on the kth subcarrier is $T^{(p)}[m,k] = \sqrt{\frac{E_s}{PN}}\, X[m,k]\, e^{-j\frac{2\pi k d_p}{N}}$, where $E_s = NE_c$ is the average received symbol energy, E_c is the average received chip energy, d_p is the number of unit cyclic shifts applied to the pth transmit antenna, and T_c is the time-domain chip duration equal to the sampling period. A cyclic prefix (CP) or guard of length GT_c is appended [108] to facilitate frequency-domain equalization at the receiver.

5.3 Channel Model

We consider time-varying multipath-Rayleigh-fading channels. Considering any receive antenna $q \in \{1, \cdots, Q\}$, where Q is the total number of receive antennas, the discrete channel frequency response corresponding to the kth subcarrier of the mth symbol and pth transmit antenna is $H^{(p,q)}[m,k] = \frac{1}{\sqrt{N}} \sum_{l=0}^{L-1} h^{(p,q)}[m,l]\, e^{-j2\pi kl/N}$ for $p = 1, \cdots, P$ and $k = 0, 1, \cdots, N-1$, where L is the number of channel taps, and $h^{(p,q)}[m,l]$ is a zero mean complex Gaussian distributed channel coefficient associated with the lth ($l = 0, 1, \cdots, L-1$) path between the pth transmit and qth receive antenna. The frequency response vector corresponding to the pth transmit and qth receive antenna pair is $\mathbf{H}^{(p,q)}[m] = \frac{1}{\sqrt{N}}\, \mathbb{F}\, \mathbf{h}^{(p,q)}[m]$, where $\mathbf{h}^{(p,q)}[m] = [h^{(p,q)}[m,0],\, h^{(p,q)}[m,1],\, \cdots,\, h^{(p,q)}[m,L-1]]^T$; $\mathbf{H}^{(p,q)}[m] = [H^{(p,q)}[m,0],\, H^{(p,q)}[m,1],\, \cdots,\, \cdots,\, H^{(p,q)}[m,N-1]]^T$ and the elements of the DFT matrix are $[\mathbb{F}]_{k,l} = e^{-j\frac{2\pi kl}{N}}$ for $k = 0, 1, \cdots, N-1$ and $l = 0, 1, \cdots, L-1$.

5.4 Proposed $\frac{E_c}{N_0}$ Estimator

After removing the cyclic prefix and applying DFT at each receiver antenna, the frequency-domain signal corresponding to the mth symbol and qth receive antenna is

$$\begin{aligned} Y^{(q)}[m,k] &= \sqrt{N}\sum_{p=0}^{P-1} H^{(p,q)}[m,k]\; T^{(p)}[m,k] + V^{(q)}[m,k] \\ &= \sum_{p=0}^{P-1}\sum_{l=0}^{L-1} h^{(p,q)}[m,l]\; T^{(p)}[m,k]\; e^{-j2\pi kl/N} + V^{(q)}[m,k]\;, \end{aligned} \tag{46}$$

where $V^{(q)}[m,k]$ are independent identically distributed (i.i.d.) additive white Gaussian noise (AWGN) samples having zero mean and variance N_0. The signals received on the different subcarriers by any receive antenna q can be arranged in a column vector as follows

$$\begin{aligned} \mathbf{Y}^{(q)}[m] &= \left[Y^{(q)}[m,0], Y^{(q)}[m,1], \cdots, Y^{(q)}[m,N-1]\right]^T \\ &= \mathbf{A}[m]\;\mathbf{h^{(q)}}[m] + \mathbf{V^{(q)}}[m];\;\; q = 1,\cdots,Q\;, \end{aligned} \tag{47}$$

where $\mathbf{h}^{(q)}[m] = \left[\mathbf{h}^{(1,q)^T}[m],\cdots,\mathbf{h}^{(P,q)^T}[m]\right]^T$ is the channel coefficient vector for the mth symbol, $\mathbf{h}^{(p,q)}[m] = [h^{(p,q)}[m,0], h^{(p,q)}[m,1],\cdots,h^{(p,q)}[m,L-1]]^T$ is the channel coefficient vector associated with the pth transmit and qth receive antenna pair, $\mathbf{V^{(q)}}[m] = \left[V^{(q)}[m,0], V^{(q)}[m,1],\cdots\;\cdots, V^{(q)}[m,N-1]\right]^T$ is the AWGN vector, and

$$\mathbf{A}[m] = \begin{bmatrix} T^{(1)}[m,0] & \cdots & T^{(P)}[m,0] & \cdots & T^{(P)}[m,0]\; e^{-j2\pi k(L-1)/N} \\ \vdots & & \vdots & & \vdots \\ T^{(1)}[m,N-1] & \cdots & T^{(P)}[m,N-1] & \cdots & T^{(P)}[m,N-1]\; e^{-j2\pi k(L-1)/N} \end{bmatrix} \tag{48}$$

is a $N\times PL$ matrix that depends on the transmitted symbol, cyclic shifts, and channel delays. The AWGN vector $\mathbf{V^{(q)}}[m]$ has zero mean and covariance $N_0\;\mathbf{I}_N$, where $\mathbf{I}_N$ denotes $N\times N$ identity matrix.

The vector obtained by applying l $(0 < l < N-1)$ cyclic shifts to the TD spreading chip vector, $\mathbf{b}^{(0)} = \{b[n]\}_{n=0}^{N-1}$ can be expressed as $\mathbf{b}^{(l)} = [b[N-l],\cdots,b[N-1],b[0],\cdots,b[N-l-1]]^T$. The corresponding frequency-domain vector is $\mathbf{B}^{(l)} = [B[0], B[1]e^{-j2\pi l/N},\cdots,B[N-1]e^{-j2\pi(N-1)l/N}]^T$. By using the expression of the transmitted signal on the kth subcarrier,

$T^{(p)}[m,k] = \sqrt{\frac{E_s}{PN}}\, s[m]B[k]\, e^{-j\frac{2\pi k d_p}{N}}$, the $N \times PL$ matrix $\mathbf{A}[m]$ given in (38) can be expressed as

$$\mathbf{A}[m] \;=\; \sqrt{\frac{E_s}{PN}}\, s[m]\, \mathbf{B} \;, \tag{4}$$

where the $N \times PL$ matrix $\mathbf{B} = \left[\mathbf{B}^{(0)_N}, \cdots, \mathbf{B}^{(L-1)_N}, \cdots\cdots, \mathbf{B}^{(d_P)_N}, \cdots, \mathbf{B}^{(d_P+L-1)_N}\right]$ does not depend on the transmitted symbol, and $(\cdot)_N$ denotes modulo-N operation. Thus, the received frequency-domain signal vector at the qth antenna can be expressed as

$$\mathbf{Y}^{(q)}[m] \;=\; \sqrt{\frac{E_s}{PN}}\, s[m]\, \mathbf{B}\, \mathbf{h^{(q)}}[m] + \mathbf{V^{(q)}}[m]. \tag{5}$$

Lemma 1: The matrix $\mathbf{B}$ is full rank, only if the following conditions on cyclic delays are satisfied

$$\begin{aligned} 0 \le d_p \le N - L, \qquad & \forall\, p \in \{1, 2, \cdots, P\}; \\ |d_p - d_{p-1}| \;\ge\; L, \qquad & \forall\, p \in \{2, 3, \cdots, P\}. \end{aligned} \tag{6}$$

Proof: If $N - L < d_p < N$ or $|d_p - d_{p-1}| < L$, the columns of $\mathbf{B}$ are no longer unique (independent). As a consequence of the conditions given by (6), the number of transmit antennas must be upper bounded by $P \le \lfloor \frac{N}{L} \rfloor$, where $\lfloor x \rfloor$ denotes the largest integer less than or equal to x.

When the cyclic delays applied for achieving transmit diversity satisfy the conditions of (6), by using the auto-orthogonal property of the complex quadratic spreading sequences, we have $\mathbf{B}^{(k)^H}\mathbf{B}^{(l)} = N\delta_{kl}$, and $\mathbf{B}^H\mathbf{B} = N\, \mathbf{I}_N$, where δ_{kl} is the Kronecker delta function. Thus, $E\left[\,\|\, \mathbf{Y}^{(q)}[m] \,\|^2\right] = E_s + NN_0$.

The channel and AWGN vectors can be separated as shown in (41) for the alternative expression of the received signal vector at the qth antenna. Let the column space (also known as range or signal subspace) and left-null space of matrix $\mathbf{B}$ be denoted as $\mathcal{R}(\mathbf{B})$ and $\mathcal{N}(\mathbf{B}^T)$, respectively. If the conditions of Lemma 1 are satisfied, matrix $\mathbf{B}$ has full rank, i.e., $\dim(\mathcal{R}(\mathbf{B})) = PL$ and $\dim(\mathcal{N}(\mathbf{B}^T)) = N - PL$. For simplicity, let the cyclic delays be

$d_p = (p-1)L$ for $p = 1, 2, \cdots, P$. From (40), the basis of $\mathcal{R}(\mathbf{B})$ and $\mathcal{N}(\mathbf{B}^T)$, respectively, are $\frac{1}{\sqrt{N}} \left\{\mathbf{B}^{(0)}, \mathbf{B}^{(1)}, \cdots, \mathbf{B}^{(PL-1)}\right\}$ and $\frac{1}{\sqrt{N}} \left\{\mathbf{B}^{(PL)}, \mathbf{B}^{(PL+1)}, \cdots, \mathbf{B}^{(N-1)}\right\}$. If $\tilde{\mathbf{Y}}^{(q)}[m]$ is the projection of $\mathbf{Y}^{(q)}[m]$ onto the entire left-null space then

$$\begin{aligned} E\left[\| \tilde{\mathbf{Y}}^{(q)}[m] \|^2\right] &= \frac{1}{N} E\left[\sum_{d=PL}^{N-1} \left|\langle \mathbf{B}^{(d)}, \mathbf{Y}^{(q)}[m]\rangle\right|^2\right] \\ &= \frac{1}{N} \sum_{d=PL}^{N-1} E\left[\left|\mathbf{B}^{(d)H} \mathbf{V}^{(\mathbf{q})}[m]\right|^2\right] \\ &= (N - PL) N_0 \ , \end{aligned} \tag{7}$$

where $\langle \mathbf{x}, \mathbf{y}\rangle = \mathbf{x}^H \mathbf{y}$. Because $N >> PL$, the dimension of $\mathcal{N}(\mathbf{B}^T)$ is large compared to the dimension of the signal subspace, $\mathcal{R}(\mathbf{B})$. Using the Pythagorean theorem, a computationally efficient expression for the AWGN variance is obtained by projecting the received signal vector onto $\mathcal{R}(\mathbf{B})$ as

$$\begin{aligned} N_0 &= \frac{1}{N - PL} E\left[\| \tilde{\mathbf{Y}}^{(q)}[m] \|^2\right] \\ &= \frac{1}{N - PL} E\left[\| \mathbf{Y}^{(q)}[m] \|^2 - \| \mathbf{Y_s}^{(q)}[m] \|^2\right] \\ &= \frac{1}{N - PL} \left(E\left[\| \mathbf{Y}^{(q)}[m] \|^2\right] - \frac{1}{N} \sum_{d=0}^{PL-1} E\left[\left|\mathbf{B}^{(d)H} \mathbf{Y}^{(q)}[m]\right|^2\right]\right), \end{aligned} \tag{8}$$

where $\mathbf{Y_s}^{(q)}[m]$ is the projection of $\mathbf{Y}^{(q)}[m]$ on the entire signal space. Thus, considering empirical averaging over multiple symbols and Q receive antennas, the $\frac{E_c}{N_0}$ estimator becomes

$$\hat{\gamma} = \widehat{\frac{E_c}{N_0}} = \frac{N - PL}{N} \cdot \frac{\sum_{m \in \mathcal{S}} \sum_{q=1}^{Q} \| \mathbf{Y}^{(q)}[m] \|^2}{\sum_{m \in \mathcal{S}} \sum_{q=1}^{Q} \left(\| \mathbf{Y}^{(q)}[m] \|^2 - \frac{1}{N} \sum_{d=0}^{PL-1} \left|\mathbf{B}^{(d)H} \mathbf{Y}^{(q)}[m]\right|^2\right)} - 1 \ , \tag{9}$$

where $\mathcal{S}$ is the set of symbol indexes over which averaging is performed.

The above $\frac{E_c}{N_0}$ estimator for the MC-CDMA-CDD system is more power and bandwidth efficient, and it requires fewer number of computations than the estimators for TDMA systems proposed in [23] and [24]. For the estimators of TDMA system, **B** depends on the training sequence or estimated data symbols. Thus, either a training sequence is required

Table 1. Computational complexity - Blind SNR Estimation

Operation	$\hat{E}[\| \mathbf{Y}^{(q)}[m] \|^2]$	$\hat{E}[\| \mathbf{Y_s}^{(q)}[m] \|^2$
Multiply	$2NQ\|\mathcal{S}\|$	$2PL(2N+1)Q\|\mathcal{S}\|+1$
Add	$2NQ\|\mathcal{S}\|-1$	$PL(3N+1)Q\|\mathcal{S}\|-1$

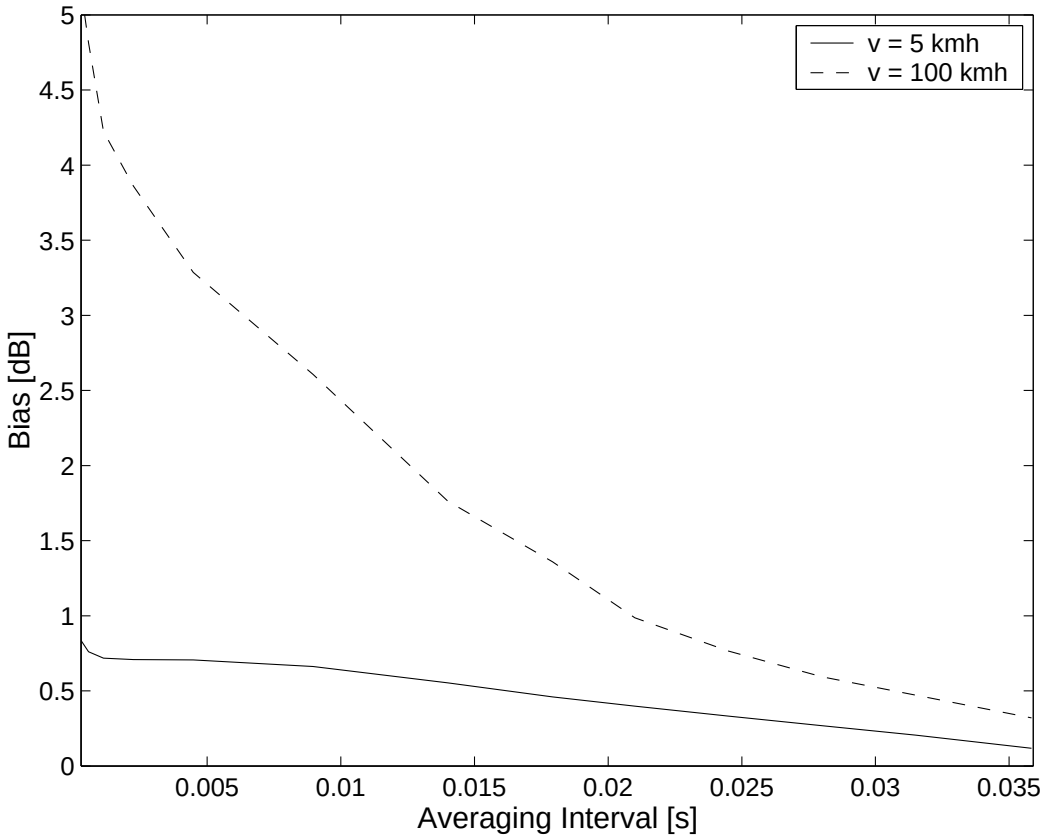

Figure 14. Bias of $\widehat{\frac{E_c}{N_0}}$ for different averaging intervals and mobile speed, $v = 5$ and 100 kmh ($P = 2,\ Q = 2,\ E_s/N_0 = 5$ dB).

or the basis of $\mathcal{R}(\mathbf{B})$ has to be computed every time $\mathbf{B}$ changes according to the symbol decisions. However, for the constant-envelope MC-CDMA-CDD system, $\mathbf{B}$ is constant, and orthonormalization is not required since the columns of $\mathbf{B}$ are orthogonal spreading sequences. Therefore, estimation of $\frac{E_c}{N_0}$ for the constant-envelope MC-CDMA-CDD system is computationally less demanding and the estimation interval can be long enough to achieve very accurate estimates without any loss of power and bandwidth. Table 1 shows the total number of real additions and multiplications required to calculate the sample means $\hat{E}[\| \mathbf{Y}^{(q)}[m] \|^2]$ and $\hat{E}[\| \mathbf{Y}_s^{(q)}[m] \|^2$ are presented.

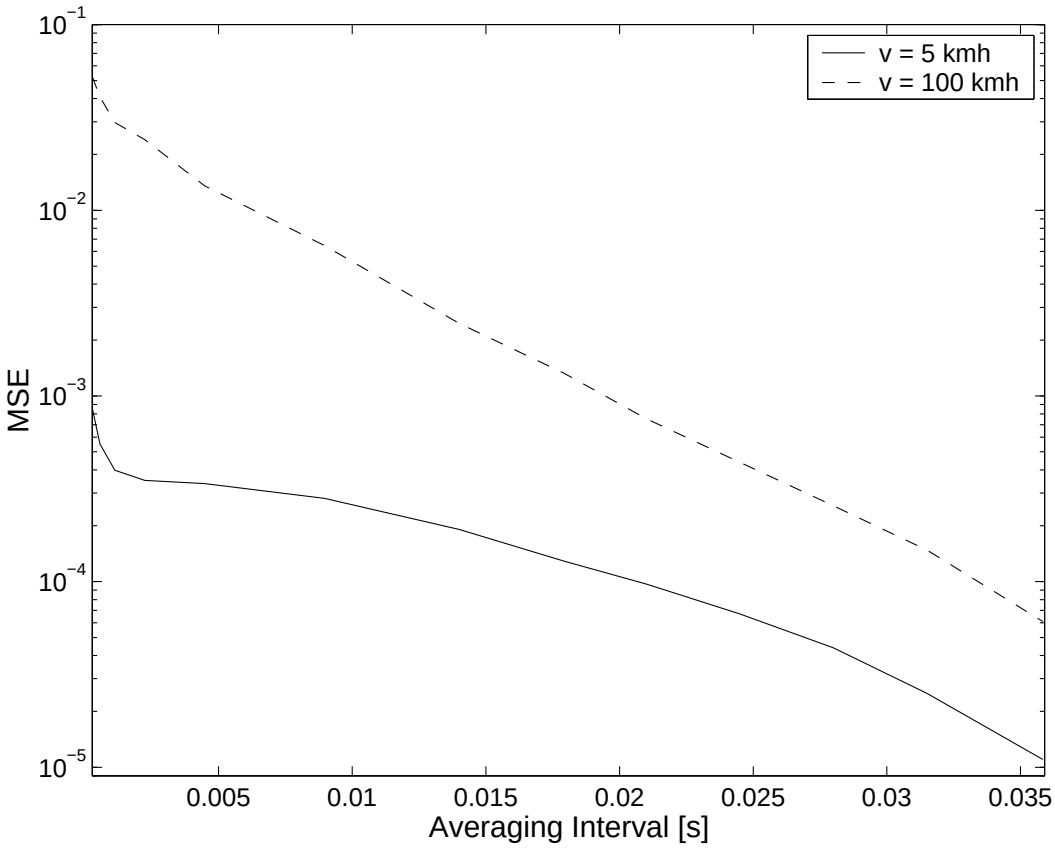

Figure 15. MSE of $\widehat{\frac{E_c}{N_0}}$ for different averaging intervals and mobile speed, $v = 5$ and 100 kmh ($P = 2$, $Q = 2$).

5.5 Numerical Results and Discussions

For all simulation results, we use two transmit antennas. Considering lemma 1, the cyclic delays are selected as $d_p = (p-1)L$ for $p = 1, 2, \cdots, P$. The delay and power profiles of the time-varying multipath-Rayleigh-fading channel are $0, 1, 2$ $[T_c]$ and $0, -3, -6$ [dB], respectively. All transmit and receive antenna pairs have same channel power and delay profiles. The carrier frequency, bandwidth, and number of subcarriers are $f_c = 5$ GHz, $B_f = 2$ MHz, and $N = 32$, respectively. Thus, the sampling period is $T_c = 0.5\mu s$, MC-CDMA symbol period including the guard interval is $T_s = (N+G)T_c = 17.5\mu s$, and Doppler frequency is $f_d = v f_c / c$, where v is the mobile velocity, and $c = 3 \times 10^8$ m/s is the light speed.

Figs. 14, 15, and 16, respectively, show the bias, mean square error (MSE), and variance

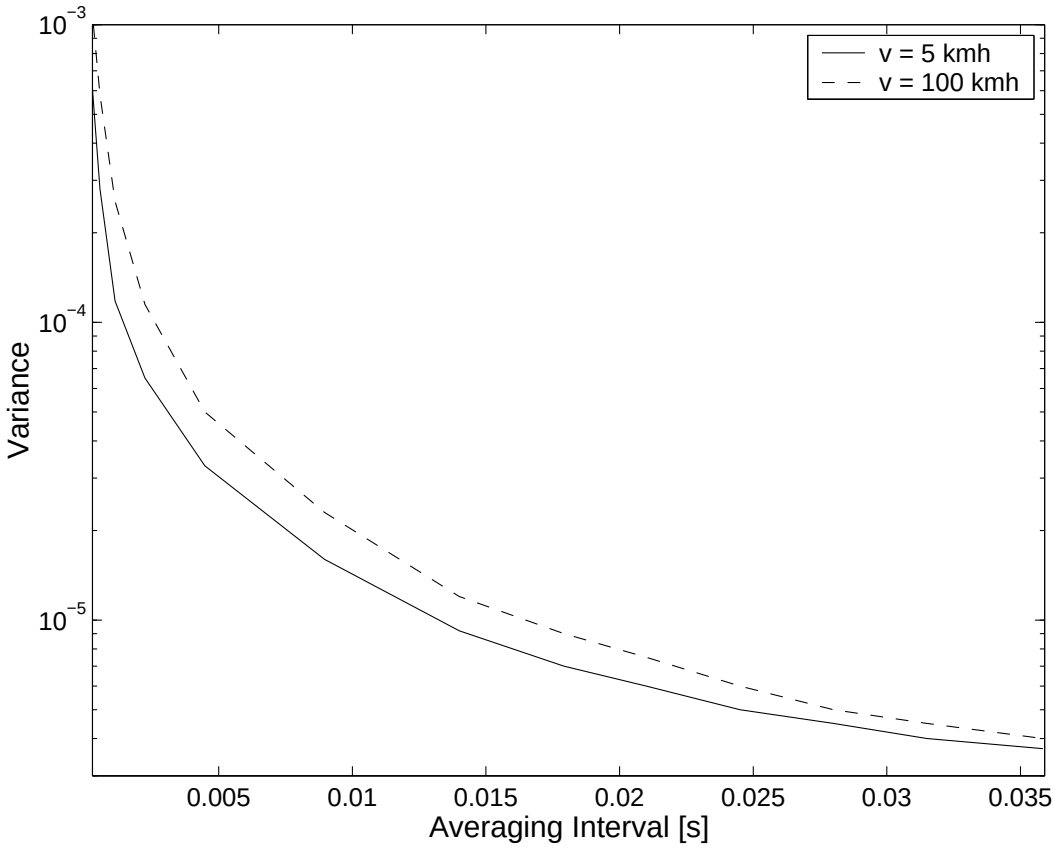

Figure 16. Variance of $\widehat{\frac{E_c}{N_0}}$ for different averaging intervals and mobile speed, $v = 5$ and 100 kmh ($P = 2$, $Q = 2$).

of $\widehat{\frac{E_c}{N_0}}$ for different averaging intervals and mobile velocity, $v = 5$ and 100 kmh when the true $\frac{E_s}{N_0} = 5$ dB at each receive antenna and two receive antennas are used. The averaging interval range is $|\mathcal{S}| = [16, 2048]$ symbols corresponding to $[0.28, 35.8]$ ms. The bias, MSE and variance of the estimate reduces as the averaging interval increases. To achieve a $\frac{E_c}{N_0}$ estimate with average error below 0.5 dB, the estimation interval should be at least 15 and 30 ms when the mobile speed is 5 and 100 kmh, respectively. We define normalized bias, MSE, and variance as follows. Bias $= E\left[\frac{\hat{\gamma}-\gamma}{\gamma}\right]$, MSE $= E\left[\left(\frac{\hat{\gamma}-\gamma}{\gamma}\right)^2\right]$, and variance $= E\left[\left(\frac{\hat{\gamma}-E[\hat{\gamma}]}{\gamma}\right)^2\right]$, where $\gamma = \frac{E_c}{N_0}$ and $\hat{\gamma}$ is expressed by (9). Figs. 17, 18, and 19 illustrate the normalized bias, MSE, and variance of $\widehat{\frac{E_c}{N_0}}$ at different $\frac{E_s}{N_0}$ when the mobile speed is 5 kmh, two transmit and one receive antennas are used. The number of symbols used for averaging is $|\mathcal{S}| = 128$, 512, and 1024.

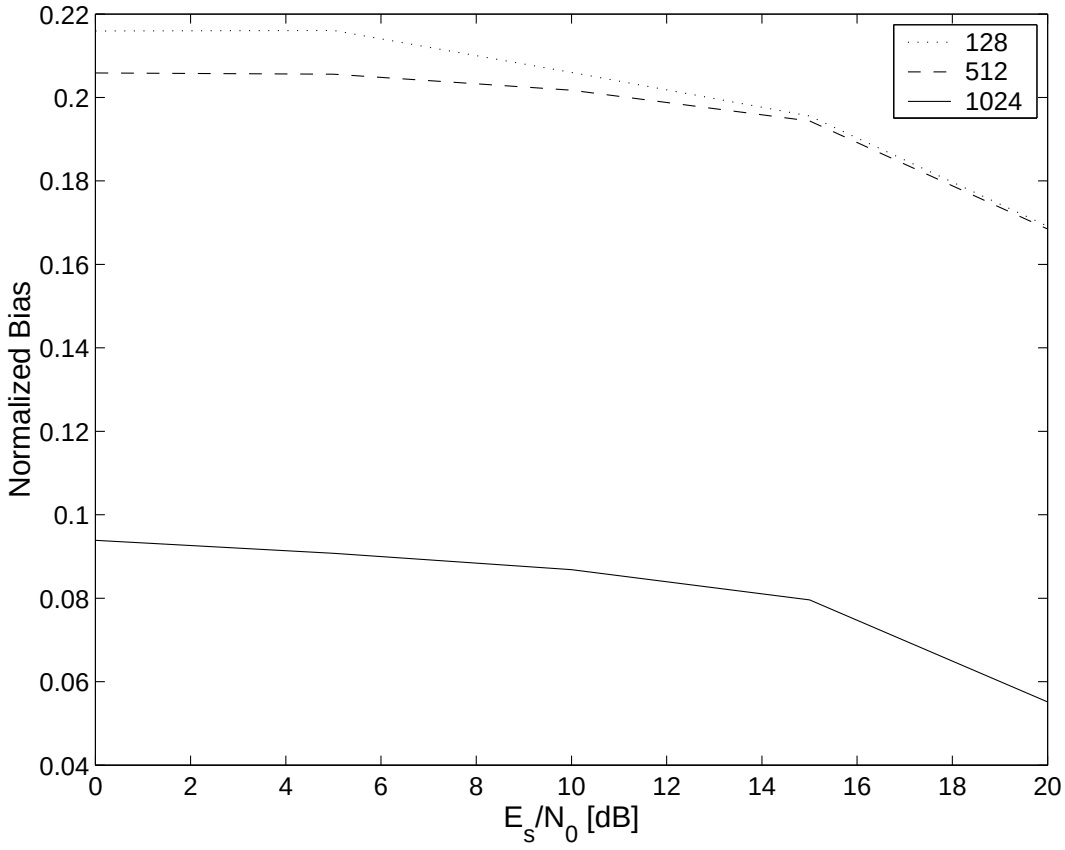

Figure 17. Normalized bias of $\widehat{\frac{E_c}{N_0}}$ for different $\frac{E_s}{N_0}$ and numbers of averaging symbols ($P = 2,\ Q = 1,\ v =$ 5 kmh).

5.6 Summary

We have introduced a signal-space projection-based SNR estimator for the single-user constant-envelope MC-CDMA system with cyclic delay diversity operating under time-varying multipath-fading channel. The proposed SNR estimator does not require training symbols or symbol decisions to operate. Therefore, long estimation intervals can be chosen to achieve high-quality SNR estimates without any power or bandwidth constraint. Numerical results illustrate the impressive performance of the estimator. The normalized bias, MSE, and variance of the estimator do not degrade much even at small E_s/N_0. The estimator can be used for post interference cancelation signal-to-noise-plus-(residual) interference/jamming ratio estimation.

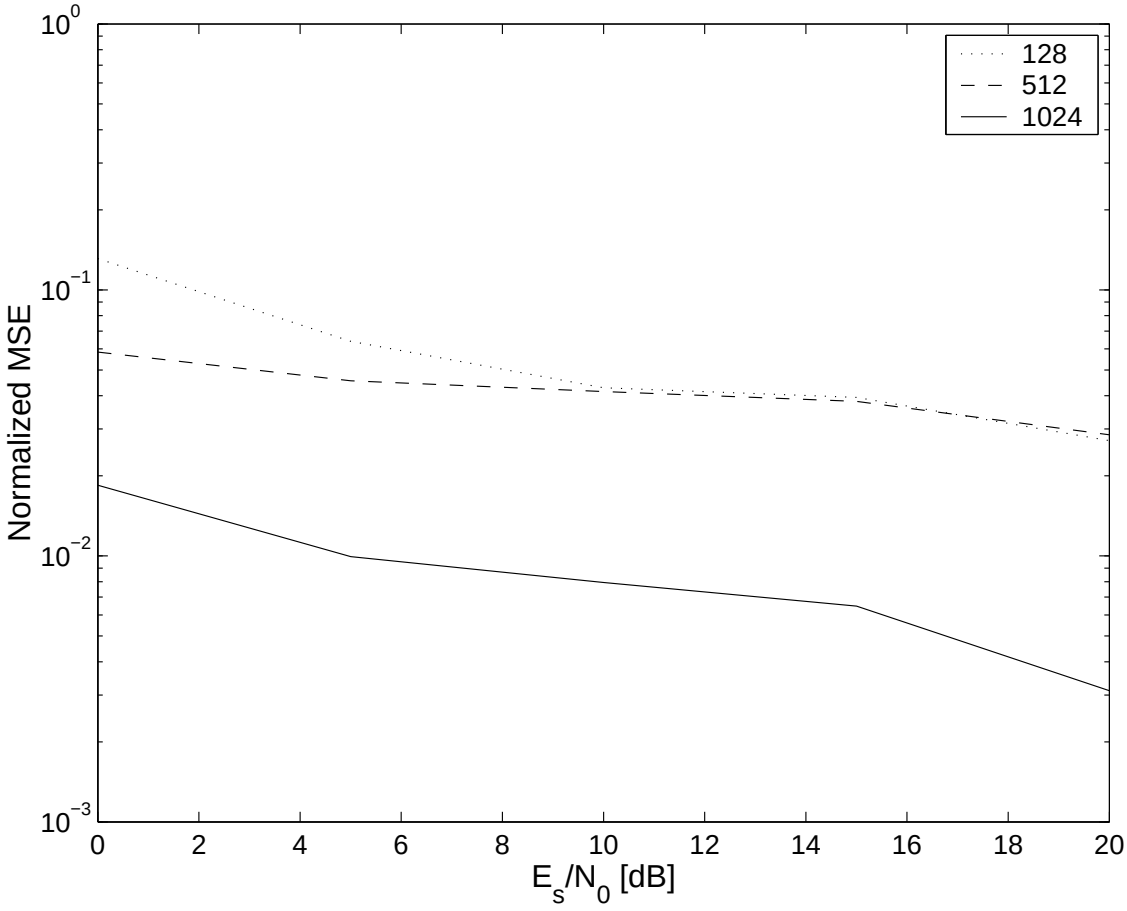

Figure 18. Normalized MSE of $\widehat{\frac{E_c}{N_0}}$ for different $\frac{E_s}{N_0}$ and numbers of averaging symbols ($P = 2$, $Q = 1$, $v = 5$ kmh).

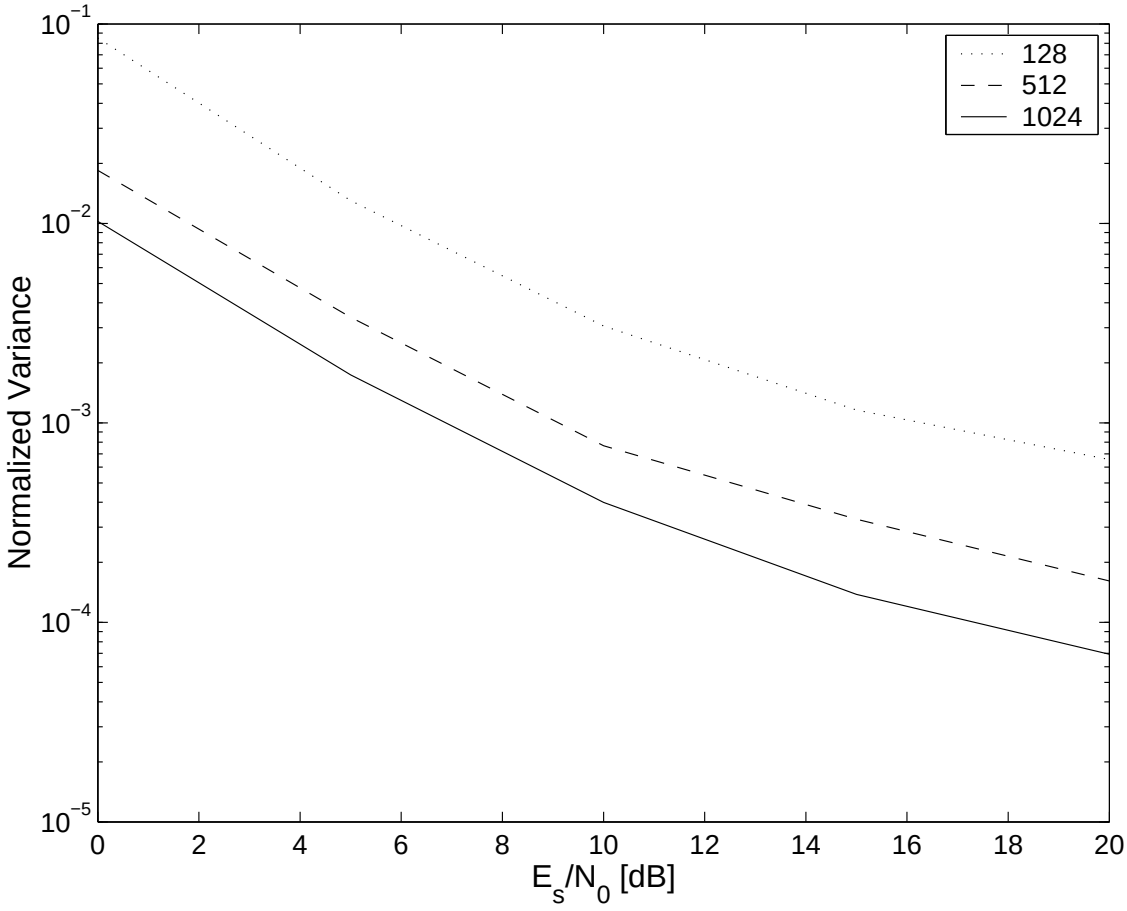

Figure 19. Normalized variance of $\widehat{\frac{E_c}{N_0}}$ for different $\frac{E_s}{N_0}$ and numbers of averaging symbols ($P = 2,\ Q = 1,\ v = 5$ kmh).

CHAPTER 6

SOFT-CHIP-COMBINING CE-MC-CDMA-CDD ANTI-JAM SYSTEMS

6.1 Overview

In an MC-CDMA system, the data symbols are spread in the frequency domain, and the spread signals, also known as chips, are transmitted over the subcarriers. The received frequency-domain signals or chips, associated with each data symbol, must be combined considering the channel's frequency response (if necessary) and noise/jamming statistics of the corresponding sub-channels, in addition to being multiplied by the complex conjugate of the frequency-domain spreading sequence. We refer to this frequency-diversity combining or weighted despreading as *chip combining*.

To achieve our goal of developing a multiuser wireless system that is robust against multipath fading and jamming, so far we have exploited the constant-envelope polyphase spreading sequences and cyclic delay diversity (CDD) at the transmitter side of the considered MC-CDMA system as shown in Chapter 4. In this chapter, we demonstrate that the proposed constant-envelope MC-CDMA-CDD (CE-MC-CDMA-CDD) system facilitates frequency- or time-domain chip combining to mitigate different types of jamming. We focus on developing *iterative receivers* that significantly improves the system performance against different types of jamming. We assume a Rayleigh-flat-fading channel and the channel coefficients are perfectly known at the receiver.

Chip combining with appropriate weights at the despreader can mitigate jamming/ interference in an MC-CDMA system, where each symbol is spread in the frequency domain (FD) and/or time domain (TD). Maximal-ratio combining (MRC) [25] [26] is optimum for unequal Gaussian-noise power on different diversity branches, where each combining weight is inversely proportional to the noise power of the associated diversity branch. For anti-jam MC-CDMA systems that employ chip combining, jammer state information (JSI),

which indicates the presence of a jamming signal in a sub-band or a time-domain chip, is essential for determining the chip-combining weights [28] [27]. Our proposed MC-CDMA-CDD system employs turbo coding. We iteratively estimate and exploit JSI to perform the appropriate chip combining so as to enhance the input signal-to-interference-plus-noise ratio (SINR) to the turbo decoder [29].

For our MC-CDMA system, time and frequency domain JSI estimation, followed by chip combining in the respective domain, is essential for effective suppression of pulse jamming (PJ) and partial-band noise jamming (PBNJ), respectively. After the discrete Fourier transform (DFT) in our MC-CDMA receiver, any PJ signal is converted into a full-band jamming signal, which is similar to AWGN and difficult to suppress. On the other hand, any PBNJ signal is transformed into a continuous PJ signal to be suppressed by time-domain chip combining in our MC-CDMA receiver. Therefore, in this chapter, anti-jam receivers estimating the JSI and using them for chip combining in frequency- and time-domains to suppress partial-band noise jamming (PBNJ) and pulse jamming (PJ), respectively, are studied for the turbo-coded constant-envelope MC-CDMA-CDD system [41]. In other words, we investigate iterative despreading (includes JSI estimation and chip combining using the estimated JSI), demapping, and decoding (IDDD) receivers that include anti-jam processing in both the frequency and time domains. The performance of the IDDD receivers is compared with that of iterative demapping and decoding (IDD) receivers [112], which use only the initial ($i = 0$) JSI estimate to perform chip combining, i.e., the iterative ($i \geq 1$) JSI estimation and chip combining of the IDDD receivers are turned off in the IDD receivers. We also propose a soft-JSI (S-JSI)-based chip-combining technique that outperforms the conventional hard-JSI (H-JSI)-based chip combining by at least 1.75 dB at BER of 10^{-4} under both types of jamming. It is also shown that with perfect channel information and without pilot-assisted *a priori* JSI, iterative despreading, demapping, and decoding (IDDD) has almost similar performance as one-shot despreading followed by iterative demapping and decoding (IDD).

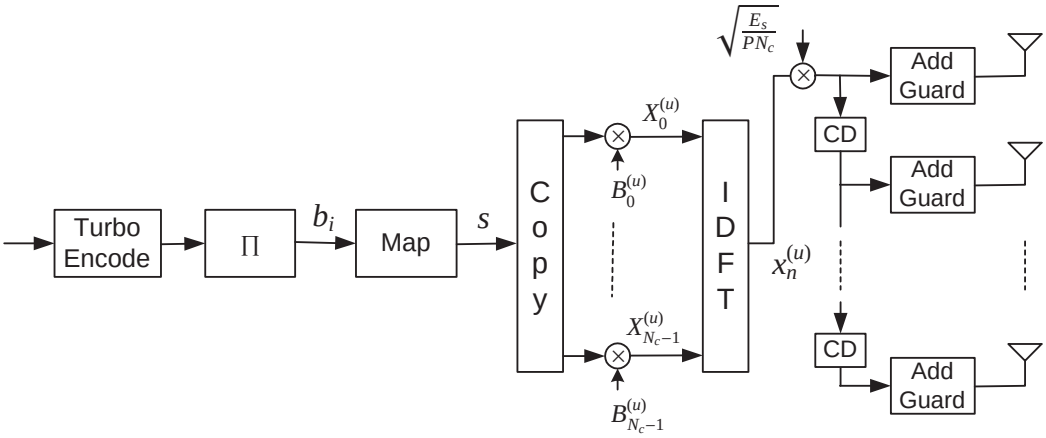

Figure 20. MC-CDMA-CDD transmitter.

The chapter is organized as follows. Section 6.2 describes the transmitter. Section 6.3 illustrates the anti-PBNJ frequency-domain receiver that includes iterative frequency-domain JSI estimation for IDDD, and soft-JSI-based chip combining. The anti-PJ time-domain receiver with iterative time-domain-JSI estimation is presented in Section 6.4. Section 6.5 presents simulation results and Section 6.6 concludes the chapter.

6.2 Transmitter

Fig. 20 shows the turbo-coded and interleaved MC-CDMA-CDD transmitter with $P(\leq N_c)$ transmit antennas, where N_c is the spreading factor. We consider M-ary phase shift keying (MPSK), since the MC-CDMA waveform with MPSK will have a constant envelope in the uplink. Each mapped symbol $s = e^{j\frac{2\pi m}{M}}$, $m \in \{0, 1, \cdots, M-1\}$ is spread by the u-th user's frequency-domain spreading sequence ($\{B_k^{(u)}\}_{k=0}^{N_c-1}$) to generate the frequency-domain signal (normalized by $\sqrt{E_s}$), $X_k^{(u)} = sB_k^{(u)}$, where E_s is the average received symbol energy. The time and frequency-domain complex-quadratic or polyphase spreading sequences [11, 28] considered here are defined as $b_n = e^{-j\frac{\pi}{8}}\, e^{j\frac{\pi n^2}{N_c}}$, $n = 0, 1, \cdots, N_c - 1$ and $B_k = e^{j\frac{\pi}{8}}\, e^{-j\frac{\pi k^2}{N_c}}$, $k = 0, 1, \cdots, N_c - 1$, respectively.

If $\{B_k\} = \{B_k^{(0)}\}$ is the frequency-domain spreading sequence assigned to the desired user ($u = 0$), the frequency-domain spreading sequence [28] for the u-th user is $B_k^{(u)} = e^{-j\frac{2\pi}{N_c}ku}\, B_k$

for $k = 0, 1, \cdots, N_c - 1$. [28] To maintain orthogonality among the signals transmitted from all transmit antennas, the following multiuser spreading code assignment is used [41]

$$u \in \mathcal{U} = \left\{ 0, P, \cdots, \left(\left\lfloor \frac{N_c}{P} \right\rfloor - 1 \right) P \right\} \quad , \tag{10}$$

where $\mathcal{U}$ is the set of multiuser codes indexed by u and $\lfloor c \rfloor$ denotes the largest integer less than or equal to c.

The frequency-domain signal is transformed by an inverse DFT (IDFT) into the time-domain signal, $x_n^{(u)} = \frac{1}{\sqrt{N_c}} \sum_{k=0}^{N_c-1} X_k^{(u)} e^{j2\pi kn/N_c} = sb_n^{(u)}$, $n = 0, \ldots, N_c$. Throughout the chapter, the number of sub-carriers is assumed equal to the spreading factor N_c. Before transmission from the p-th transmit antenna, the sequence $\{x_n^{(u)}\}$ is cyclicly delayed (CD) by pT_c, where $p \in \{0, 1, \cdots, P-1\}$ and T_c is the chip duration. A cyclic prefix (CP) or guard interval of length G is appended [108] to facilitate frequency-domain equalization at the receiver. The guard interval G is greater than or equal to the maximum channel delay spread. The MC-CDMA-CDD system with multiuser code assignment given by (10) always achieves full diversity in flat-fading channel for any number of transmit antennas, $P \leq N_c$ [41].

6.3 Anti-PBNJ Frequency-Domain Receiver

Any partial-band noise jammer (regardless of the value of the jamming fraction, η) becomes a continuous pulse jammer in the time domain with duty factor, $\alpha = 1.0$, because the jamming signal power of the jammed sub-carriers are spread evenly over all time-domain chips. Therefore, frequency-domain JSI estimation and chip combining can be used to effectively suppress a PBNJ signal for jamming fraction range $\eta = (0, 1.0)$. In the case of full-band jamming, where $\eta = 1.0$, equal-gain chip combining is optimal since all the sub-carriers are jammed in this case.

The MC-CDMA-CDD receiver for PBNJ is shown in Fig. 21. The signal received at the q-th antenna ($q = 0, 1, \cdots, Q-1$) corresponding to the n-th time-domain chip ($n =$

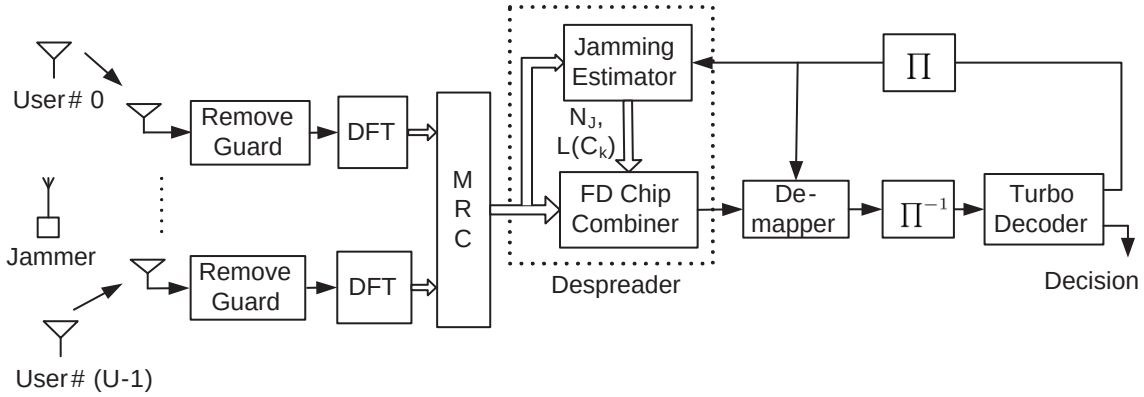

Figure 21. Anti-PBNJ receiver with frequency-domain JSI estimation and chip combining.

$0, 1, \cdots, N_c - 1$) can be expressed as

$$y_n^{(q)} = \sqrt{\frac{E_s}{PN_c}} \sum_{p=0}^{P-1} h^{(0,p,q)}\, x_{(n-p)_{N_c}}^{(0)} + \sqrt{\frac{E_s}{PN_c}} \sum_{u \in \mathcal{U}'} \sum_{p=0}^{P-1} h^{(u,p,q)}\, x_{(n-p)_{N_c}}^{(u)} + j_n^{(q)} + w_n^{(q)} \quad , (11)$$

where $h^{(u,p,q)}$ is the flat-faded channel coefficient between the p-th transmit antenna of u-th user and the q-th receive antenna. The channel coefficients $h^{(u,p,q)}$ are assumed *i.i.d.* complex Gaussian random variables with zero mean and unit variance. The second term on the right side of (11) is the multiuser interference (MUI) contributed by users $u \in \mathcal{U}' = \left\{P, \cdots, \left(\left\lfloor \frac{N_c}{P} \right\rfloor - 1\right) P \right\}$, $j_n^{(q)}$ is the time-domain PBNJ signal at the q-th receive antenna having zero mean and average (over the entire bandwidth) power spectral density (psd) N_J, and $w_n^{(q)}$ is the AWGN having zero mean and variance N_0. For simplicity of analysis, it is assumed that each sub-channel is either jammed completely or not jammed at all. If $H_k^{(u,p,q)} = H^{(u,p,q)} = \frac{1}{\sqrt{N_c}}\, h^{(u,p,q)}$ is the discrete frequency response of the flat-fading channel for $k = 0, \cdots, N_c - 1$, then the received frequency-domain signal after applying DFT at each receive antenna becomes

$$Y_k^{(q)} = \sqrt{\frac{E_s}{P}}\, H_k^{(0,q)} X_k^{(0)} + I_k^{(q)} + C_k J_k^{(q)} + W_k^{(q)} \quad , \qquad (12)$$

where $w_n^{(q)} \xrightarrow{DFT} W_k^{(q)}$, $j_n^{(q)} \xrightarrow{DFT} C_k J_k^{(q)}$, $J_k^{(q)}$ is *i.i.d.* Gaussian jamming signal at the q-th receive antenna with zero mean and variance $\sigma_J^2 = N_J/\eta$, and η is the jamming fraction. The frequency-domain JSI is $C_k = 1$ when the kth subcarrier is jammed and $C_k = 0$ when the kth subcarrier is not jammed. The total number of jammed sub-carriers is $\sum_{k=0}^{N_c-1} C_k$

and jamming fraction is $\eta = \frac{1}{N_c}\sum_{k=0}^{N_c-1} C_k$. It is assumed that jamming signals in different sub-channels are i.i.d. Gaussian random variables with equal variance σ_J^2. The equivalent frequency-domain channel coefficients and DFT of the MUI at the q-th antenna $I_k^{(q)}$, respectively, are defined as $H_k^{(u,q)} = \sum_{p=0}^{P-1} H^{(u,p,q)} e^{-j\frac{2\pi pk}{N_c}}$ and $I_k^{(q)} = \sqrt{\frac{E_s}{P}}\ \sum_{u\in\mathcal{U}'} H_k^{(u,q)} X_k^{(u)}$. After maximal-ratio combining of different receive-antenna signals, the output corresponding to the k-th subcarrier is

$$Y_k \;=\; \sqrt{\frac{E_s}{P}}\, s \sum_{q=0}^{Q-1} \left|H_k^{(0,q)}\right|^2 B_k + I_k + J_k + W_k \ , \tag{13}$$

where s is the transmitted symbol, B_k is the frequency-domain spreading chip corresponding to the k-th subcarrier, and the contributions from MUI, PBNJ, and AWGN, respectively, are $I_k = \sum_{q=0}^{Q-1} H_k^{(0,q)^*} I_k^{(q)}$, $J_k = C_k \sum_{q=0}^{Q-1} H_k^{(0,q)^*} J_k^{(q)}$, and $W_k = \sum_{q=0}^{Q-1} H_k^{(0,q)^*} W_k^{(q)}$. The J_k and W_k are Gaussian distributed with zero mean and their variances are

$$\sigma_{J_k}^2 \;=\; \begin{cases} 0 & ;\ C_k = 0 \\ \frac{N_J}{\eta}\frac{PQ}{N_c} & ;\ C_k = 1 \end{cases} \tag{14}$$

and $\sigma_{W_k}^2 = N_0\frac{PQ}{N_c}$, respectively. Assuming independent channel coefficients, independent interferer symbols with zero mean, and using the central limit theorem, the MUI contribution before despreading I_k can be approximated as Gaussian distributed with zero mean and variance $\sigma_{I_k}^2 = E_c(U-1)\frac{PQ}{N_c}$ [111], where $E_c = E_s/N_c$ is the received chip energy.

After MRC at the despreader, the input signal to the demapper can be expressed as

$$\begin{aligned} \hat{s} \;&=\; \sum_{k=0}^{N_c-1} \rho_k\, B_k^*\, Y_k \\ &=\; \sqrt{\frac{E_s}{P}}\ \sum_{k=0}^{N_c-1} \rho_k \sum_{q=0}^{Q-1} \left|H_k^{(0,q)}\right|^2 s + \tilde{I} + \tilde{J} + \tilde{W} \ , \end{aligned} \tag{15}$$

where the chip-combining weight, ρ_k, is the SINR of the corresponding sub-channel k, $k \in \{0, 1, \cdots, N_c - 1\}$. If the total number of users is U, the weights after scaling can be expressed as

$$\rho_k \;=\; \begin{cases} \gamma_0 \;=\; \frac{E_c Q}{E_c(U-1)+N_0} & ;\ C_k = 0 \\ \gamma_1 \;=\; \frac{E_c Q}{E_c(U-1)+N_J/\eta+N_0} & ;\ C_k = 1 \end{cases} \tag{16}$$

Therefore, the frequency-domain JSI, average jamming psd, and jamming fraction must be estimated before despreading. The contributions from MUI, PBNJ and AWGN at the despreader output are $\tilde{I} = \sum_{k=0}^{N_c-1} \rho_k B_k^* I_k$, $\tilde{J} = \sum_{k=0}^{N_c-1} \rho_k B_k^* J_k$, and $\tilde{W} = \sum_{k=0}^{N_c-1} \rho_k B_k^* W_k$, respectively. The MUI under flat-fading channel and perfect timing assumption is always zero [41] for equal-gain chip combining and the multiuser code assignment given by (10). Given the JSI $\{C_k\}$, weights $\{\rho_k\}$ and channel coefficients $\{H_k^{(0,q)}\}$, and i.i.d. Rayleigh faded channel assumption, the AWGN plus PBNJ variance at the despreader output is

$$\sigma_{\tilde{W}}^2 + \sigma_{\tilde{J}}^2 = \sum_{k=0}^{N_c-1} \rho_k^2 \sum_{q=0}^{Q-1} |H_k^{(0,q)}|^2 \left(N_0 + C_k \frac{N_J}{\eta} \right) \tag{17}$$

The iterative demapper uses the despreader outputs and the previous iteration's extrinsic information from the turbo decoder to generate the log likelihood ratios (LLRs) of the interleaved bits, which are then fed to the turbo decoder [112].

6.3.1 Iterative Frequency-Domain JSI Estimation

The JSI is estimated iteratively by exploiting the soft information or LLRs of the coded bits from the turbo decoder [113,114]. The LLRs from the turbo decoder are interleaved and fed back to the JSI estimator and to the soft demapper [112]. Thus, blockwise despreading (i.e., JSI estimation and chip combining using these JSI estimates for each symbol in the block), demapping, and decoding are performed on the same set of received data. Reliable LLRs from the decoder will enable refined JSI estimates as the iteration among the despreader, demapper and decoder progress. In this chapter, we call this process iterative despreading , demapping, and decoding (IDDD). Depending upon whether the hard or soft values of the JSI estimates are used in the frequency-domain chip combining at the despreader, we will further refer to this process as H-JSI-IDDD or S-JSI-IDDD, respectively.

If $p(\hat{C}_k = c)$, $c \in \{0, 1\}$ is the *a posteriori* probability of the frequency-domain JSI, C_k,

corresponding to the k-th subcarrier, then

$$\begin{aligned} p(\hat{C}_k = c) &\triangleq P\left(C_k = c \mid Y_k, \{H_k^{(0,q)}\}_{q=0}^{Q-1}\right) \\ &\propto \sum_{s\in\mathcal{S}} P\left(Y_k \mid s, C_k = c, \{H_k^{(0,q)}\}_{q=0}^{Q-1}\right) p(s)p(C_k = c) \ , \end{aligned} \tag{18}$$

where $\mathcal{S}$ denotes the set of all possible decoded symbols, the symbol probability $p(s) = \prod_{i=0}^{\log_2 M-1} P(b_i)$ is calculated using the LLR of the bits from the turbo decoder, and $\{b_{(\log_2 M-1)}, \cdots, b_0\}$ are the coded and interleaved bits associated with the symbol s. Because of bit interleaving after error-correction coding, the bits corresponding to any symbol can be handled independently from each other. Then the LLR of the JSI at i-th IDDD iteration, $i = 1, 2, \ldots,$ can be derived as

$$\begin{aligned} L(\hat{C}_k^{(i)}) &= \log\left[\frac{p(\hat{C}_k^{(i)} = 1)}{p(\hat{C}_k^{(i)} = 0)}\right] \\ &= \log\left[\frac{\sum_{s\in\mathcal{S}} P\left(Y_k \mid s, C_k = 1, \{H_k^{(0,q)}\}_{q=0}^{Q-1}\right) p(s^{(i-1)})}{\sum_{s\in\mathcal{S}} P\left(Y_k | s, C_k = 0, \{H_k^{(0,q)}\}_{q=0}^{Q-1}\right) p(s^{(i-1)})}\right] + L(\hat{C}_k^{(i-1)}) \end{aligned} \tag{19}$$

In the derivation of (19), $p(C_k = c)$ and $p(s)$ in (18) are replaced by the *a posteriori* probability of the frequency-domain JSI $p(\hat{C}_k^{(i-1)} = c)$ and decoded symbol probability $p(s^{(i-1)})$, respectively, that are obtained from the previous $(i-1)$-th IDDD iteration. The conditional probability of the received signal $P\left(Y_k|s, C_k = c, \{H_k^{(0,q)}\}_{q=0}^{Q-1}\right)$ has a Gaussian distribution with variance

$$\sigma_c^2 = \sum_{q=0}^{Q-1} |H_k^{(0,q)}|^2 \begin{cases} N_0 + E_c(U-1) & ; \ c = 0 \\ N_0 + E_c(U-1) + \hat{\sigma}_J^{2(i)} & ; \ c = 1 \end{cases} , \tag{20}$$

where the estimates of the jamming fraction and jamming signal variance used in the i-th IDDD iteration are $\hat{\eta}^{(i)} = \frac{1}{N_c}\sum_{k=0}^{N_c-1} \hat{C}_k^{(i-1)}$ and $\hat{\sigma}_J^{2(i)} = \hat{N}_J/\hat{\eta}^{(i)}$, respectively, and $\hat{N}_J$ is calculated from the sample variance of Y_k. For the initial iteration, $\hat{\sigma}_J^{2(1)} = \hat{N}_J$ is used. The hard-JSI estimates at the end of i-th IDDD iteration are obtained as $\hat{C}_k^{(i)} = 0$, if $L(\hat{C}_k^{(i)}) < 0$, and $\hat{C}_k^{(i)} = 1$, if $L(\hat{C}_k^{(i)}) > 0$.

6.3.2 Soft-JSI-Based Chip Combining

The calculation of the optimum chip-combining weights involves inversion of the noise plus interference covariance matrix of dimension N_c, which is computationally demanding [115]. However, suboptimal combining requires only the noise and interference power.

While conventional hard JSI (C_k) reveals the presence of a jamming signal in a particular subchannel, the soft JSI (LLR, $L(C_k)$) bears the same information with additional reliability information, which depends on the dominant jamming signal and MUI before despreading. In the presence of perfect JSI (ideal case), the hard values of JSI $C_k \in \{0, 1\}$ are used to determine the weights for MRC of the chips on the different subcarriers as shown in (15) and (16). With hard-JSI-IDDD (and also in hard-JSI-based despreading before IDD), the hard-JSI estimates, $\hat{C}_k^{(i)} \in \{0, 1\}$, are used to calculate the chip-combining weights at the i-th IDDD iteration as

$$\rho_k^{(i)} = \begin{cases} \gamma_0 = \frac{E_c Q}{E_c(U-1)+N_0} & , \ \hat{C}_k^{(i)} = 0 \\ \hat{\gamma}_1^{(i)} = \frac{E_c Q}{E_c(U-1)+\hat{\sigma}_J^{2(i)}+N_0} & , \ \hat{C}_k^{(i)} = 1 \end{cases} , \tag{21}$$

where $\hat{\gamma}_1^{(i)}$ and $\hat{C}_k^{(i)} \in \{0, 1\}$ are the SINR and hard-JSI estimates at the i-th ($i = 1, 2, \cdots$) IDDD iteration. The estimated LLRs given by (19) are noisy. Hence, the use of soft-JSI estimates in the despreader will yield better performance. In this chapter, we propose a simple scheme using the soft-JSI estimates to calculate the chip-combining weights by using the probabilities of the random JSI, C_k, as follows:

$$\begin{aligned} \rho_k^{(i)} &= \gamma_0 \, p(\hat{C}_k^{(i)} = 0) + \hat{\gamma}_1^{(i)} \, p(\hat{C}_k^{(i)} = 1) \\ &= \frac{E_c Q}{E_c(U-1)+N_0} \cdot \frac{1}{1+e^{L(\hat{C}_k^{(i)})}} + \frac{E_c Q}{E_c(U-1)+\hat{\sigma}_J^{2(i)}+N_0} \cdot \frac{1}{1+e^{-L(\hat{C}_k^{(i)})}} , \end{aligned} \tag{22}$$

where $\gamma_0 = \frac{E_c Q}{E_c(U-1)+N_0}$ and $\gamma_1 = \frac{E_c Q}{E_c(U-1)+\sigma_J^2+N_0}$ are the ideal SINR in the absence and presence of PBNJ, respectively. The soft-JSI-based combining weights are then used for iterative chip combining and despreading as

$$\hat{s}^{(i)} = \sum_{k=0}^{N_c-1} \rho_k^{(i)} \, B_k^* \, Y_k , \tag{23}$$

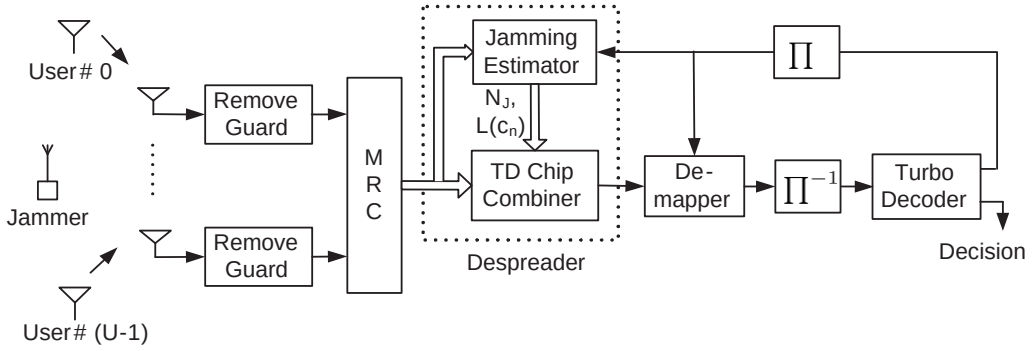

Figure 22. Anti-PJ receiver with time-domain JSI estimation and chip combining.

where $\hat{s}^{(i)}$ is the despreader (chip combiner) output at the *i*-th IDDD iteration. Throughout the thesis, we refer to this type of soft-JSI-based chip combining as *soft-chip combining*. For soft-chip combining despreading, the variance of the AWGN plus PBNJ contributions at the despreader output is calculated as

$$\sigma_{\tilde{W}}^{2(i)} + \sigma_{\tilde{J}}^{2(i)} = \sum_{k=0}^{N_c-1} \rho_k^2 \sum_{q=0}^{Q-1} |H_k^{(0,q)}|^2 \left[N_0 . \frac{1}{1 + e^{L(\hat{C}_k^{(i)})}} + (N_0 + \hat{\sigma}_J^{2(i)}) . \frac{1}{1 + e^{-L(\hat{C}_k^{(i)})}} \right] \quad (24)$$

6.4 Anti-PJ Time-Domain Receiver

With pulse jamming (PJ), the jammer intermittently jams the entire desired signal bandwidth [27]. If the average jamming power is P_J over the signal bandwidth W, the power spectral density of the jamming signal is $N_J = P_J/W$. At any time instant, the jamming pulse is present with probability α and with power P_J/α, where α is called the duty cycle [27]. If the frequency-domain receiver of Fig. 21 is used, the DFT operation at the receiver maintains the wide-band PJ signal as a full-band jamming (FBJ) signal. Therefore, time-domain-JSI estimation and chip combining is necessary for effective suppression of PJ signals. In the following, we show that the MC-CDMA-CDD receiver can be easily configured to facilitate time-domain JSI estimation and chip combining. The anti-PJ receiver is shown in Fig. 22.

The received time-domain signal at the q-th antenna ($q = 0, 1, \cdots, Q-1$) corresponding to the n-th chip ($n = 0, 1, \cdots, N_C - 1$) of a symbol is

$$\begin{aligned} y_n^{(q)} &= \sqrt{\frac{E_s}{PN_c}} \sum_{p=0}^{P-1} h^{(0,p,q)}\, x^{(0)}_{(n-p)_{N_c}} + \sqrt{\frac{E_s}{PN_c}} \sum_{u \in \mathcal{U}'} \sum_{p=0}^{P-1} h^{(u,p,q)} x^{(u)}_{(n-p)_{N_c}} + c_n j_n^{(q)} + w_n^{(q)} \\ &= \sqrt{\frac{E_s}{PN_c}} h_n^{(0,q)} s + i_n^{(q)} + c_n j_n^{(q)} + w_n^{(q)} \ , \end{aligned} \tag{25}$$

where $h^{(u,p,q)}$ is the Rayleigh-flat-fading channel between the p-th transmit antenna of u-th user and the q-th receive antenna. The channel coefficients, $h^{(u,p,q)}$ are assumed independent complex Gaussian random variables with zero mean and unit variance. The second term on the right side of (25) is the MUI, $j_n^{(q)}$ is the time-domain PJ signal at the q-th receive antenna having i.i.d. white Gaussian distribution with zero mean and psd, $\sigma_J^2 = N_J/\alpha$, and $w_n^{(q)}$ is the AWGN having zero mean and variance, N_0. For simplicity of analysis, it is assumed that each time-domain chip is either completely jammed or not jammed at all. Hence, the pulse JSI, $c_n = 1$, if the n-th chip is jammed, and $c_n = 0$, if it is not jammed. The equivalent channel plus spreading code is combined into a single coefficient as

$$h_n^{(0,q)} = \sum_{p=0}^{P-1} h^{(0,p,q)} b_{(n-p)_{N_c}} \tag{26}$$

After MRC of the signals from different receive antennas

$$\begin{aligned} y_n &= \sum_{q=0}^{Q-1} h_n^{(0,q)^*} y_n^{(q)} \\ &= \sqrt{\frac{E_s}{PN_c}} \sum_{q=0}^{Q-1} \left| h_n^{(0,q)} \right|^2 s + i_n + c_n j_n + w_n \ , \end{aligned} \tag{27}$$

where MUI, PJ and AWGN contributions are $i_n = \sum_{q=0}^{Q-1} h_n^{(0,q)^*} i_n^{(q)}$, $j_n = \sum_{q=0}^{Q-1} h_n^{(0,q)^*} j_n^{(q)}$, and $w_n = \sum_{q=0}^{Q-1} h_n^{(0,q)^*} w_n^{(q)}$, respectively. Differing from the frequency-domain receiver described for PBNJ, the above MRC eliminates the phase shift due to the spreading code along with the phase shift due to the equivalent channel. The SINR varies on the different time-domain chips depending upon whether each chip is jammed or not. Using MRC to combine the

chips corresponding to each data symbol, the chip combiner output becomes

$$\begin{aligned}\hat{s} &= \sum_{n=0}^{N_C-1} \rho_n y_n \\ &= \sqrt{\frac{E_s}{PN_c}} \sum_{n=0}^{N_C-1} \rho_n \sum_{q=0}^{Q-1} \left|h_n^{(0,q)}\right|^2 s + \tilde{i} + \tilde{j} + \tilde{w} \ , \end{aligned} \tag{28}$$

where MUI, PJ and AWGN contributions, respectively, are $\tilde{i} = \sum_{n=0}^{N_C-1} \rho_n i_n$, $\tilde{j} = \sum_{n=0}^{N_C-1} \rho_n c_n j_n$ and $\tilde{w} = \sum_{n=0}^{N_C-1} \rho_n w_n$ with time-domain JSI, $c_n \in \{0, 1\}$. In order to maximize the SINR at the combiner output, the time-domain combining weight corresponding to the n-th chip is

$$\rho_n = \begin{cases} \gamma_0 = \frac{E_c Q}{E_c(U-1)+N_0} & , \ c_n = 0 \\ \gamma_1 = \frac{E_c Q}{E_c(U-1)+N_J/\alpha+N_0} & , \ c_n = 1 \end{cases} \tag{29}$$

6.4.1 Iterative Time-Domain JSI Estimation

The time-domain JSI, c_n ($n = 0, 1, \cdots, N_C - 1$), is estimated iteratively by using the LLR from the pervious IDDD iteration of the turbo decoder [113]. Like the PBNJ case, depending on whether the hard or soft values of time-domain JSI are used for calculating the chip-combining weights at the despreader, we will refer to the process as H-JSI-IDDD or S-JSI-IDDD, respectively.

Let us define the *a posteriori* probability of the time-domain JSI, $c_n = c, \ c \in \{0, 1\}$ as

$$\begin{aligned} p(\hat{c}_n = c) &\triangleq P\left(c_n = c \mid y_n, \{h_n^{(0,q)}\}_{q=0}^{Q-1}\right) \\ &\propto \sum_{s \in \mathcal{S}} P\left(y_n \mid s, c_n = c, \{h_n^{(0,q)}\}_{q=0}^{Q-1}\right) p(s) \ p(c_n = c) \ , \end{aligned} \tag{30}$$

where the symbol probability $p(s)$ is calculated from the LLR of the coded bits from the turbo decoder and the conditional probability

$$P\left(y_n \mid s, c_n = c, \{h_n^{(0,q)}\}_{q=0}^{Q-1}\right) = \frac{1}{\pi\sigma_c^2} \exp\left(- \frac{\left| y_n - \sqrt{\frac{E_s}{PN_C}} \sum_{q=0}^{Q-1} |h_n^{(0,q)}|^2 \ s \right|^2}{\sigma_c^2} \right) \tag{31}$$

Assuming that the MUI, AWGN and PJ signal are independent from each other, the variance of y_n with known channel coefficients is equal to

$$\sigma_c^2 = \sum_{q=0}^{Q-1} |h_n^{(0,q)}|^2 \begin{cases} E_c(U-1) + N_0 & ; \quad c = 0 \\ E_c(U-1) + N_0 + N_J/\alpha & ; \quad c = 1 \end{cases} \tag{32}$$

Finally, the LLR of the time-domain JSI, c_n, at the end of i-th IDDD iteration is obtained as

$$\begin{aligned} L(\hat{c}_n^{(i)}) &= \log\left[\frac{p(\hat{c}_n^{(i)}=1)}{p(\hat{c}_n^{(i)}=0)}\right] \\ &= \log\left[\frac{\sum_{s\in\mathcal{S}} P\left(y_n \mid s, c_n=1, \{h_n^{(0,q)}\}_{q=0}^{Q-1}\right) p(s^{(i-1)})}{\sum_{s\in\mathcal{S}} P\left(y_n | s, c_n=0, \{h_n^{(0,q)}\}_{q=0}^{Q-1}\right) p(s^{(i-1)})}\right] + L(\hat{c}_n^{(i-1)}) \ , \end{aligned} \tag{33}$$

where $p(s^{(i-1)})$ is the symbol probability calculated using the LLR from the turbo decoder and $L(\hat{c}_n^{(i-1)})$ is the LLR of JSI estimated in the previous iteration. For the initial chip combining in IDDD (also in the only hard-/soft-JSI-based chip combining before IDD), we assume that $L(\hat{c}_n^{(0)}) = 0$ and all symbols are equally likely ($p(s) = 1/M$) yielding the LLR of the time-domain JSI as

$$L(\hat{c}_n^{(1)}) = \log\left[\frac{\sum_{s\in\mathcal{S}} P\left(y_n \mid s, c_n=1, \{h_n^{(0,q)}\}_{q=0}^{Q-1}\right)}{\sum_{s\in\mathcal{S}} P\left(y_n | s, c_n=0, \{h_n^{(0,q)}\}_{q=0}^{Q-1}\right)}\right]. \tag{34}$$

In order to calculate the variance of the PJ signal, we assume that the desired signal, MUI, PJ and AWGN contributions in y_n are independent random variables with zero mean. Then the variance of y_n can be calculated as $\sigma_{y_n}^2 = PQ\{E_c(Q+1) + E_c(U-1) + N_J + N_0\}$. Therefore, using the method of moments, the average jamming signal variance can be estimated from the sample variance $\hat{\sigma}_{y_n}^2 = \frac{1}{N_C-1}\sum_{n=0}^{N_C-1} \left|y_n - m_{y_n}\right|^2$ as

$$\hat{N}_J = \frac{\hat{\sigma}_{y_n}^2}{PQ} - E_c(Q+U) - N_0 \ , \tag{35}$$

where m_{y_n} is the sample average of y_n. Because the duty factor estimate is not available in the initial JSI estimate with IDDD ($i = 1$) or with JSI estimation before IDD, this value of

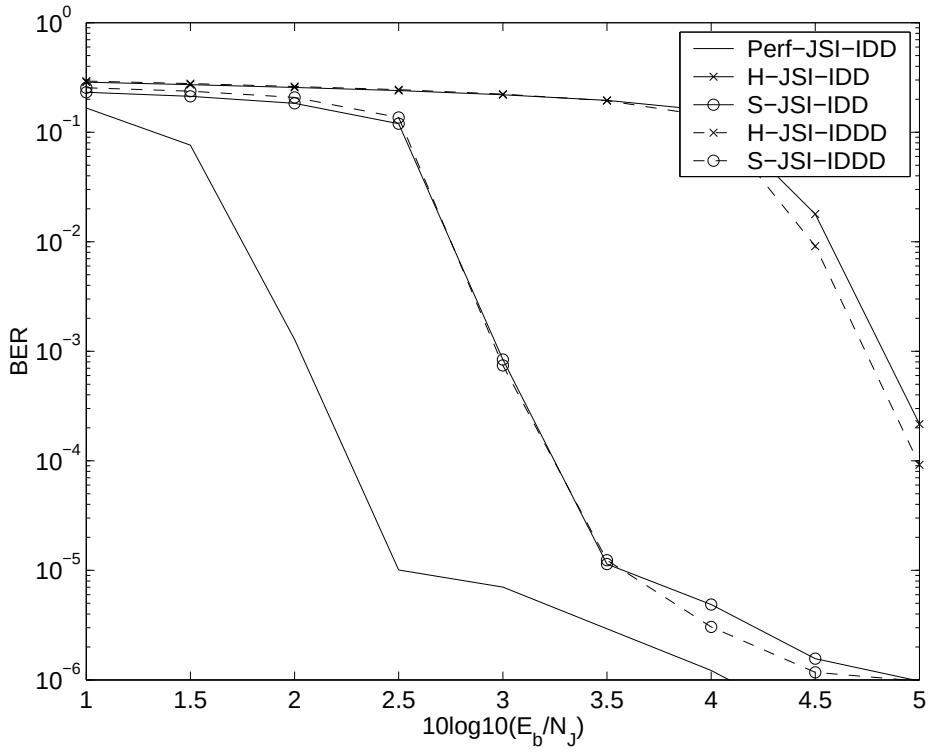

Figure 23. BER for different receiver schemes under the worst case PBNJ (η = 1.0, 4x4 iterations, E_b/N_0=20dB, P = 4, Q = 1). Soft-JSI-based chip combining improves the performance in both IDD and IDDD. IDDD has slightly better performance than IDD. [Perf/H/S-JSI: Perfect/hard/soft jammer state information, IDD: Iterative demapping and decoding, IDDD: Iterative despreading, demapping, and decoding]

$\hat{N}_J$ is used instead of $\sigma_J^2 = N_J/\alpha$ in (32) to calculate the conditional probabilities in (31) and, thus, $L(\hat{c}_n^{(1)})$ in (34). In subsequent IDDD iterations ($i \geq 2$), the estimate of the duty factor $\hat{\alpha}^{(i)} = \frac{1}{N_c}\sum_{n=0}^{N_c-1}\hat{c}_n^{(i-1)}$ is used to calculate the jamming signal variance as $\hat{\sigma}_J^2 = \hat{N}_J/\hat{\alpha}^{(i)}$.

6.4.2 Soft-JSI-Based Chip Combining

In 6.3.2, the frequency-domain soft-JSI-based weight calculation and chip combining were described in the context of PBNJ. In the presence of PJ, the same technique can be applied for time-domain soft-JSI-based ($L(\hat{c}_n^{(i)})$) chip combining.

6.5 Numerical Results and Discussions

Information bits are turbo coded before modulation, spreading and the application of cyclic delay diversity. The code polynomials used for the 16-state component encoders are G_1 =

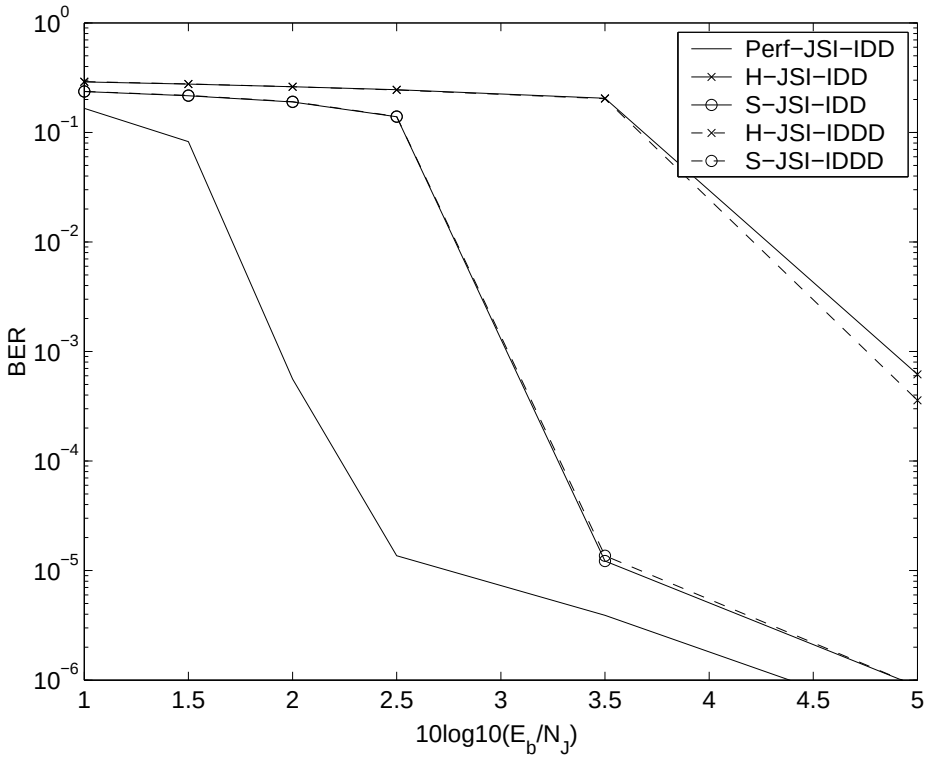

Figure 24. BER for different receiver schemes under the worst case PJ ($\alpha = 1.0$, 4x4 iterations, E_b/N_0=20 dB, $P = 4$, $Q = 1$). Soft-JSI-based combining yields much better performance than hard-JSI-based combining. [Perf/H/S-JSI: Perfect/hard/soft jammer state information, IDD: Iterative demapping and decoding, IDDD: Iterative despreading, demapping, and decoding]

21 and $G_2 = 37$, each having constraint length five. In all simulations, code blocks of 2048 bits, code rate of $R = 1/2$, QPSK modulation, four transmit antennas, and $N_c = 32$ subcarriers are used on a Rayleigh-flat-fading channel. Assuming jamming is dominant, the signal to AWGN power ratio is set at $E_b/N_0 = 20$ dB. In each IDD or IDDD iteration, four turbo iterations are performed to obtain reliable LLR from the turbo decoder.

Fig. 23 shows the BER for different signal energy-to-jamming power spectral density ratios (SJR=E_b/N_J) for different anti-jam receiver schemes with four transmit and one receive antenna under the worst case PBNJ. Compared to conventional hard-JSI-based chip combining, the soft-JSI-based chip combining improves the performance in both the IDD and IDDD cases by at least 1.75 dB at BER of 10^{-4}. On the other hand, iterative despreading with IDDD improves the performance only marginally compared with IDD.

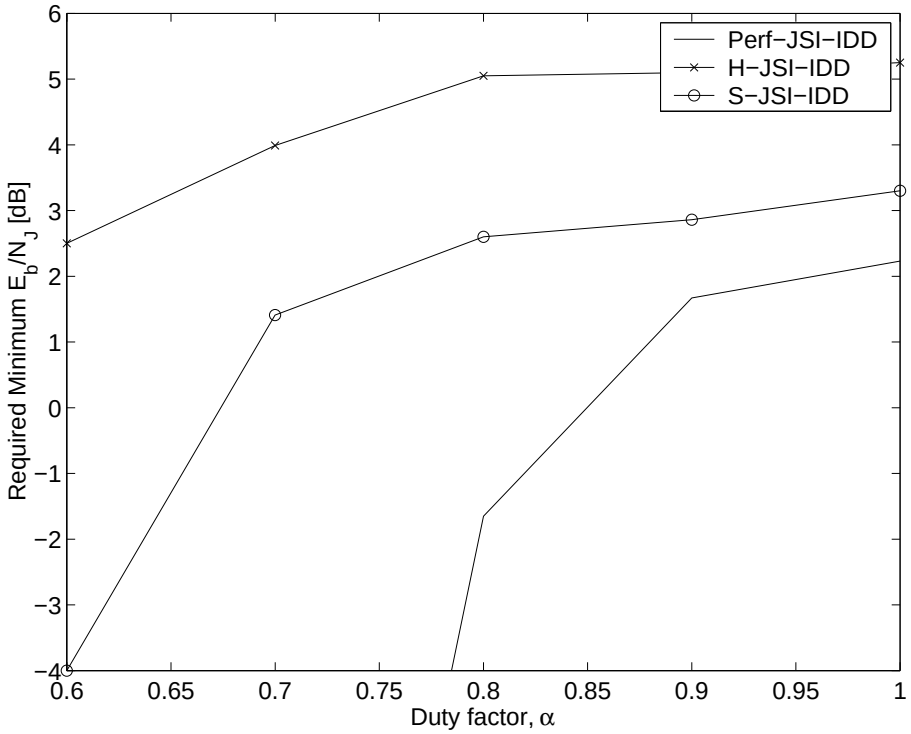

Figure 25. Comparison between hard-JSI and soft-JSI-based chip combining with IDD: Required E_b/N_J to guarantee BER of 10^{-4} under PJ with different duty factors (4x4 iterations, E_b/N_0=20 dB, $P = 4$, $Q = 1$) [Perf/H/S-JSI: Perfect/hard/soft jammer state information, IDD: Iterative demapping and decoding].

Fig. 24, shows the BER vs. SJR=E_b/N_J performance under the worst case pulse jamming ($\alpha = 1.0$) for non-iterative hard- and soft-JSI-based (given by (34)) chip combining followed by IDD, and for iterative hard- and soft-JSI-based (given by (33)) chip combining used in IDDD. For the worst case continuous pulse jamming ($\alpha = 1.0$), the performance gains of soft-JSI-based combining over the hard-JSI-based combining are 1.7 and 2.0 dB at BER of 10^{-3} and 10^{-4}, respectively. This is because the soft-JSI-based chip combining always provides more improved SINR at the input to the turbo decoder [29] after demapping than the hard-JSI-based chip combining does.

Use of pilot aided JSI estimates as *a priori* information is the most efficient way to iteratively detect the presence of interference when the interference pattern over sub-carriers or time-domain chips is constant between two consecutive pilot symbols. This has been pointed out in interference suppression (from the FM band) with OFDM digital audio

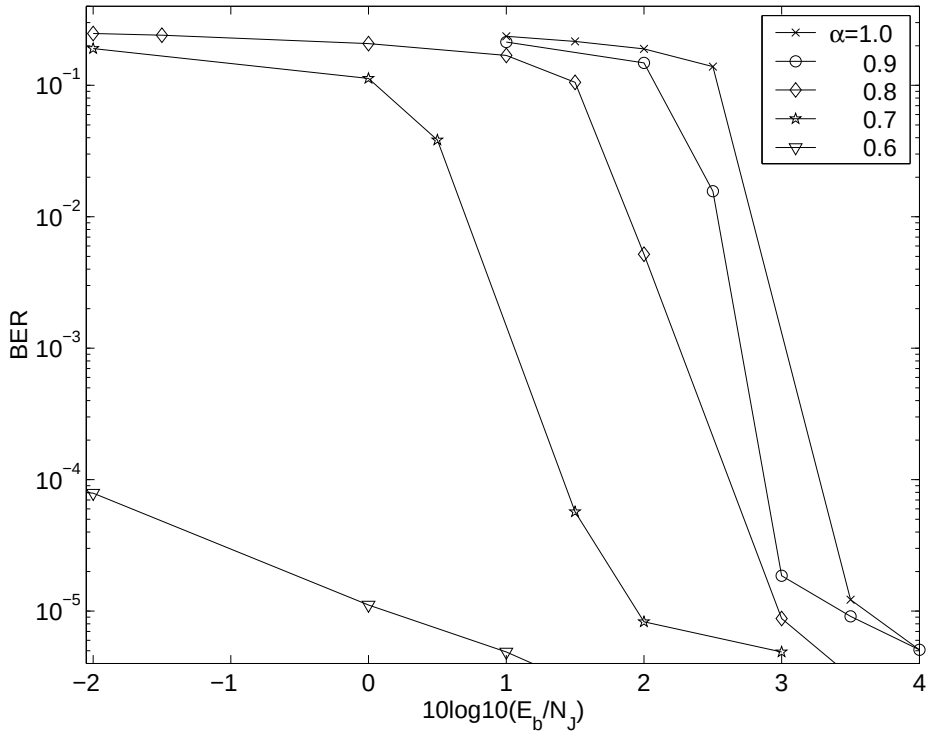

Figure 26. BER vs. E_b/N_J for soft-JSI-based IDD receivers under pulse jamming with different duty factors (4x4 iterations, E_b/N_0=20 dB, $P = 4$, $Q = 1$).

broadcasting [116]. Since the jamming pattern can randomly change from symbol to symbol, the pilot aided JSI estimates can not be used as *a priori* information during the chip combining of data symbols. Because the JSI used in both IDD and every IDDD iteration is estimated under the same instantaneous jamming signal, AWGN, and MUI present in the data symbols, iterative estimation of JSI does not reap any significant new information in the subsequent IDDD iterations. Thus, the performance of IDDD does not improve much over the IDDD iterations, yielding similar performance as IDD. Hence, soft-JSI-IDD receiver is a better option to combat jamming than soft-JSI-IDDD because of the increased complexity of the IDDD receivers. In order to illustrate the superiority of soft-JSI-IDD over hard-JSI-IDD, Fig. 25 shows the required minimum E_b/N_J to guarantee the BER $\leq 10^{-4}$ under PJ for different values of the duty factor. The performance gain of the soft-JSI-IDD over hard-JSI-IDD increases as the duty factor decreases. Fig. 26 shows the BER vs. E_b/N_J performance of the soft-JSI-IDD receiver under PJ with different values of the duty cycle.

6.6 Summary

In this chapter, we have demonstrated that the proposed receivers for the constant-envelope MC-CDMA system using cyclic delay diversity are indeed capable of estimating the JSI and combining the chips in both the frequency and time domains for effective mitigation of PBNJ and PJ, respectively. This configurability makes the receiver more robust against different types of jamming. A simple but elegant soft-JSI-based weight calculation method for chip combining is proposed that enhances the SINR at the despreader output and outperforms the conventional hard-JSI-based chip combining under both PBNJ and PJ. The soft-JSI-based chip-combining method can be applied to any MC-CDMA or OFDM system under jamming or interference from other systems having unequal power. Also, iterative JSI estimators with frequency- or and time-domain despreading, demapping, and decoding (IDDD) are investigated. Without the use of pilot aided JSI estimates as *a priori* information and with perfect channel information, the IDD and IDDD schemes have similar performances.

CHAPTER 7

JOINT ITERATIVE CHANNEL AND JAMMING-PARAMETER ESTIMATION WITH SUFFICIENT-STATISTIC CHIP COMBINING FOR CE-MC-CDMA-CDD ANTI-JAM SYSTEMS

7.1 Overview

In Chapter 6, we have shown that the constant-envelope MC-CDMA system using cyclic delay diversity (CDD) facilitates frequency- or time-domain chip combining to mitigate different types of jamming. Jammer state information (JSI) and jamming-signal-power-assisted chip combining have been used at the despreader for the constant envelope MC-CDMA-CDD system, where each symbol is spread into chips in the frequency or time domain. We have only considered flat-fading channels, and the channel coefficients are assumed perfectly known at the receiver thus far. In this chapter, the time-varying multiple-input multiple-output (MIMO) frequency-selective-fading-channel coefficients and jamming parameters are jointly estimated to suppress the adverse effects of partial-band noise jamming (PBNJ). These jamming parameters include JSI and jamming-signal power.

Channel estimation is necessary for coherent demodulation, combining different receive antenna signals, and estimation of JSI and jamming-signal power. Conversely, knowledge of the jamming-signal power and JSI can improve the accuracy of the channel estimates. For systems with multiple transmit antennas, any received signal is the superposition of the signals from multiple transmit antennas, which makes channel estimation even more challenging. If the signals transmitted from each antenna have equal power, then the received signal-to-interference-plus-noise ratio (SINR) is always less than or equal to 0 dB and, hence, the mean square error (MSE) of the channel estimates is very large [100]. Hence, special parameter estimation approaches are needed when using transmit diversity or space-time coding [39]. In [36], the time-varying channel for an MC-CDMA system is estimated using a Slepian basis expansion [102] that does not require complete knowledge

of the second-order channel statistics. A maximum-likelihood (ML) channel acquisition and least mean square (LMS) channel tracking method for a single transmit antenna MC-CDMA system is presented in [37]. However, neither of these papers consider transmit diversity or the presence of any jamming signal.

In this chapter, the MIMO channel coefficients, jamming-signal power, and JSI are jointly estimated for a convolutional-coded single-user MC-CDMA-CDD system [41] operating on a time-varying multipath-fading channel in the presence of partial-band noise jamming. To increase the system's robustness against jamming, we use multiple receive antennas at the receiver. We derive pilot-assisted weighted least square error (LSE) and linear minimum mean square error (MMSE) channel estimators that iteratively use the JSI estimates associated with the pilot symbols to update the noise covariance matrix. On the other hand, the JSI associated with the pilot symbols is iteratively estimated by using the updated channel estimates. We also specify the constraints on cyclic delays that are essential for the LSE channel estimator to exist and minimize the LSE and MMSE channel-estimation errors under full-band noise jamming (FBNJ).

Using the sufficient-statistic criterion of information theory, we show that the optimum chip-combining weights are inversely proportional to the PBNJ-plus-AWGN variance of the corresponding subcarriers. The chip combiner requires the JSI; hence, the JSI for the data symbols is iteratively estimated using the decoder output. For data detection, we use the iterative despreading, demapping, and decoding (IDDD) receiver. The despreading process consists of two steps: 1) JSI estimation using the decoder outputs and 2) chip combining based on the estimated JSI. The performance of the IDDD receiver is compared with that of an iterative demapping and decoding (IDD) receiver [112], where the JSI estimation and chip combining are performed just once without using the decoder output, i.e., the iterative ($i > 1$) JSI estimation and chip combining of the IDDD receiver are turned off in the IDD receiver. Simulation results demonstrate that the proposed iterative despreading (includes JSI estimation and chip combining), demapping, and decoding (IDDD) receiver

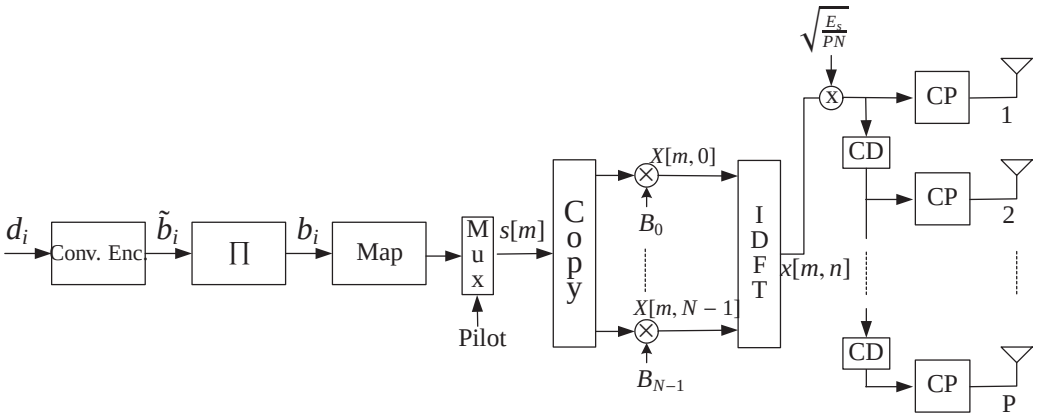

Figure 27. Constant-envelope MC-CDMA transmitter using cyclic delay diversity.

with soft-JSI (S-JSI)-assisted channel estimation and chip combining is very robust against PBNJ. The anti-jam techniques proposed in this chapter for PBNJ can be applied to suppress PJ in a straight forward fashion.

The remainder of the chapter is organized as follows. Section 7.2 illustrates the MC-CDMA-CDD transmitter. The signal model is discussed in Section 7.3. Pilot-assisted channel estimation and optimum (sufficient statistics) chip combining under PBNJ are described in Sections 7.4 and 7.5, respectively. Section 7.6 presents the estimation techniques of different jamming parameters. The computational complexities of the proposed anti-jam algorithms are discussed in Section 7.7. Section 7.8 presents the simulation results and Section 7.9 concludes the chapter.

7.2 Transmitter

Fig. 27 shows the convolutional-coded MC-CDMA-CDD transmitter with $P(\leq N)$ transmit antennas, where N is the number of subcarriers, which is also equal to the spreading factor. The subcarriers are uniformly spread over the system bandwidth so that the frequency diversity of the channel can be well exploited. The use of any M-ary phase shift keying (MPSK) provides a constant envelope in the frequency or time domain for uplink. For the purpose of parameter estimation, one pilot symbol is inserted every N_t symbols. The sets

of pilot and data symbol positions are denoted by $\mathcal{P}$ and $\mathcal{D}$, respectively. Throughout the chapter, the following notations are used: $(\cdot)^*$, $(\cdot)^T$, and $(\cdot)^H$ denote conjugate, transpose, and conjugate transpose, respectively.

The mth mapped symbol, $s[m]$, is spread by the frequency-domain spreading sequence $\{B[k]\}$, $k = 0, 1, \cdots, N-1$, to generate the frequency-domain signal, $X[m,k] = s[m]B[k]$ for $m \in \mathcal{P} \cup \mathcal{D}$, where $\cup$ denotes the union of sets. The time- and frequency-domain complex-quadratic polyphase spreading sequences [28] considered here are same as the previous chapters, which are defined as $b[n] = e^{-j\pi/8}\, e^{j\pi n^2/N}$, $n = 0, 1, \cdots, N-1$ and $B[k] = e^{j\pi/8}\, e^{-j\pi k^2/N}$, $k = 0, 1, \cdots, N-1$, respectively. If the corresponding time- and frequency-domain chips without any cyclic shifts are arranged in vector form as $\mathbf{b}^{(0)} = [b[0], b[1], \cdots, b[N-1]]^T$ and $\mathbf{B}^{(0)} = [B[0], B[1], \cdots, B[N-1]]^T$, respectively, then $\mathbf{B}^{(0)} = \mathbf{F}\ \mathbf{b}^{(0)}$, where the elements of the discrete Fourier transform (DFT) matrix are $[\mathbf{F}]_{k,n} = e^{-j\frac{2\pi kn}{N}}$; $k, n = 0, 1, \cdots, N-1$.

The frequency-domain signal is transformed by an inverse DFT (IDFT) into the time-domain signal as $x[m,n] = 1/\sqrt{N}\ \sum_{k=0}^{N-1} X[m,k]\, e^{j2\pi kn/N} = s[m]b[n]$, where $n = 0, 1, \ldots, N-1$ is the time-domain chip index. Before transmission from the p-th ($1 \le p \le P$) antenna, the sequence, $\{x[m,n]\}_{n=0}^{N-1}$, is cyclic delayed by $d_p T_c$ so that the transmitted signal on the kth subcarrier is $T^{(p)}[m,k] = \sqrt{E_s/(PN)}\, X[m,k]\, e^{-j2\pi k d_p/N}$, where E_s is the average received symbol energy, d_p is the number of unit cyclic shifts applied to the pth transmit antenna, and T_c is the time-domain chip duration equal to the sampling period. For simplicity, no cyclic delay is applied to the signal transmitted from the first antenna, i.e., $d_1 = 0$. A cyclic prefix or guard of length GT_c is appended [108] to facilitate frequency-domain equalization at the receiver. The guard interval is greater than or equal to the maximum excess delay of the channel.

7.3 Signal Model

We consider time-varying multipath-Rayleigh-fading channels. Considering any receive antenna $q \in \{1, \cdots, Q\}$, where Q is the total number of recieve antennas, the discrete channel frequency response corresponding to the kth subcarrier of the mth symbol and pth transmit antenna is $H^{(p,q)}[m,k] = 1/\sqrt{N} \sum_{l=0}^{L-1} h^{(p,q)}[m,l]\, e^{-j2\pi kl/N}$ for $p = 1, \cdots, P$ and $k = 0, 1, \cdots, N-1$, where L is the number of channel taps, and $h^{(p,q)}[m,l]$ is a zero mean complex Gaussian distributed channel coefficient associated with the lth ($l = 0, 1, \cdots, L-1$) path between the pth transmit and qth receive antenna. The frequency response vector corresponding to the pth transmit and qth receive antenna pair is $\mathbf{H}^{(p,q)}[m] = 1/\sqrt{N}\, \mathbf{F}\, \mathbf{h}^{(p,q)}[m]$, where the elements of the DFT matrix are $[\mathbf{F}]_{k,l} = e^{-j2\pi kl/N}$ for $k = 0, 1, \cdots, N-1$ and $l = 0, 1, \cdots, L-1$; $\mathbf{h}^{(p,q)}[m] = [h^{(p,q)}[m,0], h^{(p,q)}[m,1], \cdots, h^{(p,q)}[m, L-1]]^T$; and $\mathbf{H}^{(p,q)}[m] = [H^{(p,q)}[m,0], H^{(p,q)}[m,1], \cdots, \cdots, H^{(p,q)}[m, N-1]]^T$.

We assume that the channel coefficients among different transmit and receive antenna pairs and among different multipaths are independent identically distributed (i.i.d.). The correlation [48] of the channel coefficients are $E[h^{(p,q)}[m_1,l]\, h^{(p,q)^*}[m_2,l]] = E[|h^{(p,q)}[m,l]|^2]$ $J_0(2\pi f_d(m_1 - m_2)T_s)$, where $J_0(\cdot)$ is the *zero*th order Bessel function of first kind, $T_s = (N+G)T_c$ is the MC-CDMA symbol period, $f_d = v f_c/c$ is the maximum Doppler frequency for mobile velocity, v m/s, carrier frequency, f_c Hz, and light speed, $c = 3 \times 10^8$ m/s. The fading statistics are exploited when the pilot-assisted channel estimates are filtered [7] to obtain the channel estimates for the data symbol positions.

The partial-band noise jammer transmits a jamming signal with a power of P_J watts over a bandwidth ηB_f Hz, where B_f is the signal bandwidth, and η is the fraction of bandwidth jammed (also called jamming fraction), hence, $\eta \in (0, 1]$. The average power spectral density (psd) of the jammer is $N_J = P_J/B_f$. The power spectral density of the jammer is N_J/η in the jammed frequency band and zero in the unjammed band [28].

The complete anti-jam receiver having the channel, jamming-signal power, and JSI estimators and the chip combiner is shown in Fig. 28. After removing the cyclic prefix

and applying DFT, the frequency-domain signal corresponding to the mth symbol and qth receive antenna is

$$\begin{aligned} Y^{(q)}[m,k] &= \sqrt{N}\sum_{p=0}^{P-1} H^{(p,q)}[m,k]\; T^{(p)}[m,k] + C[m,k]\; J^{(q)}[m,k] + W^{(q)}[m,k] \\ &= \sum_{p=0}^{P-1}\sum_{l=0}^{L-1} h^{(p,q)}[m,l]\; T^{(p)}[m,k]\; e^{-j2\pi kl/N} + C[m,k]J^{(q)}[m,k] + W^{(q)}[m,k] \end{aligned} \quad (36)$$

where $W^{(q)}[m,k]$ are independent identically distributed (i.i.d.) additive white Gaussian Noise (AWGN) samples having zero mean and variance N_0, $C[m,k] \in \{0,1\}$ is the jammer state information (JSI), and $J^{(q)}[m,k]$ is the i.i.d. Gaussian jamming signal at the qth receive antenna having zero mean and variance $\sigma_J^2 = N_J/\eta$. The JSI associated with the mth symbol and kth subcarrier is $C[m,k] = 1$ when the kth subcarrier of the mth symbol is jammed, and $C[m,k] = 0$ when the kth subcarrier is not jammed. The JSI for a subcarrier changes independently over the MC-CDMA symbols. For simplicity of analysis, it is assumed that each subchannel is either completely jammed or not jammed at all. The total number of jammed subchannels is $\sum_{k=0}^{N-1} C[m,k]$ and the jamming fraction is $\eta = 1/N \sum_{k=0}^{N-1} C[m,k]$. Therefore, $\eta = 1.0$ under FBNJ. The goal of the anti-jam receiver is to sense the JSI and exploit the JSI estimates to suppress the adverse effects of jamming on channel estimation by updating noise covariance matrix and on despreading by weighted despreading or chip combining.

The signals received on different subcarriers by any receive antenna q can be arranged in a column vector as follows

$$\begin{aligned} \mathbf{Y}^{(q)}[m] &= \left[Y^{(q)}[m,0], Y^{(q)}[m,1], \cdots, Y^{(q)}[m,N-1]\right]^T \\ &= \mathbf{A}[m]\,\mathbf{h^{(q)}}[m] + \mathbf{V^{(q)}}[m];\;\; q = 1, \cdots, Q\;, \end{aligned} \quad (37)$$

where $\mathbf{h}^{(q)}[m] = \left[\mathbf{h}^{(1,q)^T}[m], \cdots, \mathbf{h}^{(P,q)^T}[m]\right]^T$ is the channel coefficient vector for the mth symbol, $\mathbf{h}^{(p,q)}[m] = [h^{(p,q)}[m,0], h^{(p,q)}[m,1], \cdots, h^{(p,q)}[m,L-1]]^T$ is the channel-coefficient vector associated with the pth transmit and qth receive antenna pair, $\mathbf{V^{(q)}}[m] = \Big[V^{(q)}[m,0]$, $V^{(q)}[m,1], \cdots \;\cdots, V^{(q)}[m,N-1]\Big]^T$ is the AWGN-plus-PBNJ vector, where $V^{(q)}[m,k] =$

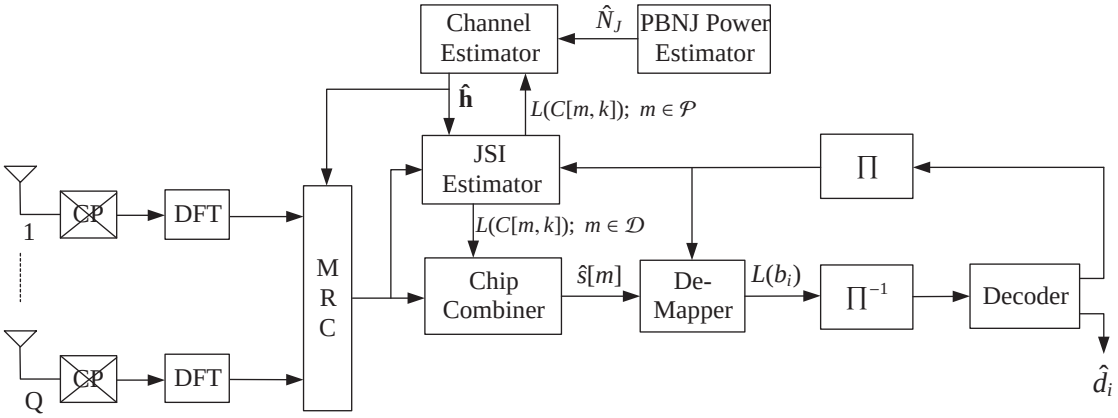

Figure 28. Iterative anti-jam receiver with channel, jamming power, and JSI estimators; and soft chip combiner.

$C[m,k]\ J^{(q)}[m,k] + W^{(q)}[m,k]$, and

$$\mathbf{A}[m] = \begin{bmatrix} T^{(1)}[m,0] & \cdots & T^{(P)}[m,0] & \cdots & T^{(P)}[m,0]\ e^{-j2\pi k(L-1)/N} \\ \vdots & \ddots & \vdots & \ddots & \vdots \\ T^{(1)}[m,N-1] & \cdots & T^{(P)}[m,N-1] & \cdots & T^{(P)}[m,N-1]\ e^{-j2\pi k(L-1)/N} \end{bmatrix} \quad (38)$$

is a $N \times PL$ matrix that depends on the transmitted symbol, cyclic shifts, and channel delays. Because the AWGN and PBNJ signals are independent random processes, the AWGN-plus-PBNJ signal vector $\mathbf{V}^{(\mathbf{q})}[m]$ has zero mean and covariance

$$\mathbf{C}_V[m] = E\left[\mathbf{V}^{(q)}[m]\mathbf{V}^{(q)}[m]^H\right] = \frac{N_J}{\eta}\begin{bmatrix} C[m,0] & 0 & \cdots & 0 \\ 0 & C[m,1] & \cdots & 0 \\ \vdots & \vdots & \ddots & \vdots \\ 0 & 0 & \cdots & C[m,N-1] \end{bmatrix} + N_0\ \mathbf{I}_N\ , \quad (39)$$

where $\mathbf{I}_N$ is $N \times N$ identity matrix.

The vector obtained by applying l $(0 < l < N-1)$ cyclic shifts to the time-domain spreading chip vector, $\mathbf{b}^{(0)} = \{b[n]\}_{n=0}^{N-1}$, can be expressed as $\mathbf{b}^{(l)} = [b[N-l], \cdots, b[N-1], b[0], \cdots, b[N-l-1]]^T$. The corresponding frequency-domain vector is $\mathbf{B}^{(l)} = [B[0], B[1]e^{-j2\pi l/N}, \cdots, B[N-1]e^{-j2\pi(N-1)l/N}]^T$. By using the expression of the kth subcarrier transmitted signal, $T^{(p)}[m,k] = \sqrt{E_s/(PN)}\ s[m]B[k]\ e^{-j2\pi k d_p/N}$, the $N \times PL$ matrix, $\mathbf{A}[m]$ in

(38), can be expressed as

$$\begin{aligned}\mathbf{A}[m] &= \sqrt{\frac{E_s}{PN}}\, s[m]\left[\mathbf{B}^{(0)_N}, \cdots, \mathbf{B}^{(L-1)_N}, \cdots\cdots, \mathbf{B}^{(d_P)_N}, \cdots, \mathbf{B}^{(d_P+L-1)_N}\right] \\ &= \sqrt{\frac{E_s}{PN}}\, s[m]\, \mathbf{B}; \;\; m \in \mathcal{P} \cup \mathcal{D} \;, \end{aligned} \tag{40}$$

where $(\cdot)_N$ denotes modulo-N operation. The $N \times PL$ matrix, $\mathbf{B} = \left[\mathbf{B}^{(0)_N}, \cdots, \mathbf{B}^{(L-1)_N}, \cdots\cdots, \mathbf{B}^{(d_P)_N}, \cdots, \mathbf{B}^{(d_P+L-1)_N}\right]$, does not depend on the transmitted symbol. Thus, the received frequency-domain signal vector can be expressed as

$$\mathbf{Y}^{(q)}[m] = \sqrt{\frac{E_s}{PN}}\, s[m]\, \mathbf{B}\, \mathbf{h^{(q)}}[m] + \mathbf{V^{(q)}}[m]; \;\; q = 1, \cdots, Q \;, \tag{41}$$

7.4 Pilot-Assisted Channel Estimation

The task of channel estimation is challenging for transmit diversity [39]. This is mainly because every subcarrier at each receive antenna entails multiple channel parameters associated with the multiple transmit antennas. The presence of a jamming signal makes channel estimation even more difficult. Since the channel estimates are used in JSI estimation, the quality of the JSI estimates depends on the available channel estimates. On the other hand, the initial channel estimates, which are estimated without JSI, can be refined by using the JSI estimates as they become available during the later iterations.

Because the number of subcarriers is usually much larger than the product of the number of transmit antennas and the channel length (i.e., $N > PL$), the estimation of $\mathbf{h}^{(p,q)}[m]$ involves fewer unknowns than the estimation of $\mathbf{H}^{(p,q)}[m]$. Therefore, for any transmitted symbol, it suffices to estimate the parameters, $\{h^{(p,q)}[m,l]\}$ for $l = 0, \cdots, L-1$ and $p = 1, \cdots, P$, from the received signal at each antenna. Because both the received signal vector and the unknown channel vector are Gaussian distributed, the posterior density function, $f(\mathbf{h^{(q)}}|\mathbf{Y}^{(q)})$, is also Gaussian distributed. Therefore, for each receive antenna $q \in \{1, \cdots, Q\}$, the LSE and MMSE channel estimators can be derived as [117]

$$\hat{\mathbf{h}}^{(q)}_{LSE}[m] = \sqrt{\frac{PN}{E_s}}\left(\mathbf{B}^H \mathbf{C}_V^{-1}[m]\mathbf{B}\right)^{-1} \mathbf{B}^H \left(\mathbf{C}_V^{-1}[m]\, \tilde{\mathbf{Y}}^{(q)}[m]\right); \; m \in \mathcal{P} \tag{42}$$

and

$$\hat{\mathbf{h}}^{(q)}_{MMSE}[m] = \sqrt{\frac{E_s}{PN}}\left(\mathbf{C}_h^{-1} + \frac{E_s}{PN}\,\mathbf{B}^H\mathbf{C}_V^{-1}[m]\mathbf{B}\right)^{-1}\mathbf{B}^H\left(\mathbf{C}_V^{-1}[m]\;\tilde{\mathbf{Y}}^{(q)}[m]\right);\; m\in\mathcal{P}\;, \quad (43)$$

respectively, where $\mathbf{C}_h = E\{\mathbf{h}^{(q)}[m]\mathbf{h}^{(q)H}[m]\}$ is the covariance matrix of the zero-mean channel-coefficient vector, and $\tilde{\mathbf{Y}}^{(q)}[m] = s^*[m]\,\mathbf{Y}^{(q)}[m]$. Because the AWGN-plus-PBNJ signal is Gaussian distributed and $\mathbf{C}_V^{-1}[m]$ is a diagonal matrix with diagonal elements $[C[m,k]N_J/\eta\; + N_0]^{-1}$, the cost function for LSE channel estimation can be viewed as a summation of weighted squares of different error elements. Thus, the maximum-likelihood channel estimator is same as the weighted-LSE channel estimator given in (42). Finally, the channel frequency response estimates are calculated as $\hat{\mathbf{H}}^{(p,q)}[m] = 1/\sqrt{N}\;\mathbf{F}\;\hat{\mathbf{h}}^{(p,q)}[m]$, where $\hat{\mathbf{h}}^{(p,q)}[m]$ is either $\hat{\mathbf{h}}^{(p,q)}_{LSE}[m]$ or $\hat{\mathbf{h}}^{(p,q)}_{MMSE}[m]$.

The noise covariance matrix depends on the jamming-signal variance and JSI as shown in (39). Therefore, $\sigma_J^2 = N_J/\eta$ and $\{C[m,k]\}_{k=0}^{N-1}$ for $m\in\mathcal{P}$ must be estimated for accurate channel estimation, especially when $\eta < 1.0$. The average PBNJ psd (N_J) is blindly estimated by projecting the received signal vector onto the entire column space of $\mathbf{A}[m]$ as described later in Section 7.6.1. Because the jamming pattern over the subcarriers changes randomly from symbol to symbol, $\{C[m,k]\}_{k=0}^{N-1}$ has to be estimated during every symbol position, $m\in\mathcal{P}\cup\mathcal{D}$, for either channel estimation or chip combining. The hard or soft JSI and corresponding noise covariance matrix, and thus, the channel coefficients, are iteratively estimated as described in Section 7.6.2.

Lemma 1: The LSE channel estimator exists, only if the following conditions on cyclic delays are satisfied

$$\begin{aligned} &0 \le d_p \le N-L, \qquad \forall\, p\in\{1,2,\cdots,P\};\\ &|d_p - d_{p-1}| \;\ge\; L, \qquad \forall\, p\in\{2,3,\cdots,P\}. \end{aligned} \quad (44)$$

Proof: In order for the LSE channel estimator to exist, $\mathbf{B}$ must be full rank, i.e., $rank[\mathbf{B}] = PL$ when $PL \le N$. If $N-L < d_p < N$ or $|d_p - d_{p-1}| < L$, the columns of $\mathbf{B}$ are no longer unique (independent); hence, the LSE channel estimator does not exist. As

a consequence of the conditions given by (44), the number of transmit antennas must be upper bounded by $P \leq \lfloor N/L \rfloor$, where $\lfloor x \rfloor$ denotes the largest integer less than or equal to x.

■

7.4.1 Mean Square Error (MSE)

The mean square errors of the LSE (or ML) and MMSE channel estimators can be expressed as [117]

$$MSE_{LSE} = \frac{N}{E_s L}\, tr\left\{\left(\mathbf{B}^H \mathbf{C}_V^{-1}[m]\mathbf{B}\right)^{-1}\right\} \tag{45}$$

and

$$MSE_{MMSE} = \frac{1}{PL}\, tr\left\{\left(\mathbf{C}_h^{-1} + \frac{E_s}{PN}\,\mathbf{B}^H \mathbf{C}_V^{-1}[m]\mathbf{B}\right)^{-1}\right\}\ , \tag{46}$$

respectively, where $tr\{\cdot\}$ denotes the trace of a matrix. The continuous full-band noise jammer inflicts the worst BER to the receiver having jammer state information [10]. Poor channel estimates deteriorate the BER further. Therefore, minimizing the channel estimation mean square errors under full-band noise jamming is an important feature of a robust channel estimator operating under PBNJ. The following lemma specifies the conditions that minimize the estimation mean square errors.

Lemma 2: Under full-band noise jamming ($\eta = 1.0$), the conditions of (44) on cyclic delays also minimize the mean square errors of both the LSE and MMSE channel estimators.

Proof: Under full-band noise jamming, the PBNJ-plus-AWGN covariance is $\mathbf{C}_V[m] = (\sigma_J^2 + N_0)\,\mathbf{I}_N$. So, the mean square errors associated with the LSE and MMSE channel estimators, respectively, are

$$MSE_{LSE}^{(\eta=1.0)} = \frac{N}{E_s L}(\sigma_J^2 + N_0)\, tr\left\{\left(\mathbf{B}^H\mathbf{B}\right)^{-1}\right\} \tag{47}$$

and

$$MSE_{MMSE}^{(\eta=1.0)} = \frac{1}{PL}\, tr\left\{\left(\mathbf{C}_h^{-1} + \frac{E_s}{PN}\frac{1}{\sigma_J^2 + N_0}\,\mathbf{B}^H\mathbf{B}\right)^{-1}\right\}. \tag{48}$$

The mean square errors of the channel estimators will be minimized if $\mathbf{B}^H\mathbf{B}$ is diagonal [118]. When the cyclic delays applied for achieving transmit diversity satisfy the conditions of (44), by using the auto-orthogonal property of the complex-quadratic spreading sequences, we have $\mathbf{B}^{(k)^H}\mathbf{B}^{(l)} = N\delta_{kl}$, and $\mathbf{B}^H\mathbf{B} = N\,\mathbf{I}_N$, where δ_{kl} is Kronecker delta function. Thus, the conditions of (44) minimize the mean square errors for both the LSE and MMSE channel estimators. ■

Assuming that all the transmit and receive antenna pairs have the same channel delay and power profiles, the minimum MSEs for LSE and MMSE estimators can be expressed as

$$MSE_{LSE,min}^{(\eta=1.0)} = \left(\frac{E_s}{\sigma_J^2 + N_0}\right)^{-1} P \tag{49}$$

and

$$MSE_{MMSE,min}^{(\eta=1.0)} = \frac{1}{L}\sum_{l=0}^{L-1}\left(\frac{1}{\sigma_h^2[l]} + \frac{E_s}{\sigma_J^2 + N_0}\,\frac{1}{P}\right)^{-1}, \tag{50}$$

respectively, where the channel-coefficient variance associated with lth path is $\sigma_h^2[l] = E\{|h^{(p,q)}[m,l]|^2\}$. The analytical and simulated minimum MSEs of the LSE and MMSE channel estimators under FBNJ are shown in Fig. 29 for a three-ray frequency-selective-fading channel with delay profile $0, 1, 2\ [T_c]$ and power profile $0, -3, -6$ [dB].

7.5 Sufficient-Statistic Chip Combining

In our MC-CDMA system, the data symbols are spread in the frequency-domain and the spread signals or chips are transmitted over the subcarriers. After removing the cyclic prefix and applying DFT at the receiver, maximal-ratio combining (MRC) is used to combine the signals received at different antennas for each subcarrier. After MRC, the frequency-domain signals, associated with each data symbol, must be combined considering the channel's frequency response (if necessary) and noise/jamming statistics of the corresponding sub-channels, in addition to being multiplied by the complex conjugate of the frequency-domain spreading sequence. We refer to this frequency-diversity combining or weighted

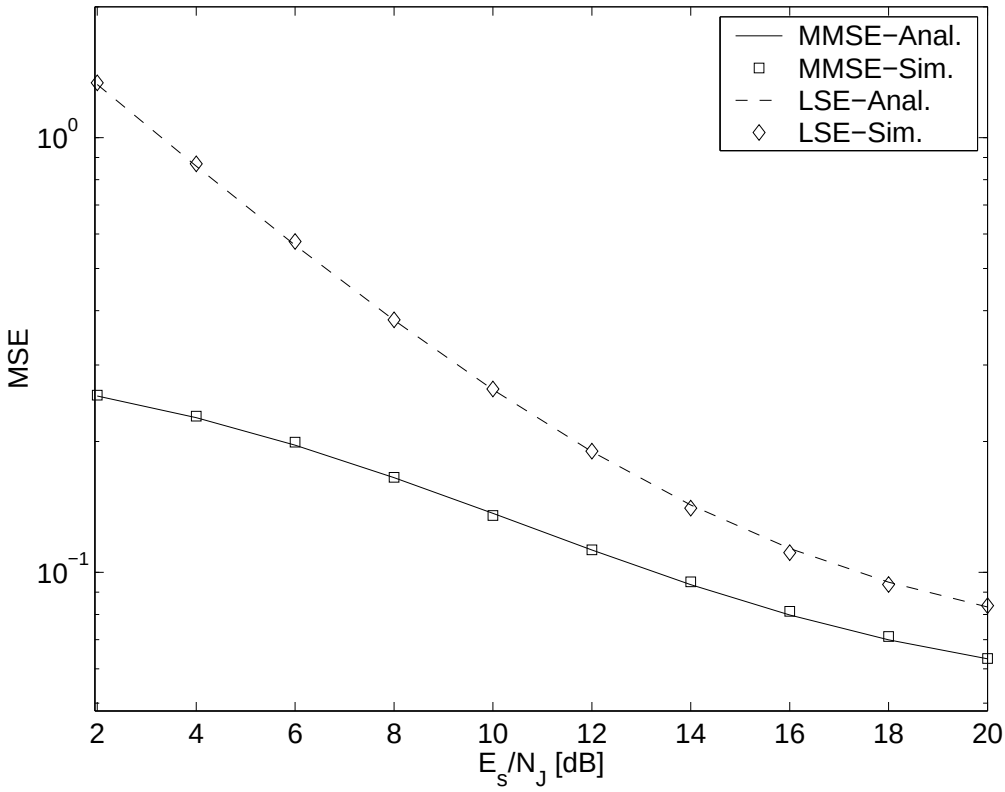

Figure 29. Minimum mean square errors of LSE and MMSE channel estimators under full-band noise jamming (Two transmit antennas, E_s/N_0 = 15 dB, three-tap channel).

despreading as *chip combining*. To calculate the chip-combining weights, different optimization criteria, e.g., MRC, MMSE [8] [7] etc., are used. In this section, we use sufficient statistics as the optimization criterion to determine the chip-combining weights.

Frequency domain JSI estimation and chip combining is necessary to suppress the PBNJ signal effectively for the jamming-fraction range $\eta = (0, 1.0]$. When JSI is available at the receiver, the worst case PBNJ is a full-band jammer, where $\eta = 1.0$ [28]. The MRC of different receive antenna signals, applied prior to chip combining, renders compensation for the channel's frequency selectivity unnecessary during chip combining, as will be evident from the derived sufficient-statistic chip-combining weights. Thus, for full-band noise jamming, equal-gain chip combining is optimal since all the subcarriers are jammed with equal noise power. However, when $\eta < 1.0$, the receiver can operate more efficiently (with a smaller required minimum E_b/N_J at a given BER) with JSI-assisted chip combining than

equal-gain chip combining, where E_b is the average received energy per information bit.

The received kth subcarrier signal after removing the cyclic prefix and applying DFT at each receive antenna can be expressed as

$$Y^{(q)}[m,k] \;=\; \sqrt{\frac{E_s}{P}}\, H^{(q)}[m,k]\, X[m,k] + C[m,k]J^{(q)}[m,k] + W^{(q)}[m,k] \;, \qquad (51)$$

where $C[m,k] \in \{0,1\}$ is the JSI, and $H^{(q)}[m,k] = \sum_{p=1}^{P} H^{(p,q)}[m,k]\, e^{-j2\pi k d_p/N}$ is the equivalent channel response or frequency-domain channel coefficient at the qth receive antenna. After maximal-ratio combining of the different receive-antenna signals, the output corresponding to the kth subcarrier of the mth symbol is

$$Y[m,k] \;=\; \sqrt{\frac{E_s}{P}}\, s[m] \sum_{q=1}^{Q} \left|H^{(q)}[m,k]\right|^2 B[k] + J[m,k] + W[m,k] \;, \qquad (52)$$

where $s[m]$ ($m \in \mathcal{P} \cup \mathcal{D}$) is the transmitted pilot or data symbol, $B[k]$ is the frequency-domain spreading chip associated with the kth subcarrier, and the contributions from PBNJ and AWGN, respectively, are $J[m,k] = C[m,k] \sum_{q=1}^{Q} H^{(q)}[m,k]^* J^{(q)}[m,k]$ and $W[m,k] = \sum_{q=1}^{Q} H^{(q)}[m,k]^* W^{(q)}[m,k]$. Given the channel coefficients, $J[m,k]$ and $W[m,k]$ have zero-mean Gaussian distributions with variances (dropping the symbol index m from the notation)

$$\sigma^2_{J_k} \;=\; \begin{cases} 0 & , \;\; C[m,k] = 0 \\ \frac{N_J}{\eta} \sum_{q=1}^{Q} \left|H^{(q)}[m,k]\right|^2 & , \;\; C[m,k] = 1 \end{cases} \qquad (53)$$

and $\sigma^2_{W_k} = N_0 \sum_{q=1}^{Q} \left|H^{(q)}[m,k]\right|^2$, respectively.

The maximal-ratio combined frequency-domain signals corresponding to each data symbol, given in (52) for different subcarriers, are (chip-) combined, then demapped and decoded. Considering the known frequency-domain spreading sequence, the chip combiner output (input signal to the demapper) for the mth data symbol can be expressed as

$$\hat{s}[m] \;= \sum_{k=0}^{N-1} \rho[m,k]\, B^*[k]\, Y[m,k];\;\; m \in \mathcal{D} \;, \qquad (54)$$

where $\rho[m,k]$ is the chip-combining weight corresponding to the kth subchannel of the mth data symbol.

Theorem: Under Gaussian distributed PBNJ and AWGN, for any data symbol, the chip-combining weights that provide a sufficient statistic to the demapper are inversely proportional to the AWGN-plus-jamming signal variance and do not depend on the channel's frequency response.

Proof: To derive the chip-combining weights, we begin with the log-likelihood ratio (LLR) computation at the demapper. If the coded and bit-interleaved sequence corresponding to the mth symbol is denoted by $\{b_i\}_{i=0}^{\log_2 M-1}$, the log-likelihood ratio of *a posteriori* probability of b_i generated by the demapper is [112]

$$\begin{aligned} L(b_i) &= \log\left[\frac{p(b_i=1 \mid \mathbf{Y}[m], \{H^{(q)}[m,k]\}_{q=1,\ k=0}^{Q,\ N-1})}{p(b_i=0 \mid \mathbf{Y}[m], \{H^{(q)}[m,k]\}_{q=1,\ k=0}^{Q,\ N-1})}\right] \\ &= \log\left[\frac{\sum_{s\in\mathcal{S}:b_i=1} p\left(\mathbf{Y}[m] \mid s, \{H^{(q)}[m,k]\}_{q=1,\ k=0}^{Q,\ N-1}\right)\ p(s)}{\sum_{s\in\mathcal{S}:b_i=0} p\left(\mathbf{Y}[m] \mid s, \{H^{(q)}[m,k]\}_{q=1,\ k=0}^{Q,\ N-1}\right)\ p(s)}\right] , \end{aligned} \tag{55}$$

where the received signal vector associated with the mth data symbol is $\mathbf{Y}[m] = [Y[m,0], \cdots, \cdots, Y[m,N-1]]^T$, $s \in \mathcal{S}$ is the hypothetical data symbol, and $\mathcal{S}$ is the set of possible data symbols. Let us consider the conditional likelihood function, $p\left(\mathbf{Y}[m] \mid s; \{H^{(q)}[m,k]\}_{q=1,\ k=0}^{Q,\ N-1}\right)$, where the equivalent channel coefficients $\{H^{(q)}[m,k]\}_{q=1,\ k=0}^{Q,\ N-1}$ are known, and s is the random parameter of interest. After ignoring the irrelevant additive terms, the conditional log-likelihood function, can be expressed as

$$\begin{aligned} \log\ p\left(\mathbf{Y}[m] \mid s, \{H^{(q)}[m,k]\}_{q=1,\ k=0}^{Q,\ N-1}\right) &= -\sum_{k=0}^{N-1} \log\left[\pi(\sigma_{W_k}^2 + \sigma_{J_k}^2)\right] \\ &\quad - \sum_{k=0}^{N-1} \frac{1}{\sigma_{W_k}^2 + \sigma_{J_k}^2} \left| Y[m,k] - \sqrt{\frac{E_s}{P}} \sum_{q=1}^{Q} \left|H^{(q)}[m,k]\right|^2 B[k]\ s \right|^2 \\ &\approx 2\sqrt{\frac{E_s}{P}}\ \Re\mathfrak{e}\left[\left(\sum_{k=0}^{N-1} \frac{1}{N_0 + C[m,k]\frac{N_J}{\eta}}\ B^*[k]\ Y[m,k]\right) s^*\right] , \end{aligned} \tag{56}$$

where $\Re\mathfrak{e}[\cdot]$ denotes the real part of a complex number. The hypothetical parameter of interest (s) must be coupled with the sufficient statistic but not with the original received signal vector ($\mathbf{Y}[m]$). Using Fisher's factorization theorem [117] [119], the sufficient statistic for

any data symbol is

$$\mathcal{T}(\mathbf{Y}[m]) \;=\; \sum_{k=0}^{N-1} \frac{1}{N_0 + C[m,k]N_J/\eta}\, B^*[k]\; Y[m,k], \tag{57}$$

which must be provided to the demapper in order to evaluate appropriate likelihood functions for calculating the LLR of the coded and interleaved bits. Considering the term inside the summation of the sufficient statistic given in (57), the chip-combining weight for the kth subcarrier has to be the part excluding the complex conjugate of the spreading chip, $B^*[k]$ and the received frequency-domain observed signal, $Y[m,k]$. Thus,

$$\rho[m,k] \;=\; \frac{1}{N_0 + C[m,k]N_J/\eta}\;, \tag{58}$$

which is inversely proportional to the AWGN-plus-jamming signal variance of the relevant subcarriers. ■

Note that the chip-combining weights, given in (58), do not depend on the frequency selective channel response, because MRC of different receive antenna signals is applied for each subcarrier prior to chip combining. Since the numerators of the weights are constant for all the sub-carriers, we can simply say that the chip-combining weights are inversely proportional to the AWGN-plus-PBNJ variance of the corresponding subcarriers. The derived sufficient-statistic chip-combining weights also conform with the maximal-ratio linear diversity combining weights presented in [25], where the MRC weights are proportional to the rms of the signal component and inversely proportional to the average noise power of the corresponding sub-channels.

The sufficient statistic, $\mathcal{T}(\mathbf{Y}[m])$, given in (57), satisfies the condition for equality in the data processing inequality and preserves mutual information [120] as

$$I(s;\mathbf{Y}[m]) \;=\; I(s;\mathcal{T}(\mathbf{Y}[m]))\;, \tag{59}$$

where $I(s;\mathbf{Y}[m])$ denotes the mutual information between the random variable s and observed vector $\mathbf{Y}[m]$, and $I(s,t)$ is the mutual information between the random variables s

and t. After optimal (sufficient-statistics sense) chip combining at the despreader, the input signal to the demapper for the mth data symbol is expressed as

$$\hat{s}[m] \;=\; \mathcal{T}(\mathbf{Y}[m]) \;=\; \sqrt{\frac{E_s}{P}} \sum_{k=0}^{N-1} \rho[m,k] \sum_{q=1}^{Q} \left|H^{(q)}[m,k]\right|^2 s[m] + \tilde{J} + \tilde{W};\; m \in \mathcal{D}\;, \qquad (60)$$

where the chip-combining weight corresponding to the kth subchannel of the mth data symbol is

$$\rho[m,k] \;=\; \begin{cases} \gamma_0 \;=\; \frac{1}{N_0} \;, & C[m,k]=0 \\ \gamma_1 \;=\; \frac{1}{N_J/\eta + N_0} \;, & C[m,k]=1 \end{cases};\; m \in \mathcal{D}, \qquad (61)$$

which depends on the corresponding JSI and jamming variance, N_J/η. Therefore, the JSI, average jamming psd, and jamming fraction must be estimated and exploited in chip combining to pass the sufficient statistic to the demapper. The contributions from PBNJ and AWGN at the despreader output are $\tilde{J} = \sum_{k=0}^{N-1} \rho[m,k]\; B^*[k]J[m,k]$ and $\tilde{W} = \sum_{k=0}^{N-1} \rho[m,k]\; B^*[k]W[m,k]$, respectively. Thus, the log-likelihood ratio (LLR) of the interleaved bits computed by the soft demapper can be expressed in terms of the chip combiner output as

$$L(b_i) \;=\; \log\left[\frac{\sum_{s\in\mathcal{S}:b_i=1} \exp\left(2\sqrt{\frac{E_s}{P}}\,\Re\mathfrak{e}[\hat{s}[m]\;s^*]\right)\; p(s)}{\sum_{s\in\mathcal{S}:b_i=0} \exp\left(2\sqrt{\frac{E_s}{P}}\,\Re\mathfrak{e}[\hat{s}[m]\;s^*]\right)\; p(s)}\right]. \qquad (62)$$

For iterative demapping [112], the demapper uses the chip-combiner output as well as the extrinsic information from previous iterations of the convolutional decoder [121] to generate $L(b_i)$, which are then deinterleaved and fed to the convolutional decoder. The chip-combiner output has a Gaussian distribution with variance $\sigma^2 = \sigma^2_{\tilde{J}} + \sigma^2_{\tilde{W}}$. Given the JSI, chip-combining weights, and channel coefficients, and i.i.d. Rayleigh-fading-channel assumption, the AWGN-plus-PBNJ variance at the despreader output is

$$\sigma^2_{\tilde{W}} + \sigma^2_{\tilde{J}} = \sum_{k=0}^{N-1} \rho^2[m,k] \sum_{q=1}^{Q} |H^{(q)}[m,k]|^2 \left(N_0 + C[m,k]\frac{N_J}{\eta}\right). \qquad (63)$$

7.6 Jamming Parameter Estimation

7.6.1 Jamming Power Estimation

The average jamming-signal psd (N_J) is used in the channel and JSI estimators and also in the chip combiner. Hence, N_J must be estimated before performing any channel or JSI estimation. Because the JSI of the subcarriers is unknown at this stage, direct estimation of $\sigma_J^2 = \frac{N_J}{\eta}$ is difficult. A subspace-based technique is proposed in [22] to estimate the SINR for time division multiple access (TDMA) cellular systems. In [23], the interference-plus-AWGN variance is estimated by projecting the received signal onto a single vector of the left-null space of the matrix formed by the known training sequence or estimated data symbols. In [24], the interference-plus-noise variance for TDMA systems is estimated by projecting the received signal onto the entire signal subspace. The signal-projection (SP) method [24] has less complexity, shorter estimation time, and smaller estimation error than the other two methods.

In this Section, we apply the SP method that facilitates blind average jamming-signal psd estimation for the MC-CDMA-CDD system. The channel and PBNJ-plus-AWGN signal vectors can be separated as shown in (41) for the alternative expression of the received signal vector at the qth antenna. Let the column space (also known as range or signal subspace) and left-null space of matrix $\mathbf{B}$ be denoted as $\mathcal{R}(\mathbf{B})$ and $\mathcal{N}(\mathbf{B}^T)$, respectively. If the conditions of Lemma 1 are satisfied, matrix $\mathbf{B}$ has full rank, i.e., $\dim(\mathcal{R}(\mathbf{B})) = PL$ and $\dim(\mathcal{N}(\mathbf{B}^T)) = N - PL$. For simplicity, let the cyclic delays be $d_p = (p-1)L$ for $p = 1, 2, \cdots, P$. From (40), the basis of $\mathcal{R}(\mathbf{B})$ and $\mathcal{N}(\mathbf{B}^T)$, respectively, are $1/\sqrt{N}\ \left\{\mathbf{B}^{(0)}, \mathbf{B}^{(1)}, \cdots, \mathbf{B}^{(PL-1)}\right\}$ and $1/\sqrt{N}\ \left\{\mathbf{B}^{(PL)}, \mathbf{B}^{(PL+1)}, \cdots, \mathbf{B}^{(N-1)}\right\}$. If $\tilde{\mathbf{Y}}^{(q)}[m]$ is the projection of $\mathbf{Y}^{(q)}[m]$ onto the entire left-null space then

$$\begin{aligned} E\left[\| \tilde{\mathbf{Y}}^{(q)}[m] \|^2\right] &= \frac{1}{N} E\left[\sum_{d=PL}^{N-1} \left|\langle \mathbf{B}^{(d)}, \mathbf{Y}^{(q)}[m]\rangle\right|^2\right] \\ &= \frac{1}{N} \sum_{d=PL}^{N-1} E\left[\left|\mathbf{B}^{(d)H}\mathbf{V}^{(\mathbf{q})}[m]\right|^2\right] \\ &= (N-PL)(N_J + N_0)\ , \end{aligned} \tag{64}$$

where $\langle \mathbf{x}, \mathbf{y} \rangle = \mathbf{x}^H \mathbf{y}$. Assuming that $N >> PL$, the dimension of $\mathcal{N}(\mathbf{B}^T)$ is large compared to the dimension of the signal subspace, $\mathcal{R}(\mathbf{B})$. Using the Pythagorean theorem, a computationally efficient expression for the PBNJ signal psd is obtained by projecting the received signal vector onto $\mathcal{R}(\mathbf{B})$ as

$$\begin{aligned} N_J &= \frac{1}{N-PL} E\left[\| \tilde{\mathbf{Y}}^{(q)}[m] \|^2 \right] - N_0 \\ &= \frac{1}{N-PL} \left(E\left[\| \mathbf{Y}^{(q)}[m] \|^2 \right] - \frac{1}{N} \sum_{d=0}^{PL-1} E\left[\left| \mathbf{B}^{(d)H} \mathbf{Y}^{(q)}[m] \right|^2 \right] \right) - N_0. \end{aligned} \quad (65)$$

Thus, considering empirical averaging over multiple symbols of all receive antennas, the average jamming-signal psd estimator becomes

$$\hat{N}_J = \frac{1}{(N-PL)Q|\mathcal{S}_I|} \sum_{m \in \mathcal{S}_I} \sum_{q=1}^{Q} \left(\| \mathbf{Y}^{(q)}[m] \|^2 - \frac{1}{N} \sum_{d=0}^{PL-1} \left| \mathbf{B}^{(d)H} \mathbf{Y}^{(q)}[m] \right|^2 \right) - N_0 \ , \quad (66)$$

where $\mathcal{S}_I$ is the set of symbol indexes over which averaging is performed.

The above jamming-signal psd estimator for the MC-CDMA-CDD system is more power and bandwidth efficient, and it requires fewer number of computations than the estimators for TDMA systems proposed in [23] and [24]. For TDMA system estimators, **B** depends on the training sequence or estimated data symbols. Thus, either a training sequence is required or the basis of $\mathcal{R}(\mathbf{B})$ has to be computed every time **B** changes. However, for the constant-envelope MC-CDMA-CDD system, **B** is constant, and orthonormalization is not required, since the columns of **B** are orthogonal spreading sequences. Therefore, estimation of N_J for the constant-envelope MC-CDMA-CDD system is computationally less demanding and the estimation interval can be long enough to achieve very accurate estimates without the loss of power and bandwidth. Figs. 30 and 31, respectively, show the mean and variance of $\hat{N}_J$ for $\eta = 1.0$ (E_s/N_J = 1 to 10 dB) and $\eta = 0.6$ (E_s/N_J = -10 to 8 dB) with estimation intervals, $|\mathcal{S}_I|$ = 32 and 128 symbols.

7.6.2 JSI Estimation for Channel Estimation

The JSI associated with the pilot symbols are iteratively estimated to update the noise covariance matrix necessary for pilot-assisted channel estimation as shown in (39), (42) and

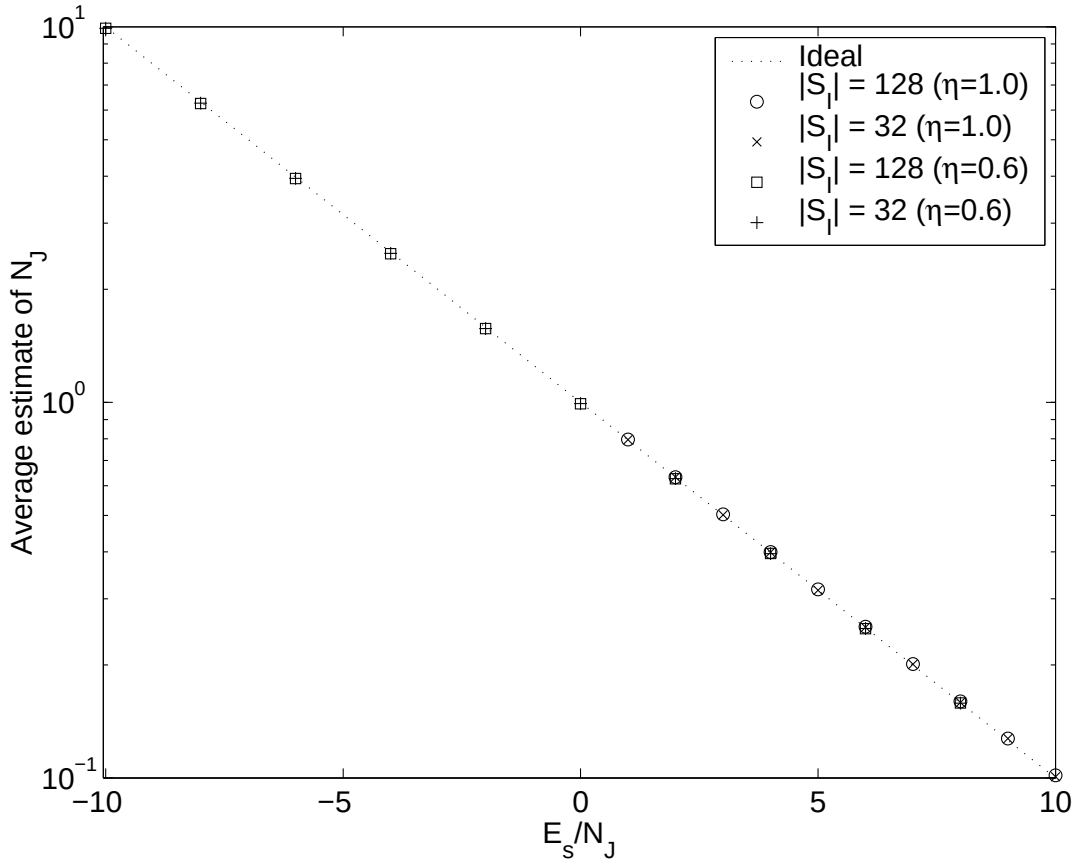

Figure 30. Average jamming power estimated using signal-projection method (2x2 MIMO, three-tap channel, mobile velocity 90 km/h).

(43). The updated channel estimates are used for JSI estimation in the next iteration. Let $p(C[m,k]=c)$, $c \in \{0,1\}$, be defined as the *a posteriori* probability of the JSI corresponding to the mth symbol and kth subcarrier, where $m \in \mathcal{P}$ and $k \in \{0,1,\cdots,N-1\}$. The jamming pattern, i.e., the set of subcarriers jammed changes independently from symbol to symbol. Since the jamming signal is independent of the transmitted pilot symbol and channel coefficients, $p(C[m,k]=c)$ can be expressed as

$$\begin{aligned} p\left(C[m,k]=c\right) &\triangleq P\left(C[m,k]=c \mid Y[m,k], s[m], \{H^{(q)}[m,k]\}_{q=1}^{Q}\right) \\ &\propto P\left(Y[m,k] \mid s[m], C[m,k]=c, \{H^{(q)}[m,k]\}_{q=1}^{Q}\right)\ p(C[m,k]=c)\ , \end{aligned} \tag{67}$$

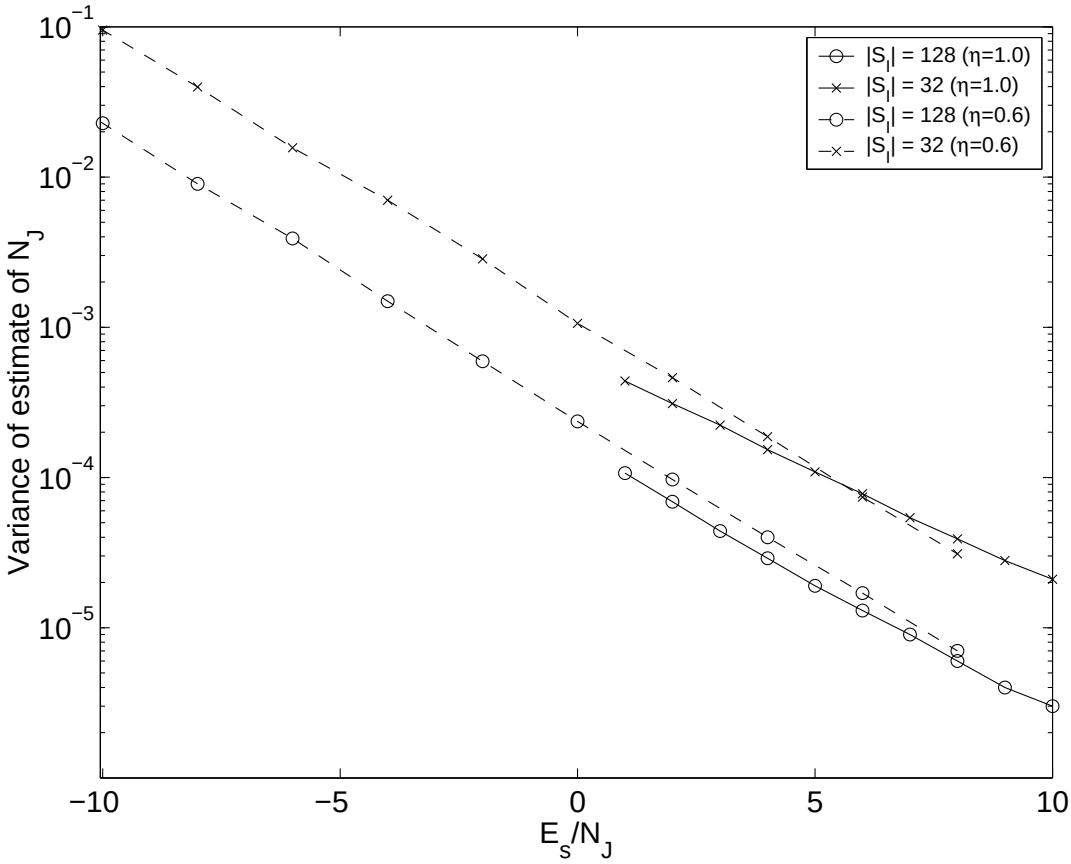

Figure 31. Variance of $\hat{N}_J$ using signal-projection method (2x2 MIMO, three-tap channel, mobile velocity 90 km/h).

where $s[m]$, $m \in \mathcal{P}$, is the known pilot symbol, and $p(C[m,k] = c)$ is the *a priori* probability that $C[m,k] = c$ for $c \in \{0,1\}$. The conditional probability can be expressed as

$$P\left(Y[m,k] \mid s[m], C[m,k] = c, \{H^{(q)}[m,k]\}_{q=1}^{Q}\right) = \frac{1}{\pi\sigma_c^2} \cdot \exp\left(-\frac{\left|Y[m,k] - \sqrt{\frac{E_s}{P}}\sum_{q=1}^{Q}|H^{(q)}[m,k]|^2\, s[m]B[k]\right|^2}{\sigma_c^2}\right), \tag{68}$$

where the variance of $Y[m,k]$ given the channel coefficients is

$$\sigma_c^2 = \sum_{q=1}^{Q}|H^{(q)}[m,k]|^2 \begin{cases} N_0 & ; \quad c = 0 \\ (N_0 + \sigma_J^2) & ; \quad c = 1 \end{cases}. \tag{69}$$

The log-likelihood ratio of $C[m,k]$ for the ith iteration ($i = 1, 2, \cdots$) is

$$\begin{aligned} L(C^{(i)}[m,k]) &= \log\left[\frac{p(C^{(i)}[m,k]=1)}{p(C^{(i)}[m,k]=0)}\right] \\ &= \log\left[\frac{\hat{\eta}^{(i)}[m]\,\hat{\beta}_1^{(i)}[m]}{(1-\hat{\eta}^{(i)}[m])\,\beta_0}\right] + \\ &\quad \frac{\left|\frac{Y[m,k]}{\sqrt{E_s}} - \sqrt{\frac{1}{P}}\sum_{q=1}^{Q}|\hat{H}^{(q)(i)}[m,k]|^2\; s[m]B[k]\right|^2}{\sum_{q=1}^{Q}|\hat{H}^{(q)(i)}[m,k]|^2}\,(\beta_0 - \hat{\beta}_1^{(i)}[m]);\; m \in \mathcal{P}\ , \end{aligned} \quad (70)$$

where the iteratively estimated jamming fraction at the ith iteration is $\hat{\eta}^{(i)}[m] = 1/N \sum_{k=0}^{N-1} \hat{C}^{(i-1)}[m,k]$ with $\hat{\eta}^{(1)}[m] = 1$ (assuming all subcarriers are equally likely to be jammed), equivalent frequency-domain channel-coefficient estimates are $\hat{H}^{(q)(i)}[m,k] = \sum_{p=1}^{P} \hat{H}^{(p,q)(i)}[m,k]\; e^{-j2\pi k d_p/N}$, $\hat{H}^{(p,q)(i)}[m,k]$ is the estimate of channel frequency response, $\beta_0 = E_s/N_0$, $\hat{\beta}_1^{(i)}[m] = E_s/(N_0 + \hat{\sigma}_J^{2(i)}[m])$, and $\hat{\sigma}_J^{2(i)}[m] = \hat{N}_J/\hat{\eta}^{(i)}[m]$. Thus, the hard-JSI at the end of the ith iteration can be obtained as $\hat{C}^{(i)}[m,k] = 0$, if $|Y[m,k]/\sqrt{E_s} - 1/\sqrt{P}\sum_{q=1}^{Q}|\hat{H}^{(q)(i)}[m,k]|^2\; s[m]B[k]|^2 < (\sum_{q=1}^{Q}|\hat{H}^{(q)(i)}[m,k]|^2)/(\beta_0 - \hat{\beta}_1^{(i)}[m]) \log\left[((1-\hat{\eta}^{(i)}[m])\,\beta_0)/(\hat{\eta}^{(i)}[m]\,\hat{\beta}_1^{(i)}[m])\right]$; $\hat{C}^{(i)}[m,k] = 1$, otherwise.

The channel and JSI estimators update each other as the new estimates are available. During the initial ($i = 1$) pilot aided channel estimation, the JSI estimates of the corresponding symbols ($m \in \mathcal{P}$) are not available. Hence, all subcarriers are assumed jammed, and the noise covariance matrix is approximated as $\hat{\mathbf{C}}_V^{(1)}[m] = (\hat{N}_J + N_0)\,\mathbf{I}_N$. Next, the initial channel estimates ($\hat{H}^{(p,q)(1)}[m,k]$) and the average PBNJ psd ($\hat{N}_J$) are used to perform JSI estimation for the pilot symbols ($m \in \mathcal{P}$). Once the JSI estimates are available, they are used for updating the noise covariance matrix and subsequently for refining the channel estimates using (39) and (42) or (43). Given the hard- or soft-JSI estimates, the noise covariance matrix for the next channel-estimation iteration is updated as

$$\left[\hat{\mathbf{C}}_V^{(i+1)}[m]\right]_{kk} = \begin{cases} N_0 & ;\ \hat{C}^{(i)}[m,k] = 0 \\ \hat{\sigma}_J^{2(i)}[m] + N_0 & ;\ \hat{C}^{(i)}[m,k] = 1 \end{cases} \quad (71)$$

and

$$\left[\hat{\mathbf{C}}_V^{(i+1)}[m]\right]_{kk} = N_0\; p(C^{(i)}[m,k]=0) + \left(\hat{\sigma}_J^{2(i)}[m] + N_0\right)\; p(C^{(i)}[m,k]=1)\ , \quad (72)$$

respectively, which yields the channel estimates, $\hat{\mathbf{h}}^{(q)(i+1)}[m]$, for $m \in \mathcal{P}$ at the $(i+1)$th iteration.

7.6.3 JSI Estimation for Data Detection

The JSI, associated with the data symbols ($m \in \mathcal{D}$), is iteratively estimated by exploiting the LLR of the coded bits provided by the convolutional decoder [121]. These JSI estimates are used during chip combining. The decoded soft information (LLR) from the convolutional decoder is interleaved and fed back to the JSI estimator as well as to the demapper [112]. Thus, blockwise despreading (JSI estimation and chip-combining using these JSI estimates for each symbol in the codeblock), demapping and decoding are performed on the same set of received signals. Reliable LLR from the decoder will enable the JSI estimator to achieve refined JSI estimates for the data symbols as the iterations among the despreader, demapper, and decoder progress. Similar as Chapter 6, we name this process as iterative despreading, demapping, and decoding (IDDD). Moreover, upon whether the hard or soft values of the estimated JSI are used in the frequency-domain chip combining at the despreader, we will refer to this process as H-JSI-IDDD or S-JSI-IDDD, respectively. For the sake of simplicity, the iteration superscript is omitted from the notation of the channel coefficients.

Let $p(C[m,k]=c)$, $c \in \{0,1\}$, be the *a posteriori* probability of the JSI associated with the kth subcarrier of the mth symbol, where $m \in \mathcal{D}$. Then $p(C[m,k]=c)$ can be expressed as

$$\begin{aligned} p(C[m,k]=c) &\triangleq P\left(C[m,k]=c \mid Y[m,k], \{H^{(q)}[m,k]\}_{q=1}^{Q}\right) \\ &\propto \sum_{s\in\mathcal{S}} P\left(Y[m,k] \mid s, C[m,k]=c, \{H^{(q)}[m,k]\}_{q=1}^{Q}\right)\ p(s)\ p(C[m,k]=c)\ , \quad (73) \end{aligned}$$

where $\mathcal{S}$ denotes the set of all possible decoded symbols, the symbol probability, $p(s) = \prod_{i=0}^{\log_2 M-1} P(b_i)$, is calculated using the LLR of the bits from the convolutional decoder, and $\{b_{(\log_2 M-1)}, \cdots, b_0\}$ is the coded and bit-interleaved sequence associated with symbol, s. Because of bit interleaving after error correction coding, the bits corresponding to any symbol can be treated as being independent from each other. The LLR of the JSI at ith

IDDD iteration, $i = 1, 2, \ldots$, can be derived as

$$\begin{aligned} L(C^{(i)}[m,k]) &= \log\left[\frac{p(C^{(i)}[m,k]=1)}{p(C^{(i)}[m,k]=0)}\right] \\ &= \log\left[\frac{\sum_{s\in\mathcal{S}} P\left(Y[m,k] \mid s, C^{(i)}[m,k]=1, \{\hat{H}^{(q)}[m,k]\}_{q=1}^{Q}\right)\ p(s^{(i-1)})}{\sum_{s\in\mathcal{S}} P\left(Y[m,k] \mid s, C^{(i)}[m,k]=0, \{\hat{H}^{(q)}[m,k]\}_{q=1}^{Q}\right)\ p(s^{(i-1)})}\right] \\ &\quad + L(C^{(i-1)}[m,k]); \quad m \in \mathcal{D}\ , \end{aligned} \tag{74}$$

where $\hat{H}^{(q)}[m,k] = \sum_{p=1}^{P} \hat{H}^{(p,q)}[m,k]\ e^{-j2\pi k d_p/N}$, and $\hat{H}^{(p,q)}[m,k]$ is the channel frequency response estimate for the data symbol position ($m \in \mathcal{D}$) obtained by Wiener filtering of the pilot position channel estimates.

In the derivation of (74), $p(C[m,k]=c)$ and $p(s)$ in (73) are replaced by the JSI probability, $p(C^{(i-1)}[m,k]=c)$, and decoded symbol probability, $p(s^{(i-1)})$, respectively, which are obtained from the previous $(i-1)$-th IDDD iteration. The conditional probability of the received signal, $P\left(Y[m,k] \mid s, C[m,k]=c, \{\hat{H}^{(q)}[m,k]\}\right)$, has the Gaussian distribution given in (68) with variance given by

$$\sigma_c^2 = \sum_{q=1}^{Q} |\hat{H}^{(q)}[m,k]|^2 \begin{cases} N_0 & ;\ c=0 \\ N_0 + \hat{\sigma}_J^{2(i)}[m] & ;\ c=1 \end{cases}\ , \tag{75}$$

where the estimates of the jamming-signal variance and jamming fraction used in the ith IDDD iteration are $\hat{\sigma}_J^{2(i)}[m] = \hat{N}_J/\hat{\eta}^{(i)}[m]$ and $\hat{\eta}^{(i)}[m] = 1/N \sum_{k=0}^{N-1} \hat{C}^{(i-1)}[m,k]$, respectively, with initial jamming fraction, $\hat{\eta}^{(1)}[m] = 1$. The hard-JSI estimates at the end of ith IDDD iteration are obtained as $\hat{C}^{(i)}[m,k] = 0$ if $L(C^{(i)}[m,k]) < 0$; otherwise $\hat{C}^{(i)}[m,k] = 1$.

Following JSI estimation in each IDDD iteration, we apply the soft-JSI estimates to calculate the chip-combining weights, which we have named as *soft-chip combining*. While conventional hard-JSI estimates ($\hat{C}[m,k] \in \{0,1\}$) only reveal the presence of a jamming signal in a particular subchannel, the soft-JSI estimates ($L(C[m,k])$) bears the same information with additional reliability information, which depends on the dominant jamming signal. In the presence of perfect JSI (optimum case), the values of JSI, $C[m,k] \in \{0,1\}$, are utilized to determine the optimum weights for combining the signals on different subcarriers, as shown in (54) and (61). In the ith ($i = 1, 2, \cdots$) iteration of hard-JSI-based

IDDD (H-JSI-IDDD), also in hard-JSI-based despreading before IDD, conventional hard-JSI estimates, $\hat{C}^{(i)}[m,k] \in \{0,1\}$, are used to calculate the chip combining weights as

$$\hat{\rho}^{(i)}[m,k] \;=\; \begin{cases} \gamma_0 \;=\; \frac{1}{N_0} \quad , \;\; \hat{C}^{(i)}[m,k]=0 \\ \hat{\gamma}_1^{(i)} \;=\; \frac{1}{\hat{\sigma}_J^{2(i)}[m]+N_0} \quad , \;\; \hat{C}^{(i)}[m,k]=1 \end{cases} . \tag{76}$$

The estimated JSI given by (74) is noisy. So, its intuitive that the use of soft-JSI estimates in the despreder will yield better performance. To calculate the chip-combining weights, we propose an *ad hoc* scheme by considering the probability of the random JSI. Based on the available LLR of the JSI associated with each subcarrier at the ith IDDD iteration, we compute the average value of $\rho[m,k]$ (soft-chip combining weight) as

$$\begin{aligned} \hat{\rho}^{(i)}[m,k] &= \gamma_0 \; p(C^{(i)}[m,k]=0) + \hat{\gamma}_1^{(i)} \; p(C^{(i)}[m,k]=1) \\ &= \frac{1}{N_0} \, \frac{1}{1+e^{L(C^{(i)}[m,k])}} \;+\; \frac{1}{\hat{\sigma}_J^{2(i)}[m]+N_0} \, \frac{1}{1+e^{-L(C^{(i)}[m,k])}} \;, \end{aligned} \tag{77}$$

where $\gamma_0 = 1/N_0$ and $\gamma_1 = 1/(\sigma_J^2 + N_0)$ are proportional to the ideal inverse noise variances in the absence and presence of PBNJ, respectively. The soft-JSI-based combining weights are then used for iterative weighted despreading (chip combining) as

$$\hat{s}^{(i)}[m] \;=\; \sum_{k=0}^{N-1} \hat{\rho}^{(i)}[m,k] \; B^*[k] \; Y[m,k]; \;\; m \in \mathcal{D} \;, \tag{78}$$

where $\hat{s}^{(i)}[m]$ is the despreader output at the end of the ith IDDD iteration. For soft-JSI-based despreading, the variance of the AWGN-plus-PBNJ contributions at the despreader output is calculated as

$$\begin{aligned} \sigma_{\tilde{J}+\tilde{W}}^{2(i)} \;=\; & \sum_{k=0}^{N-1} \hat{\rho}^2[m,k] \sum_{q=1}^{Q} |\hat{H}^{(q)}[m,k]|^2 \left[N_0 \, \frac{1}{1+e^{L(C^{(i)}[m,k])}} \right. \\ & \left. + \; (N_0 + \hat{\sigma}_J^{2(i)}[m]) \, \frac{1}{1+e^{-L(C^{(i)}[m,k])}} \right]. \end{aligned} \tag{79}$$

7.7 Complexity Analysis

Table 2 shows the order of real number operations (multiplications and additions) required for JSI estimation, pilot-assisted channel estimation, and chip combining for each symbol

Table 2. Computational Complexity - JSI-assisted Channel Estimation and Chip Combining

Function	Number of operations
Pilot-assisted channel estimation	$\mathcal{O}(2NP^2L^2 + P^3L^3 + 3P^2L^2)$
JSI estimation for pilot-assisted channel estimation	$\mathcal{O}(3N(2P+1)Q)$
JSI estimation for chip comb.	$\mathcal{O}(3N((2P+1)Q+3M))$
$\hat{C}_V$ update or chip comb. weight calculation (soft JSI)	$\mathcal{O}(5N)$
Chip comb.	$\mathcal{O}(10N)$

and for each channel-estimation or IDDD iteration. We have not considered the complexity resulting from channel interpolation, demapping, and LLR computation performed by the decoder, since these functions are common to both the IDD and IDDD receivers. Because LSE and MMSE channel estimators have the same order of complexity, we have presented a unified complexity count for the pilot-assisted channel estimators. In measuring the complexity of the channel estimators, we have exploited the symmetric property of the matrix, $\mathbf{G} = \mathbf{B}^H\mathbf{C}_V^{-1}[m]\mathbf{B}$. Considering the cyclic delays at the transmit antennas or by the channel, the elements of $\mathbf{G}$ can be simplified as $[\mathbf{G}]_{l_1,l_2} = \sum_{k=0}^{N-1}[\mathbf{C}_V^{-1}[m]]_{k,k}\ e^{j2\pi k(l_1-l_2)/N}$ for $l_1, l_2 = 0, 1, \ldots, PL-1$. The exponential values, $e^{j2\pi k(l_1-l_2)/N}$, can be read from a look up table using the index (l_1, l_2), whereas the matrix elements, $[\mathbf{C}_V[m]]_{k,k}$ for $k = 0, \ldots, N-1$, are updated using the JSI estimates for the pilot symbols.

The IDDD receivers have same complexity as the IDD receivers, except *iterative despreading*, where the JSI for the data symbols are iteratively estimated and used for iterative chip combining. Therefore, the additional number of operations required for iterative despreading ($i > 1$) of the IDDD receivers is approximately N_{id} times of that required for the only and initial despreading of the IDD receivers, where N_{id} denotes the extra number of despreading performed in the IDDD receivers. The complexity, resulting from soft-JSI-based covariance matrix update for channel estimation, or soft-JSI-based chip combining for data detection, is $\mathcal{O}(5N)$, which is very small compared to the complexity of pilot-assisted channel estimation. In contrast, the complexity for weighted chip combining itself, excluding calculation of the weights, is $\mathcal{O}(10N)$.

7.8 Numerical Results and Discussions

Information bits are convolutional coded before being bit-interleaved, mapped, spread, and cyclicly delayed. The code polynomials used for the 16-state recursive systematic encoder are $G_1 = 21$ and $G_2 = 37$, having constraint length five. Considering the lemmas of Section 7.4, the cyclic delays are selected as $d_p = (p-1)L,\ p = 1, 2, \cdots, P$, which minimizes the channel-estimation mean square errors under full-band noise jamming (FBNJ). In all simulations, code blocks of 2048 bits, pilot insertion interval $N_t = 9$ symbols, code rate $R_c = 1/2$, QPSK modulation, two transmit and two receive antennas are used. The pilot and data symbols have identical power. The delay and power profiles of the time-varying multipath-Rayleigh-fading channel are $0, 1, 2$ $[T_c]$ and $0, -3, -6$ [dB], respectively. All transmit and receive antenna pairs have the same channel power and delay profiles. The channel model order and guard length are $L = 3$ and $G = 3$, respectively. Assuming a dominant jammer, the symbol energy-to-AWGN ratio is $E_s/N_0 = 15$ dB. The carrier frequency, bandwidth, and number of sucarriers are $f_c = 5$ GHz, $B_f = 2$ MHz, and $N = 32$, respectively. Thus, the sampling period is $T_c = 0.5\mu s$. We consider a time-varying channel with mobile speed, $v = 90$ kmh (normalized Doppler rate, $f_d T_s = 0.0073$).

The channel and JSI estimators exchange and exploit each other's outputs iteratively for pilot positions, $m \in \mathcal{P}$. Five iterations between the channel and JSI estimators are performed (six channel estimation iterations including the initial one). The pilot-assisted channel estimates are used to interpolate the channel estimates for the data symbol positions ($m \in \mathcal{D}$) using Wiener filtering [7], which is optimal in MMSE sense. A total of eight filter taps are used for channel interpolation.

The characteristics of the proposed jamming estimator, especially, the knowledge about $\hat{\eta}$ is used to enhance the performance under PBNJ. Simulation results show that average $\hat{\eta}$ increases monotonically with the increase of true jamming fraction, η at any E_s/N_0 and E_s/N_J. Because equal-gain combining is optimal only for FBNJ ($\eta = 1.0$) and errors occur in JSI estimation resulting in $\hat{\eta} < 1.0$, the estimated jamming fraction is compared with

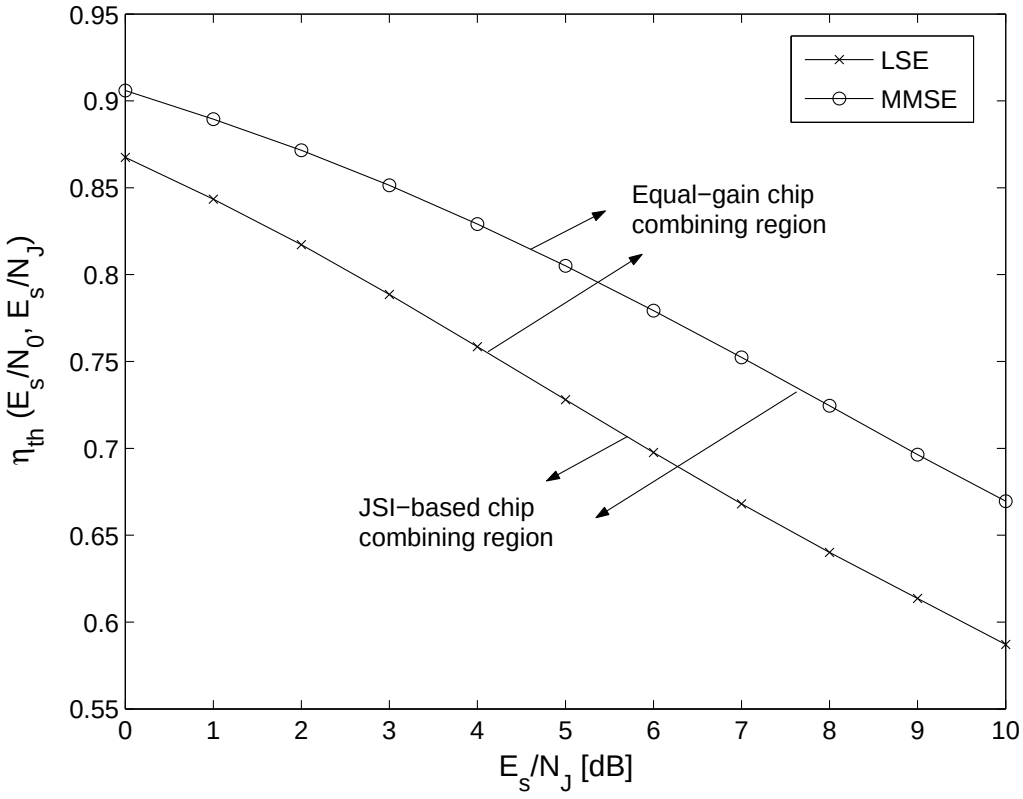

Figure 32. Jamming estimator characteristics under full-band noise jamming: Average of $\hat{\eta}$ with MMSE and LSE channel estimation at E_s/N_0 = 15 dB for different E_s/N_J (2x2 MIMO, three-tap channel, mobile velocity 90 km/h) [η_{th}: Jamming-fraction threshold].

a threshold, η_{th} to determine whether equal-gain or JSI-based chip combining should be performed. The jamming-fraction threshold, which depends on E_s/N_J and E_s/N_0, is the empirical average of $\hat{\eta}$ determined by simulation under FBNJ. Fig. 32 shows η_{th} vs. E_s/N_J characteristic at $E_s/N_0 = 15$ dB. At higher E_s/N_J, the jamming signal is weaker, and the JSI is less likely to be detected accurately. Therefore, the higher E_s/N_J is, the smaller η_{th} is.

Figs. 33(a) and (b) show the BER for different signal-to-jamming ratios (SJR = E_b/N_J) under FBNJ ($\eta = 1.0$) for different anti-jam receiver schemes with the LSE and MMSE channel estimators, respectively. The dotted and solid lines correspond to the results using

iterative demapping and decoding (IDD) and iterative despreading, demapping, and decoding (IDDD) receivers, respectively. The crosses and circles correspond to the receivers using hard JSI (H-JSI) and soft JSI (S-JSI), respectively, for channel estimation as well as chip combining. For the IDD receivers, chip combining is performed just once with either perfect or the initial JSI estimates (hard-JSI or soft-JSI) before beginning iterative demapping and decoding. For each curve, six IDD or IDDD iterations are performed with six channel estimation iterations including the initial one. The effective bit energy-to-jammer noise ratio is defined as $E_b/N_J = E_s/N_J \cdot 1/(R_c \log_2(M)) \cdot (N+G)/N \cdot N_t/(N_t-1)$. The soft-JSI-based channel estimation and chip combining yields smaller BER than conventional hard-JSI-based channel estimation and chip combining, and this effect is evident both in IDD and IDDD receivers. At BER of 10^{-3}, the gains of using soft-JSI over hard-JSI are 1.24 and 1.19 dB for the IDD and IDDD receivers, respectively, with MMSE or LSE channel estimation. The reason is the soft-JSI-based chip combining provides a more improved SINR to the convolutional decoder [29] after demapping than the hard-JSI-based chip combining does.

Figs. 33(a) and (b) also illustrate that under full-band noise jamming, the IDDD schemes outperform the IDD schemes for the same type of JSI. With LSE channel estimation at BER of 10^{-3}, compared to the IDD schemes, the IDDD schemes have a performance gain of 0.51 and 0.46 dB with hard and soft JSI, respectively. With MMSE channel estimation at BER of 10^{-3}, the performance gains with hard and soft JSI are 0.40 and 0.34 dB, respectively. The reason is that a more reliable JSI yields a larger SINR at the demapper output. In IDDD schemes, the JSI is iteratively estimated using the LLR of the coded and interleaved bits from the decoder. However, in IDD schemes, the JSI is estimated just once assuming that all symbols are equally likely (i.e., the LLR of coded bits are zero). Since the initial JSI estimates are not as reliable as those obtained during the later iterations of IDDD schemes, the IDDD schemes achieve smaller BER than the IDD schemes.

The BER of the soft-JSI-based IDDD (S-JSI-IDDD) receiver with LSE and MMSE

channel estimators is plotted in Fig. 34 for different jamming fractions. Under PBNJ with $\eta < 1.0$, this type of receiver with MMSE channel estimation can operate more efficiently (with smaller E_b/N_J) than with LSE channel estimation. Since the quality of the JSI estimates is commensurate with that of the channel estimates, the MMSE channel estimator is more robust against PBNJ than the LSE channel estimator at different jamming fractions. However, an exception occurs at higher E_b/N_J under FBNJ, where the LSE channel estimator yields slightly smaller BER than the MMSE channel estimator. The reasons are as follow.

Both the LSE and MMSE channel estimators use the jamming variance ($\sigma_J^2 = N_J/\eta$) estimates through the noise covariance matrix, $\mathbf{C}_V[m]$ as shown in (42) and (43), respectively. Given a fixed E_b/N_J, the jamming signal in FBNJ is spread over the entire bandwidth, which makes it harder to estimate the average jamming psd, N_J, compared to the narrowband case. So, the noise covariance estimates for $\eta = 1.0$ are less reliable than the covariance estimates when $\eta < 1.0$. The jamming variance estimates, under full-band noise jamming, become even more unreliable with an increase in E_b/N_J, since the jamming-signal power diminishes. The larger estimation error of PBNJ variance estimates at higher E_b/N_J affects the MMSE channel estimator more than the LSE channel estimator because of the presence of the channel covariance matrix ($\mathbf{C}_h^{-1}$) as an additive term in the first set of parentheses of the MMSE channel estimator given in (43). In LSE channel estimation, the effect of PBNJ variance estimation error is alleviated due to the absence of $\mathbf{C}_h^{-1}$ in the first set of parentheses and due to the presence of $\mathbf{C}_V^{-1}[m]$ as product in both the first (inverse) and second (non-inverse) set of parentheses. Therefore, for $\eta = 1.0$, the LSE channel estimator performs slightly better than the MMSE channel estimator at $E_b/N_J \geq 5$ dB. Fig. 35 shows the minimum E_b/N_J required to guarantee BER $\leq 10^{-4}$ for different values of the jamming fraction with MMSE channel estimator.

7.9 Summary

In this chapter, we have investigated joint iterative channel and jamming-parameter estimation techniques for the constant-envelope MC-CDMA cyclic delay diversity system under PBNJ. The jamming parameters included jammer state information and jamming-signal variance. The weighted LSE and MMSE channel estimators are derived and constraints on the cyclic delays are also identified to minimize the corresponding mean square errors under full-band jamming. The signal-space projection-based power estimation technique is applied to our system that works efficiently without training sequences or data symbol decisions. The simple but elegant soft-JSI-based channel estimation and chip-combining method enhances the SINR at the despreader output and outperforms conventional hard-JSI-based channel estimation and chip combining. Our proposed iterative despreading, demapping, and decoding (IDDD) receiver with soft-JSI-based MMSE channel estimation and chip combining is robust against PBNJ with various jamming fractions. The soft-JSI-based channel estimation and chip-combining technique can be applied to any MC-CDMA system operating under jamming or interference from other systems.

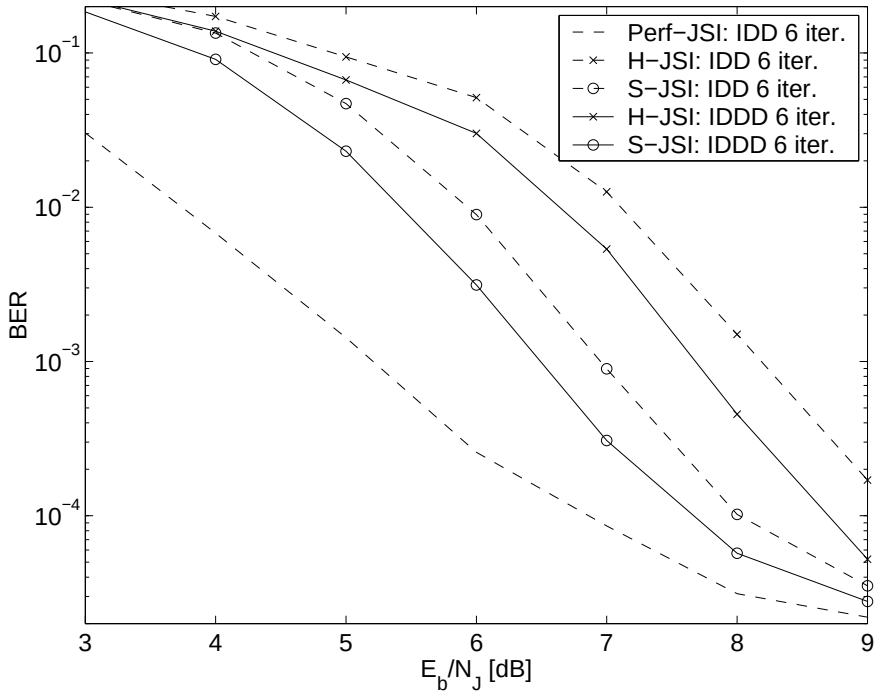

(a) LSE channel estimation

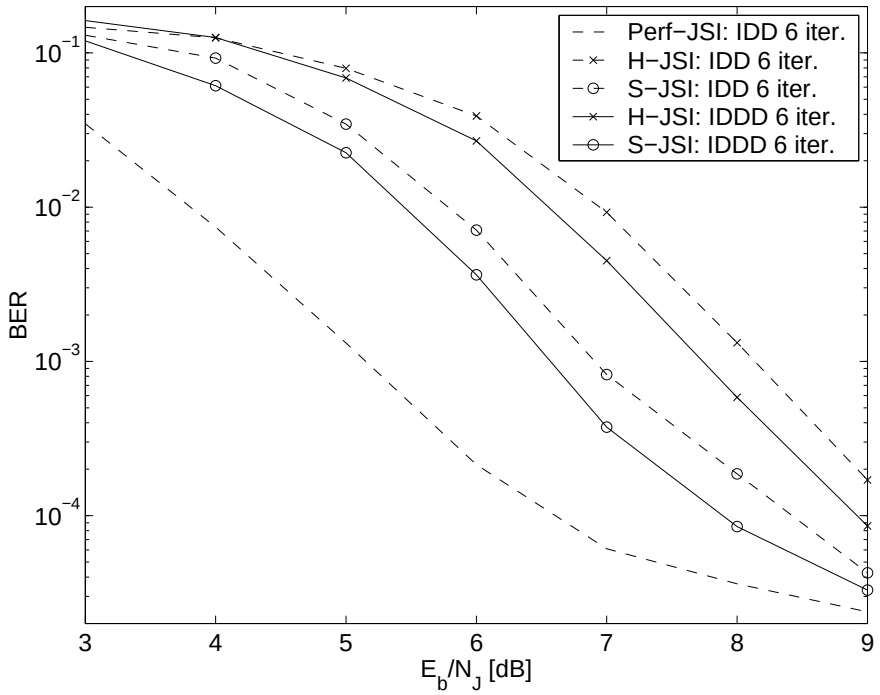

(b) MMSE channel estimation

Figure 33. BER with (a) LSE and (b) MMSE channel estimators for different receiver schemes under full-band noise jamming (Six iterations, E_b/N_0 = 15 dB, 2x2 MIMO, three-tap channel, mobile velocity 90 km/h). [Perf/H/S-JSI: Perfect/hard/soft jammer state information, IDD: Iterative demapping and decoding, IDDD: Iterative despreading, demapping, and decoding]

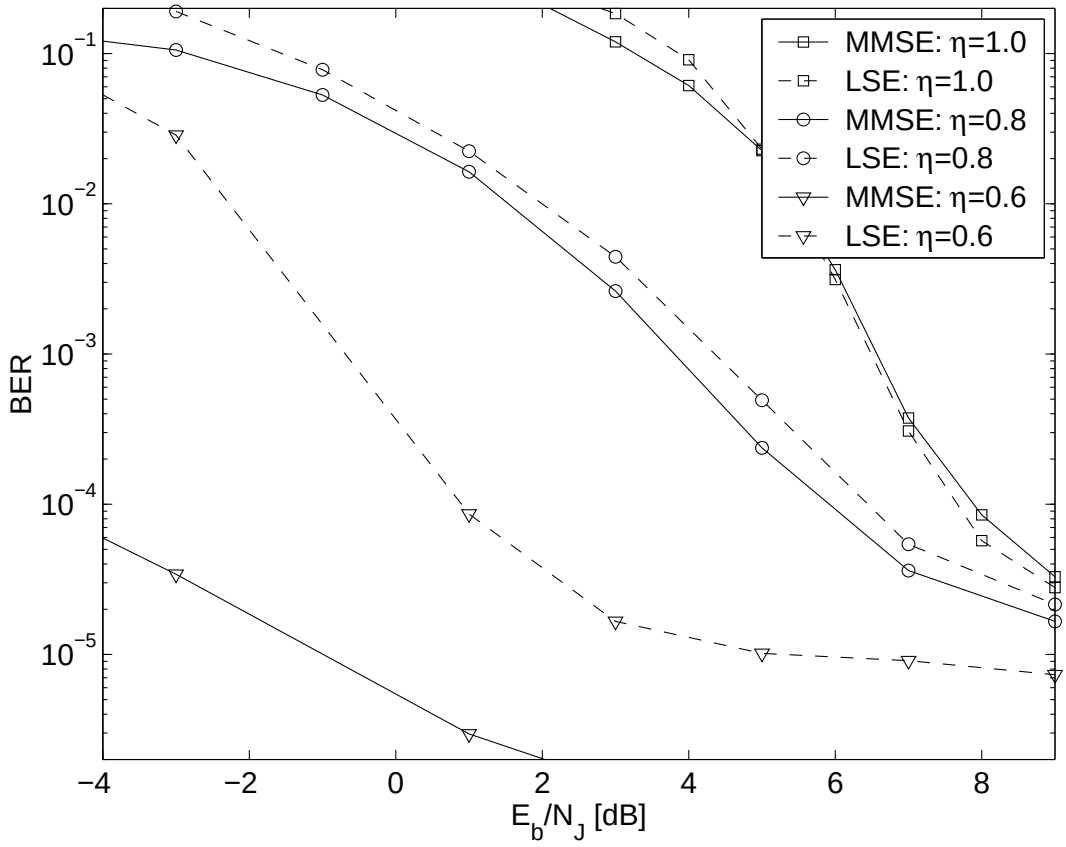

Figure 34. BER of soft-JSI-assisted iterative despreading, demapping, and decoding (S-JSI: IDDD) receiver with LSE and MMSE channel estimation for different values of the jamming fraction (Six iterations, 2x2 MIMO, three-tap channel, mobile velocity 90 km/h).

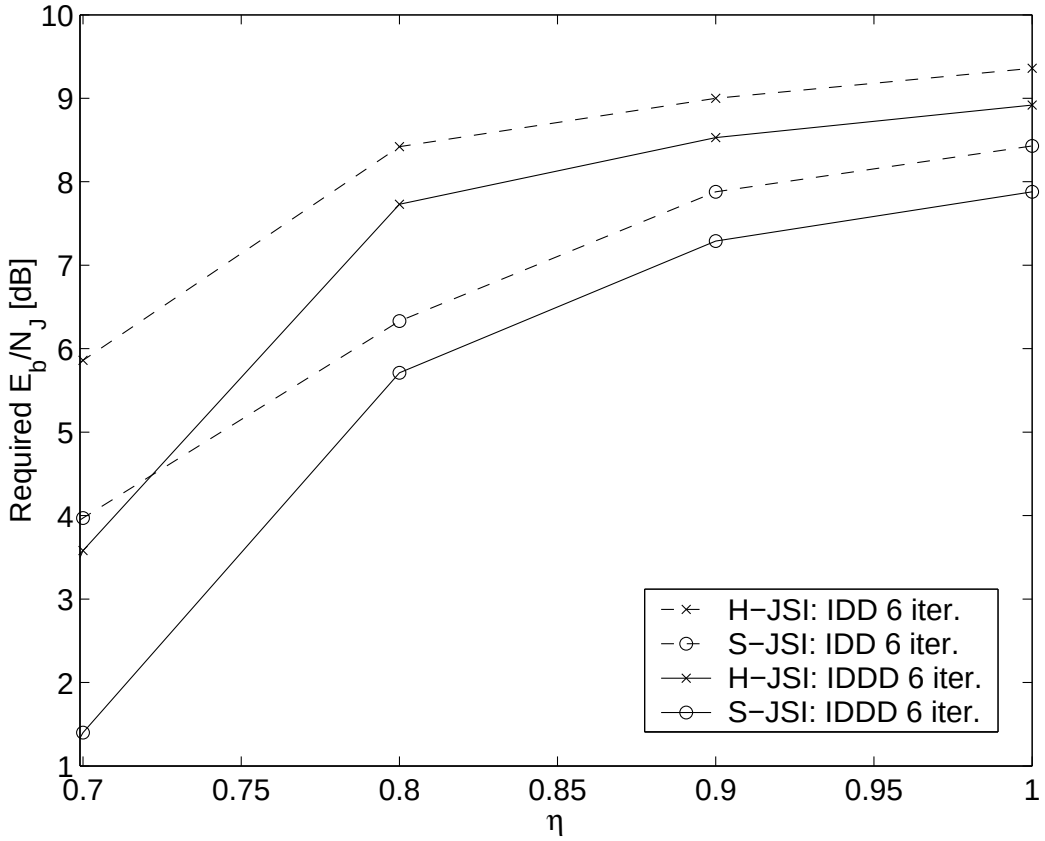

Figure 35. Comparison between hard- and soft-JSI-based IDD and IDDD receivers with MMSE channel estimation: Required E_b/N_J to guarantee BER of 10^{-4} for different jamming fractions (2x2 MIMO, three-tap channel, mobile velocity 90 km/h). [IDD: Iterative demapping and decoding, IDDD: Iterative despreading, demapping, and decoding]

CHAPTER 8

JOINT EM CHANNEL AND COVARIANCE ESTIMATION WITH SUFFICIENT-STATISTIC CHIP COMBINING FOR A SIMO MC-CDMA ANTI-JAM SYSTEM

8.1 Overview

In the previous two chapters, we have shown that chip combining with appropriate despreading weights can mitigate jamming in an MC-CDMA system where each symbol is spread in the frequency domain [43]. In Chapter 7, we have estimated the jammer state information (JSI) and used the JSI estimates for channel estimation and chip combining [44, 45] for the constant-envelope anti-jam MC-CDMA-CDD system. In addition to the JSI, these chip-combining and channel-estimation techniques required knowledge of the individual AWGN and jamming-signal variances for each subcarrier [27, 28]. However, estimation of the JSI increases the computational complexity of the receiver, and obtaining accurate estimates of the AWGN variance in the presence of a jamming signal, or vice versa, is difficult. Hence, it is desirable to design an anti-jam receiver that does not require knowledge of the JSI and individual variances of AWGN and jamming signal on each subcarrier for the purposes of channel estimation and chip combining.

This chapter considers joint estimation of the single-input multiple-output (SIMO) channel coefficients and AWGN-plus-jamming covariance for a convolutional-coded single-user MC-CDMA system operating on a slowly time-varying multipath-Rayleigh-fading channel with partial-band noise jamming (PBNJ). We apply a code-aided expectation-maximization (EM) algorithm [122] to derive the estimators [46, 47]. The initial EM iteration uses pilot-assisted estimates. However, the later EM iterations use pilot symbols as well as the log-likelihood ratios (LLR) of the coded and channel-interleaved bits provided by the decoder. An expectation-maximization algorithm for semi-blind channel estimation of single-input multiple-output flat-fading channels in spatially-correlated noise is studied

in [123] for a single-carrier system. However, the paper does not consider the presence of a jamming signal that occupies some or all the system bandwidth in an on-off fashion.

So far we have only considered the constant-envelope MC-CDMA system using cyclic delay diversity. In this chapter, we consider a generic MC-CDMA system that does not employ any transmit diversity. However, we consider multiple receive antennas because receive diversity provides robustness against jamming and fading channel. The sufficient-statistic chip combiner introduced in Chapter 7 guarantees no loss of information in the soft output generated by the demapper. Hence, we use the sufficient-statistic chip combiner where the chip-combining weights are inversely proportional to the AWGN-plus-PBNJ variances of the corresponding subcarriers. At each iteration, the estimates of channel coefficients and AWGN-plus-PBNJ variance associated with each subcarrier are used for either sufficient-statistic chip combining or minimum mean square error (MMSE) chip combining, which is widely used in MC-CDMA systems [7]. In our approach, the channel estimator or the chip combiner only requires the AWGN-plus-PBNJ power of each subcarrier to suppress jamming. Therefore, significant complexity reduction is achieved because the receiver does not need to estimate the JSI and individual variances of the AWGN and PBNJ on each subcarrier. We consider a single-user rather than a multiuser scenario in order to observe the efficacy of the estimators and chip combiner over the EM iterations, rather than to observe the soft interference cancellation performance in a multiuser scenario. The performance of the estimators is verified with both the MMSE and sufficient-statistic chip-combining techniques, to illustrate the sensitivity of these two different types of chip combining to estimation errors. Simulation results show that the sufficient-statistic chip combiner always offers smaller bit-error rate (BER) than the minimum mean square error (MMSE) chip combiner provided that reliable estimates of the channel impulse response and AWGN-plus-PBNJ covariance are available.

The remainder of this chapter is organized as follows. Section 8.2 describes the signal and system model including the generic MC-CDMA transmitter and receiver, channel

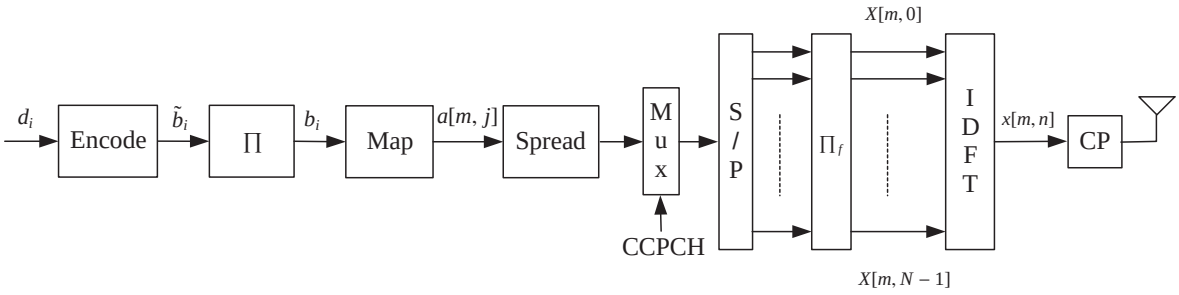

Figure 36. MC-CDMA transmitter.

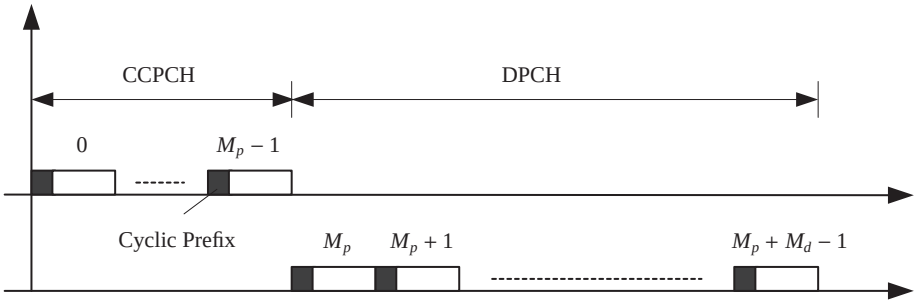

Figure 37. Frame structure.

model, and jamming signal model. Section 8.3 briefly reviews pilot-assisted channel estimation. The proposed joint channel and covariance estimator is presented in Section 8.4, and the optimum chip combiner (in a sufficient statistic sense) is revisited in Section 8.5 for the generic MC-CDMA system. Section 8.6 presents some simulation results and Section 8.7 concludes the chapter.

8.2 Signal and System Model

8.2.1 MC-CDMA Transmitter and Receiver

Fig. 36 depicts a convolutional-coded MC-CDMA transmitter with N subcarriers. Information bits are coded, channel interleaved, and mapped to M-ary phase shift keying (MPSK) data symbols before spreading and converting to MC-CDMA symbols. In the following we shall use the term *MC symbol* to refer to an MC-CDMA symbol. Fig. 37 shows

the frame structure. The frames are formed by multiplexing M_p common control physical channel (CCPCH) and M_d dedicated physical channel (DPCH) MC symbols. Each CCPCH MC symbol carries N_p pilot symbols for training purposes and/or other control signals. On the other hand, the mth ($m \in \{M_p, \cdots, M_p + M_d - 1\}$) DPCH MC symbol of a frame is formed by spreading J data symbols $\{a[m,0], \cdots a[m, J-1]\}$. Spreading of the jth data symbol associated with the mth MC symbol yields the frequency-domain signal $a[m, j] \times \{B[0], \cdots, B[N_s - 1]\}$ for $j \in \{0, 1, \cdots, J-1\}$, where the spreading sequence is $\mathbf{B} = [B[0], \cdots, B[N_s - 1]]^T$, and $N_s = N/J$ is the spreading factor.

The frequency block-interleaver $\Pi_f(j, s)$ ($j = 0, \cdots, J-1$ and $s = 0, \cdots, N_s - 1$) permutes the MC symbols over the system bandwidth to exploit the frequency diversity of the channel. Thus, the signal transmitted on the $k_{j,s}$th subcarrier of the mth MC symbol is $X[m, k_{j,s}] = \sqrt{E_s/N_s}\ a[m, j]B[s]$, where $k_{j,s} = \Pi_f(j, s) \in \{0, 1, \cdots, N-1\}$ for $j = 0, 1, \cdots, J-1$ and $s = 0, 1, \cdots, N_s - 1$. Applying the inverse discrete Fourier transform (IDFT), the frequency-domain signal is transformed into the time domain signal as

$$x[m, n] = \sqrt{\frac{E_s}{N_s}} \sum_{j=0}^{J-1} \sum_{s=0}^{N_s-1} a[m, j]B[s]\, e^{j2\pi k_{j,s} n/N};\ \ n = 0, 1, \cdots, N-1\ , \qquad (80)$$

where E_s is the average received symbol energy. A cyclic prefix or guard interval of length GT_c is appended [108] to facilitate frequency-domain equalization at the receiver, where T_c is the time domain chip duration equal to the sampling period. The guard interval is assumed to be greater than or equal to the maximum excess delay of the channel. Thus, the MC symbol period and frame length are $T = (N + G)T_c$ and $T_f = (M_p + M_d)T$, respectively. The receiver with channel and covariance estimators, and chip combiner is shown in Fig. 38.

8.2.2 Channel Model

We consider a slow multipath-Rayleigh-fading channel. The channel incorporates the transmit filter, propagation channel, and receive filter. Considering any receive antenna

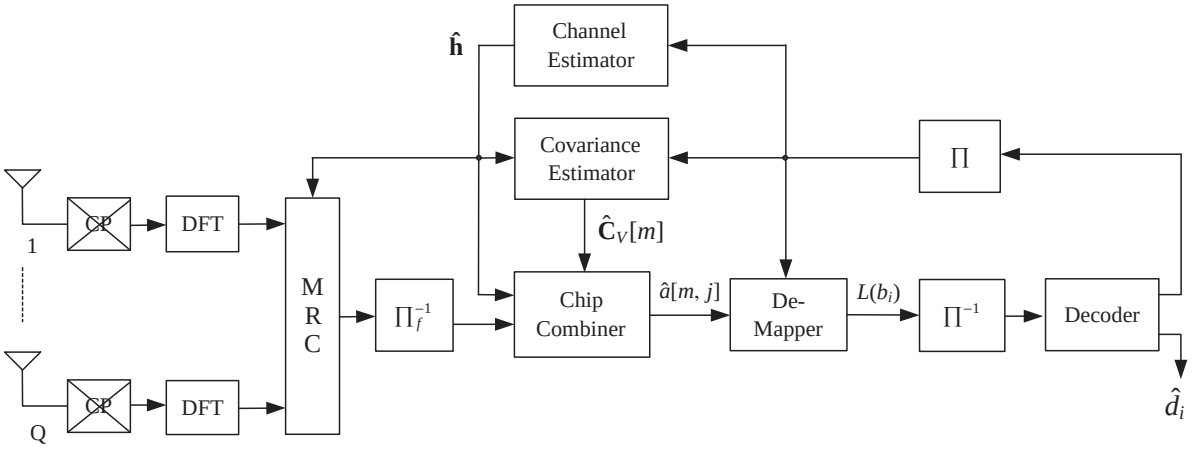

Figure 38. Iterative anti-jam receiver with joint EM channel and covariance estimation and chip combining.

$q \in \{1, \cdots, Q\}$, where Q is the number of receive antennas, the discrete channel frequency response corresponding to the kth subcarrier of the mth MC symbol is $H^{(q)}[m,k] = \sum_{l=0}^{L-1} h^{(q)}[m,l]\ e^{-j2\pi kl/N}$ for $k = 0, 1, \cdots, N-1$, where L is the number of channel taps, and $h^{(q)}[m,l]$ is a zero mean complex Gaussian distributed channel coefficient associated with the lth ($l = 0, 1, \cdots, L-1$) path between the transmit and qth receive antenna. We consider spatially uncorrelated channels. The frequency-response vector corresponding to the qth receive antenna is $\mathbf{H}^{(q)}[m] = \mathbf{F}\ \mathbf{h}^{(q)}[m]$, where the elements of the DFT matrix are $[\mathbf{F}]_{k,l} = e^{-j\frac{2\pi kl}{N}}$ for $k = 0, 1, \cdots, N-1$ and $l = 0, 1, \cdots, L-1$; $\mathbf{h}^{(q)}[m] = [h^{(q)}[m,0], h^{(q)}[m,1], \cdots, h^{(q)}[m,L-1]]^T$; and $\mathbf{H}^{(q)}[m] = [H^{(q)}[m,0], H^{(q)}[m,1], \cdots, H^{(q)}[m,N-1]]^T$.

8.2.3 Jamming Signal Model

Like the previous chapters, the partial-band jammer transmits a jamming signal continuously with a power of P_J watts over a bandwidth ηB_f Hz, where B_f is the signal bandwidth and η is the fraction of bandwidth jammed (also called jamming fraction), hence, $\eta \in (0, 1]$. The average power spectral density of the jammer is $N_J = P_J/B_f$. The power spectral density (PSD) of the jammer in the jammed frequency band is N_J/η and zero in the unjammed band [28]. After removing the cyclic prefix and applying a DFT, the frequency-domain

signal at the qth receive antenna of the mth ($m = 0, \cdots, M_p + M_d - 1$) MC symbol is

$$Y^{(q)}[m,k] \;=\; \sum_{l=0}^{L-1} h^{(q)}[m,l]\, X[m,k]\, e^{-j2\pi kl/N} + C[m,k]J^{(q)}[m,k] + W^{(q)}[m,k] \;, \quad (81)$$

where the $W^{(q)}[m,k]$ are independent identically distributed (i.i.d.) AWGN samples having zero mean and variance N_0, $C[m,k] \in \{0,1\}$ is the JSI associated with the kth subcarrier of the mth MC symbol, and $J^{(q)}[m,k]$ is the i.i.d. Gaussian jamming signal at the qth receive antenna having zero mean and variance $\sigma_J^2 = N_J/\eta$. The JSI $C[m,k] = 1$ when the kth subcarrier of the mth symbol is jammed, and $C[m,k] = 0$ otherwise. For simplicity of analysis, it is assumed that each subchannel is either completely jammed or not at all.

8.3 Pilot-Assisted Channel Estimation

Pilot-assisted channel estimates provide the initial channel estimates for the first EM iteration ($\mu = 0$). The unknown covariance matrices for the CCPCH MC symbols ($m = 0, \cdots, M_p - 1$) are assumed to be $\mathbf{C}_V[m] = \mathbf{I}_N$ during the initial channel estimation, where $\mathbf{I}_N$ denotes $N \times N$ identity matrix. Because the number of subcarriers is usually much larger than the number of discrete channel taps (i.e., $N \gg L$), the estimation of $\mathbf{h}^{(q)}[m]$ involves fewer unknowns than the estimation of $\mathbf{H}^{(q)}[m]$. Therefore, for any transmitted pilot symbols over the CCPCH, it suffices to estimate the parameters $\{h^{(q)}[m,l]\}_{l=0}^{L-1}$ from the received signal at each antenna.

The signals received on the different subcarriers at any receive antenna q can be arranged in a column vector as follows

$$\begin{aligned} \mathbf{Y}^{(q)}[m] \;&=\; \left[Y^{(q)}[m,0], Y^{(q)}[m,1], \cdots, Y^{(q)}[m,N-1]\right]^T \\ &=\; \mathbf{A}[m]\, \mathbf{h}^{(q)}[m] \;+\; \mathbf{V}^{(q)}[m] \;, \end{aligned} \quad (82)$$

where $\mathbf{h}^{(q)}[m] = [h^{(q)}[m,0], h^{(q)}[m,1], \cdots, h^{(q)}[m,L-1]]^T$ is the channel-coefficient vector, $\mathbf{V^{(q)}}[m] = \left[V^{(q)}[m,0], V^{(q)}[m,1], \cdots \;\cdots, V^{(q)}[m,N-1]\right]^T$ is the AWGN-plus-PBNJ vector with $V^{(q)}[m,k] = C[m,k]J^{(q)}[m,k] + W^{(q)}[m,k]$, $\mathbf{A}[m] = \mathbf{D}[m]\mathbf{F}$, and $\mathbf{D}[m] = \text{diag}(X[m,0], \cdots, X[m,N-1])$ is an $N \times N$ matrix that depends on the pilot (or data) symbols. Because the

AWGN and PBNJ signals are spatially and temporally uncorrelated random processes, for the mth MC-CDMA symbol, the AWGN-plus-PBNJ signal vector ($\mathbf{V^{(q)}}[m]$) at any receive antenna q has zero mean and covariance

$$\begin{aligned}
\mathbf{C}_V[m] &= E\left[\mathbf{V}^{(q)}[m]\mathbf{V}^{(q)H}[m]\right] \\
&= \text{diag}\left(C_V[m,0],\cdots,C_V[m,N-1]\right) \\
&= \frac{N_J}{\eta}\begin{bmatrix} C[m,0] & 0 & \cdots & 0 \\ 0 & C[m,1] & \cdots & 0 \\ \vdots & \vdots & \ddots & \vdots \\ 0 & 0 & \cdots & C[m,N-1] \end{bmatrix} + N_0\,\mathbf{I}_N \ , \qquad (83)
\end{aligned}$$

where $\mathbf{C}_V[m,k] = E[|V^{(q)}[m,k]|^2] = \frac{N_J}{\eta}\,C[m,k] + N_0$ is the kth ($k = 0,\cdots,N-1$) diagonal element of $\mathbf{C}_V[m]$, and $E[\ \cdot\ ]$ denotes expectation. The JSI pattern, $\{C[m,k]\}_{k=0}^{N-1}$, varies randomly over the MC symbols. Therefore, $\mathbf{C}_V[m]$ is different for different MC symbols since the set of jammed subcarriers changes randomly.

By arranging the frequency-domain signals from different received antennas in a column vector, we obtain

$$\begin{aligned}
\mathbf{Y}[m] &= \left[\mathbf{Y}^{(1)T}[m], \mathbf{Y}^{(2)T}[m], \cdots, \mathbf{Y}^{(Q)T}[m]\right]^T \\
&= \mathbf{S}[m]\,\mathbf{h}[m] \ + \ \mathbf{V}[m] \ , \qquad (84)
\end{aligned}$$

where the channel-coefficient and AWGN-plus-PBNJ vectors associated with all receive antennas of the mth MC-CDMA symbol are $\mathbf{h}[m] = [\mathbf{h}^{(1)T}[m], \cdots, \mathbf{h}^{(Q)T}[m]]^T$, $\mathbf{V}[m] = [\mathbf{V}^{(1)T}[m], \cdots, \mathbf{V}^{(Q)T}[m]]^T$, and the $QN \times QL$ matrix, $\mathbf{S}[m]$, is defined as

$$\mathbf{S}[m] = \begin{bmatrix} \mathbf{A}[m] & \mathbf{0} & \cdots & \mathbf{0} \\ \mathbf{0} & \mathbf{A}[m] & \cdots & \mathbf{0} \\ \vdots & \vdots & \ddots & \vdots \\ \mathbf{0} & \mathbf{0} & \cdots & \mathbf{A}[m] \end{bmatrix}. \qquad (85)$$

Because AWGN and jamming signal are spatially uncorrelated, the covariance of $\mathbf{V}[m]$ is

a $QN \times QN$ matrix given as

$$\begin{aligned}\tilde{\mathbf{C}}_V[m] &= E\left[\mathbf{V}[m]\mathbf{V}^H[m]\right] \\ &= \begin{bmatrix} \mathbf{C}_V[m] & \mathbf{0} & \cdots & \mathbf{0} \\ \mathbf{0} & \mathbf{C}_V[m] & \cdots & \mathbf{0} \\ \vdots & \vdots & \ddots & \vdots \\ \mathbf{0} & \mathbf{0} & \cdots & \mathbf{C}_V[m] \end{bmatrix}. \end{aligned} \tag{86}$$

To derive the channel estimator, we assume that the channel is quasi-static over a frame, i.e., $\mathbf{h}[m] \approx \mathbf{h}$ for $m = 0, 1, \cdots, M_p + M_d - 1$, but later we will dispense this assumption when evaluating its performance. The frequency-domain signal vectors (given in (84)) corresponding to the CCPCH MC symbols can be arranged in a column vector as

$$\mathbf{Y}_p = \mathbf{S}_p\mathbf{h} + \mathbf{V}_p \ , \tag{87}$$

where $\mathbf{Y}_p = [\mathbf{Y}^T[0], \ldots, \mathbf{Y}^T[M_p - 1]]^T$, $\mathbf{S}_p = [\mathbf{S}^T[0], \ldots, \mathbf{S}^T[M_p - 1]]^T$, and $\mathbf{V}_p = [\mathbf{V}^T[0], \cdots, \mathbf{V}^T[M_p - 1]]^T$ with covariance, $\mathbf{C}_{V_p} = \text{diag}\ (\tilde{\mathbf{C}}_V[0], \cdots, \tilde{\mathbf{C}}_V[M_p - 1])$. Because the AWGN-plus-PBNJ signal is Gaussian distributed and $\mathbf{C}_V^{-1}[m]$ is diagonal with diagonal elements $\left[C[m,k]\frac{N_J}{\eta} + N_0\right]^{-1}$, the maximum-likelihood (ML) channel estimator can be derived by maximizing the log-likelihood function, $\Lambda\left(\tilde{\mathbf{h}}\right) = \log\ p\left(\mathbf{Y}_p \mid \mathbf{S}_p, \tilde{\mathbf{h}}\right)$ with respect to the channel vector $\tilde{\mathbf{h}}^{(q)}$. For the initial EM iteration ($\mu = 0$), the unknown covariance is assumed as $\mathbf{C}_{V_p} = \mathbf{I}_{NQM_p}$. Thus, the maximum-likelihood channel estimator is obtained as [117]

$$\hat{\mathbf{h}}_{ML} = \left(\mathbf{S}_p{}^H\mathbf{S}_p\right)^{-1}\mathbf{S}_p{}^H\,\mathbf{Y}_p \ . \tag{88}$$

Simplifying (88), we derive at the ML channel-estimate vector for the qth ($q \in \{1, 2, \ldots, Q\}$) receive antenna as

$$\hat{\mathbf{h}}_{ML}^{(q)} = \left(\mathbf{F}^H\left[\sum_{m=0}^{M_p-1}\mathbf{D}^H[m]\mathbf{D}[m]\right]\mathbf{F}\right)^{-1}\mathbf{F}^H\left[\sum_{m=0}^{M_p-1}\mathbf{D}^H[m]\,\mathbf{Y}^{(q)}[m]\right]. \tag{89}$$

8.4 Joint Channel and Covariance Estimation

8.4.1 EM Principle

Expectation-maximization algorithm [122] provides a systematic-iterative method to find the maximum-likelihood estimates when the signal model can be formulated in terms of *complete (unobserved)* and *incomplete (observed)* data. Let us denote the complete and incomplete data as $\mathbf{z}$ and $\mathbf{y}$, respectively. The hypothetical complete data space must be larger than the observed data space and related by some many-to-one mapping as $\mathbf{y} = f(\mathbf{z})$. Let θ be the parameter set to be estimated from the observation $\mathbf{y}$.

First, a complete data set is obtained, and θ is initialized with a feasible estimate $\hat{\theta}(0)$. Then, for any iteration $\mu > 0$, the following two steps are iterated:

- Step 1: Expectation of the log-likelihood function of the complete data given the observation and current estimate of θ with respect to the complete data space yields

$$Q\left(\theta|\hat{\theta}(\mu)\right) \;=\; E_{\mathbf{z}}\left[\log\; p\,(\mathbf{z}|\theta)\,|\,\mathbf{y}, \hat{\theta}(\mu)\right] \tag{90}$$

- Step 2: Maximization of $Q\left(\theta|\hat{\theta}(\mu)\right)$ with respect to θ to find the new estimate

$$\hat{\theta}(\mu+1) \;=\; \arg\max_{\theta}\; Q\left(\theta|\hat{\theta}(\mu)\right) \tag{91}$$

Dempster [122] proved that given a good initial estimate $\hat{\theta}(0)$, the EM algorithm always converges. Therefore, the incomplete data log-likelihood function given the estimates is nondecreasing with each EM iteration, i.e.,

$$p\left(\mathbf{y}\,|\,\hat{\theta}(\mu+1)\right) \;\geq\; p\left(\mathbf{y}\,|\,\hat{\theta}(\mu)\right). \tag{92}$$

8.4.2 Iterative Channel and Covariance Estimation

The incomplete or observed data is obtained by organizing the frequency-domain received signal vectors associated with a frame in a column vector as

$$\begin{aligned}\mathbf{Y} \;&=\; [\mathbf{Y}^T[0], \ldots, \mathbf{Y}^T[M_p-1], \mathbf{Y}^T[M_p], \ldots, \mathbf{Y}^T[M_p+M_d-1]]^T \\ &=\; \mathbf{S}\,\mathbf{h} \;+\; \mathbf{V}\;,\end{aligned} \tag{93}$$

where the channel-coefficient vector is $\mathbf{h} = [\mathbf{h}^{(1)^T}, \ldots, \mathbf{h}^{(Q)^T}]^T$, $\mathbf{S} = [\mathbf{S}^T[0], \ldots, \mathbf{S}^T[M_p - 1], \mathbf{S}^T[M_p], \ldots, \mathbf{S}^T[M_p + M_d - 1]]^T$, and the AWGN-plus-PBNJ vector is $\mathbf{V} = [\mathbf{V}^T[0], \ldots, \mathbf{V}^T[M_p - 1], \mathbf{V}^T[M_p], \ldots, \mathbf{V}^T[M_p + M_d - 1]]^T$ with covariance matrix $\mathbf{C}_V = \text{diag}\,(\tilde{\mathbf{C}}_V[0], \ldots, \tilde{\mathbf{C}}_V[M_p - 1], \tilde{\mathbf{C}}_V[M_p], \cdots, \tilde{\mathbf{C}}_V[M_p + M_d - 1])$.

We are interested in estimating the channel vector $\mathbf{h}$ and the diagonal elements of the covariance matrix $\{\mathbf{C}_V[m]\}_{m=0}^{M_p+M_d-1}$. Let $\theta = \{\mathbf{h}, \mathbf{C}_V\}$ be the set of parameters to be estimated. The EM algorithm starts with an initial estimate $\hat{\theta}(0) = \{\hat{\mathbf{h}}_{ML},\ \mathbf{I}_{NQ(M_p+M_d)}\}$. We choose the complete data set as $\mathbf{z} = [\mathbf{Y}, \mathbf{X}]$, where the transmitted frequency-domain signal vector corresponding to the frame is $\mathbf{X} = [\mathbf{X}^T[0], \cdots, \mathbf{X}^T[M_p - 1], \mathbf{X}^T[M_p], \cdots\cdots, \mathbf{X}^T[M_p + M_d - 1]]^T$, and the signal vector transmitted over the subcarriers during the mth MC symbol is $\mathbf{X}[m] = [X[m, 0], \cdots, X[m, N - 1]]^T$.

Since $\mathbf{X}$ and θ are independent

$$p\,(\mathbf{z}|\theta) \quad \propto \quad p\,(\mathbf{Y}|\,\mathbf{X}, \theta) \tag{94}$$

and the expectation function in (90) at iteration μ becomes

$$\begin{aligned} Q\left(\theta|\hat{\theta}(\mu)\right) &= E_{\mathbf{X}}\left[\log\ p\,(\mathbf{Y}|\mathbf{X}, \theta)\,|\,\mathbf{Y}, \hat{\theta}(\mu)\right] \\ &\propto -\log|\mathbf{C}_V| - tr\left\{\mathbf{C}_V^{-1}\mathbf{\Sigma}\right\}\ , \end{aligned} \tag{95}$$

where $|\cdot|$ and $tr\{\cdot\}$ denote the determinant and trace of a matrix, respectively, and $\mathbf{\Sigma}$ is defined as

$$\mathbf{\Sigma} \quad = \quad E_{\mathbf{X}}\left[(\mathbf{Y} - \mathbf{Sh})\,(\mathbf{Y} - \mathbf{Sh})^H\ \mid\ \mathbf{Y}, \hat{\theta}(\mu)\right]. \tag{96}$$

Maximizing $Q\left(\theta|\hat{\theta}(\mu)\right)$ with respect to $\mathbf{C}_V$ yields

$$\mathbf{C}_V \quad = \quad \mathbf{\Sigma}. \tag{97}$$

Substituting (97) in (95) yields

$$Q\left(\theta|\hat{\theta}(\mu)\right) \quad = \quad -\log|\mathbf{\Sigma}| - NQ(M_p + M_d)\ , \tag{98}$$

which does not depend on the covariance and is a function of **h** only. Now, maximizing $Q\left(\theta|\hat{\theta}(\mu)\right)$ with respect to **h** yields the new channel estimate

$$\hat{\mathbf{h}}(\mu+1) \;=\; \left(\overline{\mathbf{S}^H\mathbf{S}(\mu)}\right)^{-1}\overline{\mathbf{S}^H(\mu)}\,\mathbf{Y}\;, \tag{99}$$

where $\overline{\mathbf{S}^H\mathbf{S}(\mu)} = E_{\mathbf{X}}\left[\mathbf{S}^H\mathbf{S} \mid \mathbf{Y}, \hat{\theta}(\mu)\right]$, and $\overline{\mathbf{S}(\mu)} = E_{\mathbf{X}}\left[\mathbf{S} \mid \mathbf{Y}, \hat{\theta}(\mu)\right]$. By substituting the expressions for **S**, thus **A**[m], in (99), the new channel-coefficient estimates for the qth antenna ($q = 1, \ldots, Q$) is derived as

$$\begin{aligned}
\hat{\mathbf{h}}^{(q)}(\mu+1) &= \left(\mathbf{F}^H\sum_{m=0}^{M_p+M_d-1}\overline{\mathbf{D}^H[m]\mathbf{D}[m]}\,\mathbf{F}\right)^{-1}\mathbf{F}^H\sum_{m=0}^{M_p+M_d-1}\overline{\mathbf{D}^H[m]}\,\mathbf{Y}^{(q)}[m] \qquad (100)\\
\overline{\mathbf{D}[m]} &= \mathrm{diag}\left(\overline{X[m,0]}, \cdots, \overline{X[m,N-1]}\right)\;,\\
\overline{\mathbf{D}^H[m]\mathbf{D}[m]} &= \mathrm{diag}\left(\overline{|X[m,0]|^2}, \cdots, \overline{|X[m,N-1]|^2}\right)\;,
\end{aligned}$$

where $\overline{X[m,k_{j,s}]} = \sqrt{\frac{E_s}{N_s}}\,B[s]\,E_{\mathbf{X}}\left[a[m,j] \mid \mathbf{Y}, \hat{\theta}(\mu)\right]$ for $k_{j,s} \in \{0, \cdots, N-1\}$, and $\overline{|X[m,k_{j,s}]|^2}$ $= \frac{E_s}{N_s}\,|B[s]|^2\,E_{\mathbf{X}}\left[|a[m,j]|^2 \mid \mathbf{Y}, \hat{\theta}(\mu)\right]$. The *a posteriori* expectations are performed using the LLR from the convolutional decoder as

$$\begin{aligned}
E_{\mathbf{X}}\left[a[m,j]|\mathbf{Y}, \hat{\theta}(\mu)\right] &= \sum_{a\in\mathcal{A}} a\,P_r\left(a[m,j] = a|\mathbf{Y}, \hat{\theta}(\mu)\right)\;,\\
E_{\mathbf{X}}\left[|a[m,j]|^2|\mathbf{Y}, \hat{\theta}(\mu)\right] &= \sum_{a\in\mathcal{A}} |a|^2\,P_r\left(a[m,j] = a|\mathbf{Y}, \hat{\theta}(\mu)\right)\;, \qquad (101)
\end{aligned}$$

where $\mathcal{A}$ denotes the set of all hypothetical decoded symbols, $P_r\left(a[m,j] = a|\mathbf{Y}, \hat{\theta}(\mu)\right) = \prod_{i=0}^{\log_2 M-1} P_r(b_i|\mathbf{Y}, \hat{\theta}(\mu))$ is the *a posteriori* symbol probability, and $\{b_{(\log_2 M-1)}, \cdots, b_0\}$ is the coded and bit-interleaved code-bit sequence associated with symbol a. Because of bit interleaving after error-correction encoding, the code bits corresponding to any symbol can be treated as being independent from each other. Thus, the new channel-frequency-response estimates are calculated as $\hat{\mathbf{H}}^{(q)}(\mu+1) = \mathbf{F}\,\hat{\mathbf{h}}^{(q)}(\mu+1)$ for $q = 1, \cdots, Q$.

Given the new channel estimates, the AWGN-plus-PBNJ covariance, $\mathbf{C}_V$ given in (97), corresponding to all the MC symbols in a frame can be expressed as

$$\hat{\mathbf{C}}_V(\mu+1) \;=\; E_{\mathbf{X}}\left[\left(\mathbf{Y} - \mathbf{S}\,\hat{\mathbf{h}}(\mu+1)\right)\left(\mathbf{Y} - \mathbf{S}\,\hat{\mathbf{h}}(\mu+1)\right)^H \;\middle|\; \mathbf{Y}, \hat{\theta}(\mu)\right]\;. \tag{102}$$

We need to estimate the diagonal elements of the covariance matrices, $\{\mathbf{C}_V[m]\}_{m=M_p}^{M_p+M_d-1}$ given in (83), for calculating the chip-combining weights as explained later in Section 8.5. Since the matrices $\mathbf{C}_V$ and $\{\tilde{\mathbf{C}}_V[m]\}_{m=0}^{M_p+M_d-1}$ are diagonal, from (102), the AWGN-plus-PBNJ covariance estimate for any receive antenna $q \in \{1, 2, \ldots, Q\}$ for the mth MC-CDMA symbol is

$$\hat{\mathbf{C}}_V[m](\mu+1) = E_{\mathbf{X}}\left[\left(\mathbf{Y}^{(q)}[m] - \mathbf{D}[m]\,\hat{\mathbf{H}}^{(q)}(\mu+1)\right)\left(\mathbf{Y}^{(q)}[m] - \mathbf{D}[m]\,\hat{\mathbf{H}}^{(q)}(\mu+1)\right)^H \mid \mathbf{Y}, \hat{\theta}(\mu)\right] . \tag{103}$$

The above expectation is conditioned on $\mathbf{Y}$ and $\hat{\theta}(\mu) = \{\hat{\mathbf{h}}(\mu), \hat{\mathbf{C}}_V(\mu)\}$, both of which include the received signals and channel coefficients, respectively, associated with all the receive antennas. The AWGN-plus-PBNJ covariance during a particular MC symbol period is same for all the receive antennas. Therefore, the new estimates of $\mathbf{C}_V[m]$ can be approximated as

$$\hat{\mathbf{C}}_V[m](\mu+1) \approx \frac{1}{Q}\sum_{q=1}^{Q}\left(\mathbf{Y}^{(q)}[m] - \overline{\mathbf{D}}[m]\,\hat{\mathbf{H}}^{(q)}(\mu+1)\right)\left(\mathbf{Y}^{(q)}[m] - \overline{\mathbf{D}}[m]\,\hat{\mathbf{H}}^{(q)}(\mu+1)\right)^H . \tag{104}$$

Note that the above channel and covariance estimators given in (100) and (104), respectively, do not require the knowledge of the JSI and the individual variances of the AWGN and jamming signal.

8.5 Sufficient-Statistic Chip Combining

The chip combiner presented in this section is the same as the sufficient-statistic chip combiner presented in Chapter 7. However, we revisit the topic in the context of the MC-CDMA system shown in Fig. 36. The kth received subcarrier signal after removing the cyclic prefix and applying a DFT at each receive antenna is given in (81). After maximal-ratio combining (MRC) of the different receive-antenna signals, the output corresponding to the $k_{j,s}$th ($k_{j,s} = 0, \cdots, N-1$) subcarrier of the mth DPCH MC symbol is

$$Y[m, k_{j,s}] = \sqrt{\frac{E_s}{N_s}}\sum_{q=1}^{Q}\left|H^{(q)}[m, k_{j,s}]\right|^2 a[m, j]B[s] + J[m, k] + W[m, k] , \tag{105}$$

where the data symbols $\{a[m, j]\}_{j=0}^{J-1}$ are transmitted over the subcarriers during the mth MC symbol, and the contributions from PBNJ and AWGN are, respectively, $J[m, k_{j,s}] =$

$C[m,k_{j,s}]\ \sum_{q=1}^{Q} H^{(q)^*}[m,k_{j,s}]\ J^{(q)}[m,k_{j,s}]$ and $W[m,k_{j,s}] = \sum_{q=1}^{Q} H^{(q)^*}[m,k_{j,s}]\ W^{(q)}[m,k_{j,s}]$. Given the channel coefficients, $J[m,k_{j,s}]$ and $W[m,k_{j,s}]$ are zero-mean Gaussian distributed with variances (dropping the MC symbol index m from notations)

$$\sigma^2_{J_{k_{j,s}}} = \begin{cases} 0 & , \quad C[m,k_{j,s}] = 0 \\ \frac{N_J}{\eta} \sum_{q=1}^{Q} \left| H^{(q)}[m,k_{j,s}] \right|^2 & , \quad C[m,k_{j,s}] = 1 \end{cases} \tag{106}$$

and $\sigma^2_{W_{k_{j,s}}} = N_0 \sum_{q=1}^{Q} \left| H^{(q)}[m,k_{j,s}] \right|^2$, respectively.

The maximal-ratio combined signals in (105) for the different subcarriers are (chip) combined, then demapped and decoded. If the frequency-domain MRC output vector associated with the jth data symbol of the mth MC symbol is $\mathbf{Y}_j[m] = [Y[m,k_{j,0}], \ldots, Y[m,k_{j,N_s-1}]]^T$, and the coded and bit-interleaved sequence corresponding to the same data symbol is denoted by $\{b_i\}_{i=0}^{\log_2 M-1}$, then the LLR of *a posteriori* probability (APP) of b_i generated by the demapper is [112]

$$\begin{aligned} L(b_i) &= \log\left[\frac{p(b_i = 1 \mid \mathbf{Y}_j[m], \theta)}{p(b_i = 0 \mid \mathbf{Y}_j[m], \theta)}\right] \\ &= \log\left[\frac{\sum_{a \in \mathcal{A}: b_i = 1} p\left(\mathbf{Y}_j[m] \mid a, \theta\right)\ p(a)}{\sum_{a \in \mathcal{A}: b_i = 0} p\left(\mathbf{Y}_j[m] \mid a, \theta\right)\ p(a)}\right] , \end{aligned} \tag{107}$$

where $a \in \mathcal{A}$ is the hypothetical data symbol, and $\mathcal{A}$ is the set of all possible data symbols.

In the following, we show that under Gaussian distributed PBNJ and AWGN, the chip-combining weights that provide a sufficient statistics to the demapper are inversely proportional to the AWGN-plus-PBNJ variance [44, 45]. To determine the chip-combining weights necessary for calculating appropriate LLRs at the demapper (from an information theoretic perspective), consider the conditional likelihood function $p\left(\mathbf{Y}_j[m] \mid a, \theta\right)$, where the parameter set θ and the symbol (random parameter of interest) a are known. After

ignoring the irrelevant terms, the conditional log-likelihood function, can be expressed as

$$\begin{aligned}\log\ p\left(\mathbf{Y}_j[m]\,|\,a,\theta\right) &= -\sum_{s=0}^{N_s-1}\log\left[\pi(\sigma^2_{W_{k_{j,s}}}+\sigma^2_{J_{k_{j,s}}})\right] \\ &\quad -\sum_{s=0}^{N_s-1}\frac{1}{\sigma^2_{W_{k_{j,s}}}+\sigma^2_{J_{k_{j,s}}}}\left|Y[m,k_{j,s}]-\sqrt{\frac{E_s}{N_s}}\sum_{q=1}^{Q}\left|H^{(q)}[m,k_{j,s}]\right|^2 B[s]\,a\right|^2 \\ &\propto 2\sqrt{\frac{E_s}{N_s}}\,\Re\mathrm{e}\left[\left(\sum_{s=0}^{N_s-1}\frac{1}{N_0+C[m,k_{j,s}]\frac{N_J}{\eta}}\,B^*[s]\,Y[m,k_{j,s}]\right)a^*\right]\ , \qquad (108)\end{aligned}$$

where $\Re\mathrm{e}[\cdot]$ denotes the real part of a complex number. The hypothetical parameter of interest (a) must be coupled with the sufficient statistic but not with the observation vector ($\mathbf{Y}_j[m]$). Using Fisher's factorization theorem [117] [119], the sufficient statistic for any data symbol is $\mathcal{T}(\mathbf{Y}_j[m]) = \sum_{s=0}^{N_s-1}\frac{1}{N_0+C[m,k_{j,s}]\frac{N_J}{\eta}}\,B^*[s]\,Y[m,k_{j,s}] = \sum_{s=0}^{N_s-1}\frac{1}{\mathbf{C}_V[m,k_{j,s}]}\,B^*[s]\,Y[m,k_{j,s}]$, which must be provided to the demapper in order to evaluate appropriate likelihood functions for calculating the LLR of the coded and interleaved bits. The sufficient statistic $\mathcal{T}(\mathbf{Y}_j[m])$ satisfies the condition for equality in the data processing inequality and preserves mutual information [120] as

$$I\left(a;\mathbf{Y}_j[m]\right) = I\left(a;\mathcal{T}(\mathbf{Y}_j[m])\right)\ , \qquad (109)$$

where $I(s;\mathbf{Y}_j[m])$ denotes the mutual information between the random variable a and observed vector $\mathbf{Y}_j[m]$, and $I(a,t)$ is the mutual information between the random variables a and t. Thus, the optimum (sufficient statistic sense) chip combining weights must be inversely proportional to the AWGN-plus-PBNJ variance of the relevant subcarriers.

After chip combining at the despreader, the input signal to the demapper for the jth data symbol of the mth MC symbol is becomes

$$\begin{aligned}\hat{a}[m,j] &= \mathcal{T}(\mathbf{Y}_j[m]) = \sum_{s=0}^{N_s-1}\rho[m,k_{j,s}]\,B^*[s]\,Y[m,k_{j,s}] \\ &= \sqrt{\frac{E_s N}{N_s}}\sum_{s=0}^{N_s-1}\rho[m,k_{j,s}]\sum_{q=1}^{Q}\left|H^{(q)}[m,k_{j,s}]\right|^2 a[m,j]+\tilde{J}[m,j]+\tilde{W}[m,j]\ , \qquad (110)\end{aligned}$$

where the contributions from PBNJ and AWGN at the despreader output are $\tilde{J}[m,j] = \sum_{s=0}^{N_s-1}\rho[m,k_{j,s}]\,B^*[s]J[m,k_{j,s}]$ and $\tilde{W}[m,j] = \sum_{s=0}^{N_s-1}\rho[m,k_{j,s}]B^*[s]W[m,k_{j,s}]$, respectively.

The optimal (sufficient statistic sense) chip-combining weight corresponding to the $k_{j,s}$th subchannel of the mth MC symbol is

$$\rho[m, k_{j,s}] \quad = \quad \frac{1}{C_V[m, k_{j,s}]}. \tag{111}$$

Therefore, the AWGN-plus-PBNJ covariance matrix must be estimated and exploited in chip combining to pass the sufficient statistic to the demapper. The LLR of the interleaved bits that is computed by the soft demapper can be expressed in terms of the chip combiner output as

$$L(b_i) \quad = \quad \log\left[\frac{\sum_{a\in\mathcal{A}:b_i=1} \exp\left(2\sqrt{\frac{E_s}{N_s}}\,\Re\mathfrak{e}[\hat{a}[m,\,j]\,a^*]\right)\,p(a)}{\sum_{a\in\mathcal{A}:b_i=0} \exp\left(2\sqrt{\frac{E_s}{N_s}}\,\Re\mathfrak{e}[\hat{a}[m,\,j]\,a^*]\right)\,p(a)}\right]. \tag{112}$$

For iterative demapping [112], the demapper uses the chip-combiner output as well as the extrinsic information from previous iterations of the convolutional decoder [121] to generate the $L(b_i)$, which are then deinterleaved and fed to the convolutional decoder. The chip-combiner output has a Gaussian distribution with variance $\sigma^2 = \sigma^2_{\tilde{J}} + \sigma^2_{\tilde{W}}$. Given the chip-combining weights, channel coefficients, AWGN-plus-PBNJ covariance matrix, and *i.i.d.* Rayleigh-fading-channel assumption, the AWGN-plus-PBNJ variance at the despreader output for the jth data symbol of the mth MC symbol is

$$\sigma^2_{\tilde{W}} + \sigma^2_{\tilde{J}} = \sum_{s=0}^{N_s-1} \rho^2[m, k_{j,s}] \sum_{q=1}^{Q} |H^{(q)}[m, k_{j,s}]|^2\ \mathbf{C}_V[m, k_{j,s}]. \tag{113}$$

For MMSE chip combining, the weights are [7]

$$\rho[m, k_{j,s}] \quad = \quad \left[1 + \left(\frac{NE_s}{N_s C_V[m, k_{j,s}]} \sum_{q=1}^{Q} \left|H^{(q)}[m, k_{j,s}]\right|^2\right)^{-1}\right]^{-1} \quad , \tag{114}$$

which also requires the AWGN-plus-PBNJ covariance estimate.

8.6 Numerical Results and Discussions

Simulations are conducted to verify how the channel and covariance estimators perform along with the sufficient-statistic or MMSE chip combining. In all simulations, code blocks

of 2048 bits (i.e., the channel-interleaver size is 4096), code rate $R_c = 1/2$, QPSK symbols with Gray mapping, Walsh-Hadamard spreading sequences, and $Q = 2$ receive antennas are used. The number of subcarriers per MC symbol used is $N = 128$, and the spreading factor is $N_s = 8$. Therefore, 16 data symbols are transmitted for each DPCH MC symbol. The number of CCPCH and DPCH MC symbols per frame is $M_p = 1$ and $M_d = 8$, respectively. The number of pilot symbols transmitted on each CCPCH MC symbol is either 8 or 16 corresponding to a pilot-to-data-symbol ratio of 1/16, and 1/8, respectively. The pilot and data symbols have identical power. The number of channel taps is $L = 10$ and an exponential channel power delay profile is assumed where the average power transferred by the lth channel path is $E[|h^{(q)}[m,l]|^2] = \sigma_h^2\, e^{-l/5}$. The normalization factor σ_h^2 is chosen such that the total power of all L paths is unity. All transmit and receive antenna pairs have same channel power and power delay profiles. The carrier frequency and system bandwidth are $f_c = 5$ GHz and $B_f = 5$ MHz, respectively. Thus, the sampling period is $T_c = 0.2\,\mu s$, MC symbol period including the guard interval is $T = 27.6\,\mu s$, and Doppler frequency is $f_d = v f_c/c$, where v is the mobile velocity, and $c = 3 \times 10^8$ m/s is the light speed. We assume a slowly time-varying fading channel where $v = 30$ km/h (the normalized Doppler rate is $f_d T = 0.0038$). Assuming a dominant jammer signal, the symbol energy-to-noise ratio is fixed at $E_s/N_0 = 15$ dB. Considering the coding rate, modulation order, number of receive antennas, guard interval, and pilot/control signals, the effective information bit-energy-to-jammer noise ratio is defined as

$$\frac{E_b}{N_J} = \frac{E_s}{N_J}\frac{Q}{R_c \log_2(M)}\frac{N+G}{N}\frac{M_p + M_d}{M_d} \quad . \tag{115}$$

The channel estimates for the receiver using sufficient-statistic chip combining differ from those of the receiver using MMSE chip combining except for the initial EM iteration. The first iteration's channel coefficients are obtained through ML channel estimation using only the pilot symbols of each CCPCH MC symbol. After the first iteration, the channel estimates differ with the type of chip combining used, since the LLR of the coded bits

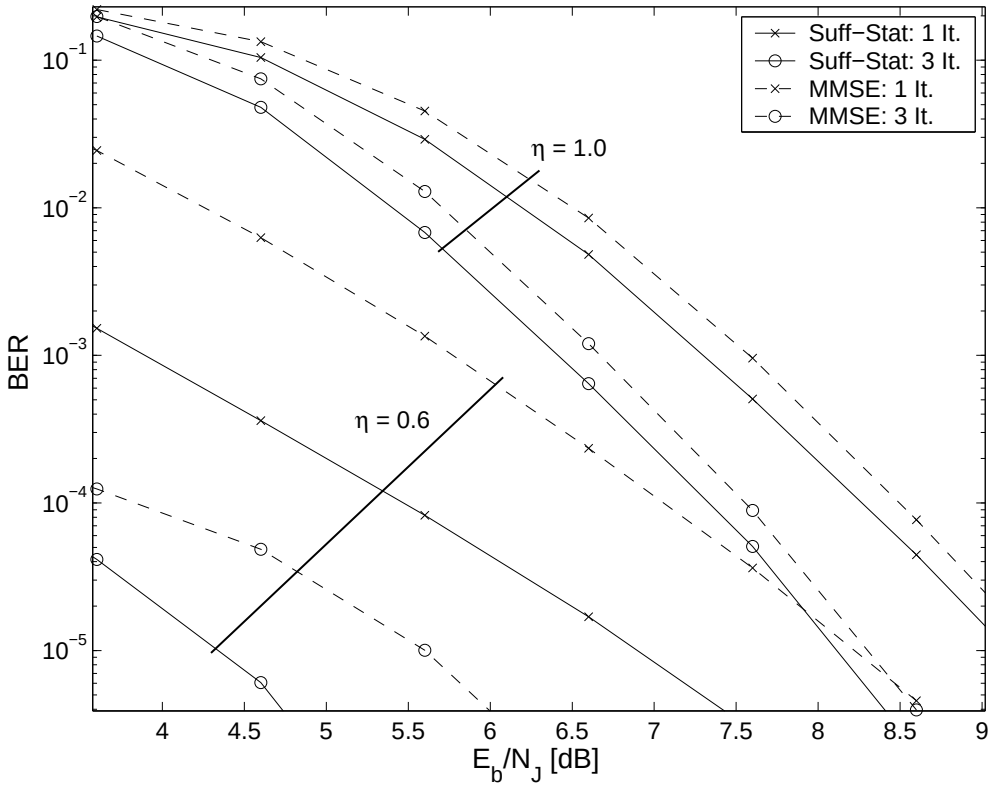

Figure 39. BER at different EM iterations under FBNJ ($\eta = 1.0$) and PBNJ ($\eta = 0.6$) when the initial channel estimation uses $N_p = 8$ pilot symbols/frame but perfect AWGN-plus-PBNJ-covariance estimates are assumed. The sufficient-statistic chip combiner always yields smaller BER than the MMSE chip combiner.

associated with the data symbols begins to contribute in the channel, and thus, the AWGN-plus-PBNJ-covariance estimates.

First, we illustrate the performance difference between the sufficient-statistic and MMSE chip combining with channel estimation only. Figs. 39 and 40 show the bit-error rate (BER) after the first and third EM iterations for $N_p = 8$ and 16, respectively, when the channel coefficients are estimated but perfect knowledge of the AWGN-plus-PBNJ covariance is assumed. Results for FBNJ ($\eta = 1.0$) and PBNJ having $\eta = 0.6$ are illustrated. The solid and dashed lines correspond to sufficient static and MMSE chip combining, respectively. The crosses and circles correspond to the first and third EM iteration, respectively. For the estimated channel coefficients obtained by using 8 pilot symbols and perfect AWGN-plus-PBNJ-covariance estimates, the sufficient statistic chip combiner outperforms the MMSE

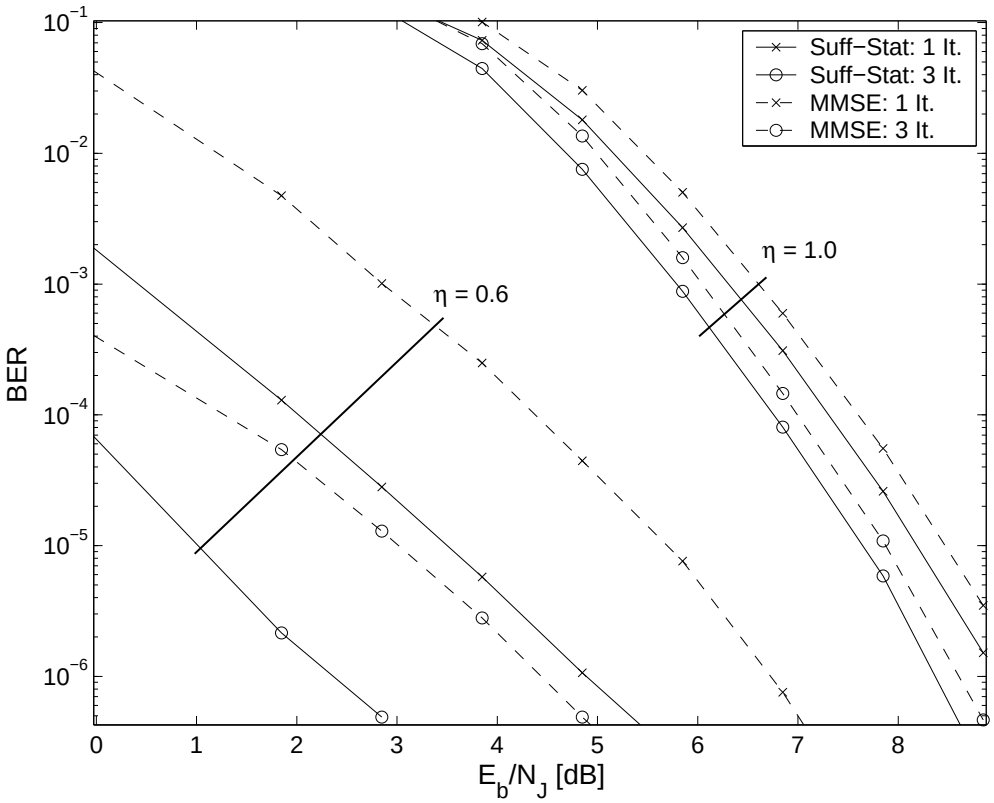

Figure 40. BER at different EM iterations under FBNJ ($\eta = 1.0$) and PBNJ ($\eta = 0.6$) when the initial channel estimation uses $N_p = 16$ pilot symbols/frame but perfect AWGN-plus-PBNJ-covariance estimates are assumed. The sufficient-statistic chip combiner always outperforms the MMSE chip combiner.

chip combiner by 0.2 and 1.3 dB when $\eta = 1.0$ and 0.6, respectively, at BER=10^{-5} after three EM iterations. When 16 pilot symbols are used for channel estimation, this gain is 0.22 and 2.0 dB for $\eta = 1.0$ and 0.6, respectively.

We now consider the BER for the receivers when both the channel and AWGN-plus-PBNJ covariance are jointly estimated. Fig. 41 shows the BER at different EM iterations for FBNJ and PBNJ with $\eta = 0.6$ when both the channel and AWGN-plus-PBNJ covariance matrix are jointly estimated and 16 pilot symbols per frame are used for initial channel estimation. Because the subcarriers are jammed with equal average power and the identity matrix is used as the initial covariance estimate, the initial covariance estimate is more appropriate for chip combining under FBNJ than for PBNJ with $\eta < 1.0$. Therefore, the initial iteration BER under FBNJ ($\eta = 1.0$) is smaller than the initial iteration BER under

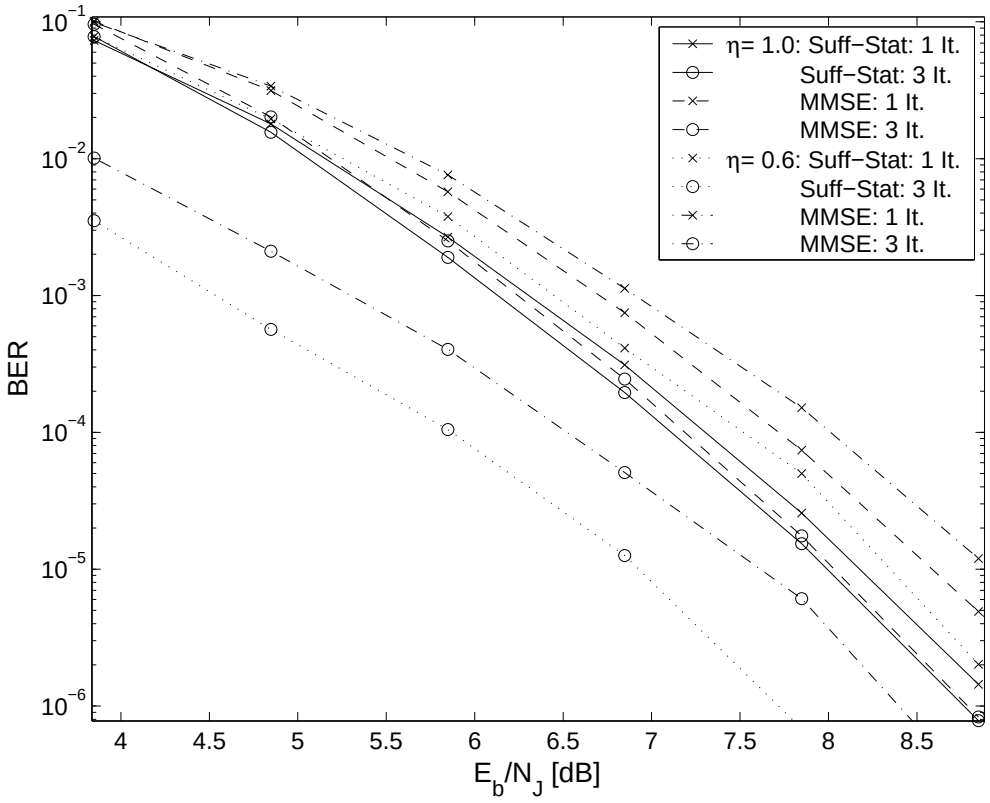

Figure 41. BER at different EM iterations under FBNJ ($\eta = 1.0$) and PBNJ ($\eta = 0.6$) when both the channel coefficients and AWGN-plus-PBNJ covariance are estimated using $N_p = 16$ pilot symbols/frame.

PBNJ with $\eta = 0.6$ at any E_b/N_J for both types of chip combining. However, the AWGN-plus-PBNJ-covariance estimate is updated at every EM iteration along with the channel estimates, and the chips are combined according to the AWGN-plus-PBNJ power to suppress the jamming signal. Hence, at any EM iteration after the first iteration, the BER for $\eta = 0.6$ is smaller than that for $\eta = 1.0$ for both types of chip combining. Under FBNJ at BER=10^{-5}, sufficient-statistic chip combining has slight gain (0.075 dB) over MMSE chip combining after three EM iterations. But this gain is 0.74 dB under PBNJ with $\eta = 0.6$.

A sufficient-statistic chip combiner that is provided with satisfactory AWGN-plus-PBNJ-covariance estimates exhibits a smaller BER than that of a MMSE chip combiner. However, exceptions may occur with unreliable covariance estimates. Fig. 42 shows the BER after three EM iterations when 8 or 16 pilot symbols per frame are used to estimate the initial channel and the receiver operates under either FBNJ or PBNJ with $\eta = 0.4$. When 16 pilot

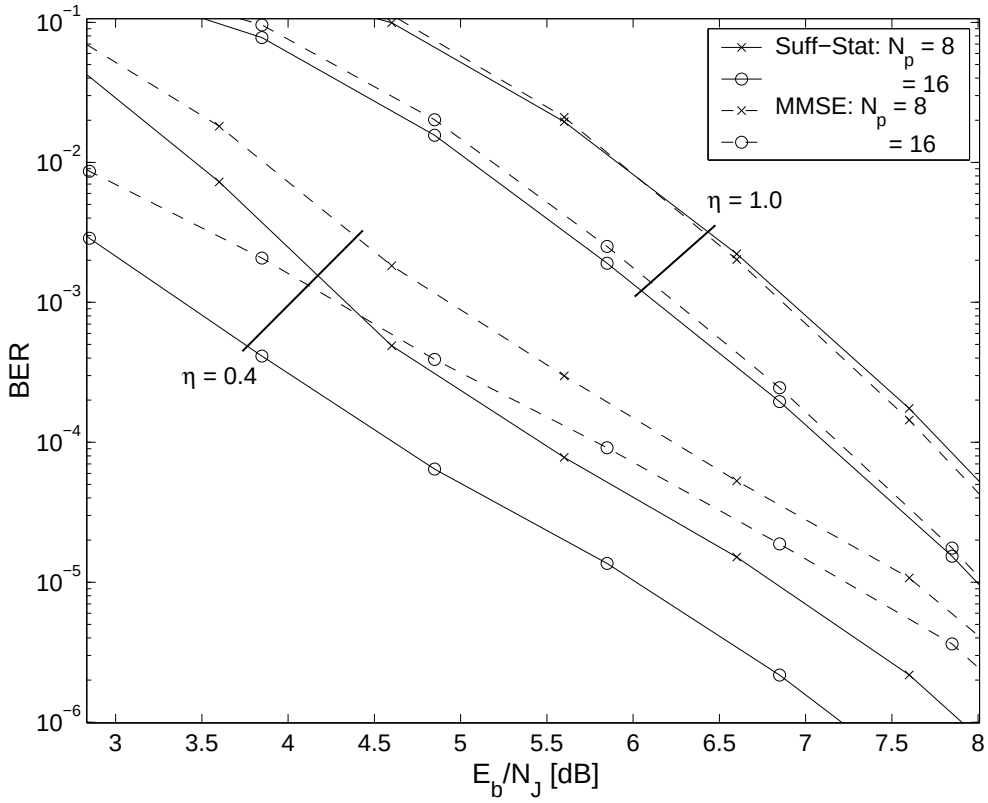

Figure 42. BER after three EM iterations under FBNJ ($\eta = 1.0$) and PBNJ ($\eta = 0.4$) when both the channel coefficients and AWGN-plus-PBNJ covariance are estimated using $N_p = 8$ and 16 pilot symbols/frame.

symbols are used for initial channel estimation, sufficient-statistic chip combining provides a smaller BER than MMSE chip combining for any $\eta \in (0, 1]$ and for all regions of E_b/N_J. However, if $N_p = 8$, exceptions occur at higher E_b/N_J region under FBNJ. The reason is as follows.

The weights of the MMSE chip combiner depend on the received chip energy (depends on channel gain) and AWGN-plus-PBNJ power. However, the weights of the sufficient-statistic chip combiner are inversely proportional to the AWGN-plus-PBNJ power estimates only. Thus, compared to MMSE chip combiner, the sufficient-statistic chip combiner is more sensitive to covariance-estimation error. Using 8 pilot symbols provides less reliable channel estimates and, thus, less reliable covariance estimates than the estimates obtained by using 16 pilot symbols. In addition, given a fixed E_s/N_J, the jamming signal in FBNJ is spread over the entire bandwidth, which makes it harder to estimate the noise power as

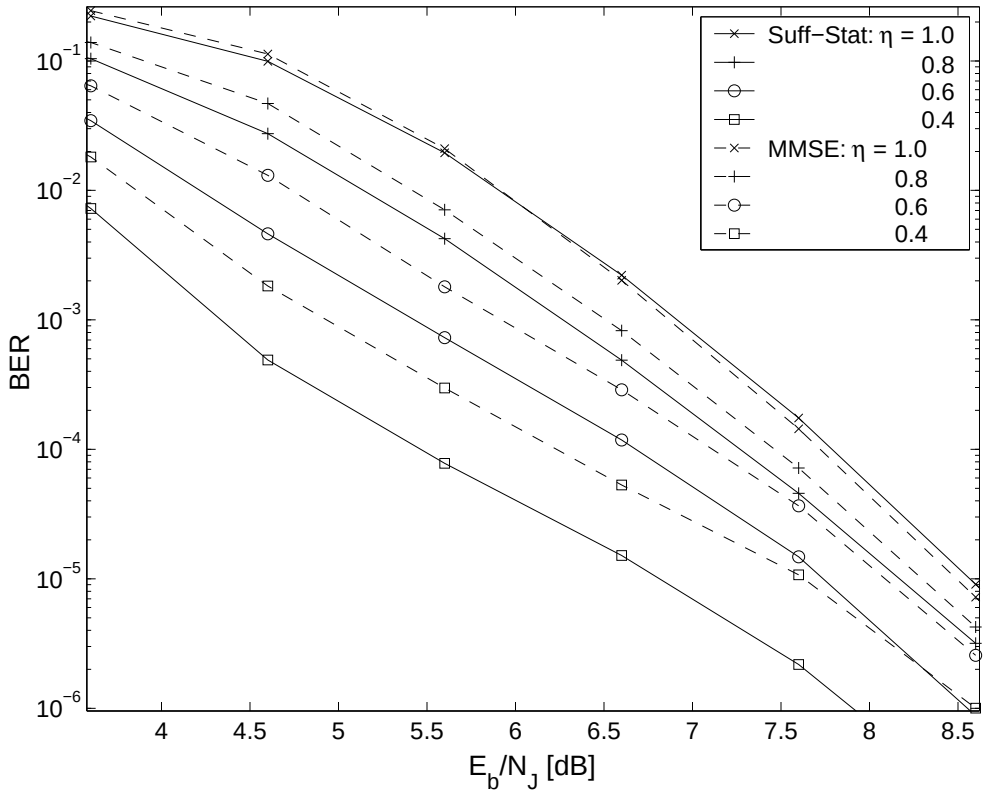

Figure 43. BER for different jamming fractions after three EM iterations when both the channel coefficients and AWGN-plus-PBNJ covariance are estimated using $N_p = 8$ pilot symbols/frame.

compared to the narrowband case. Hence, the covariance estimates for $\eta = 1.0$ are less reliable than the covariance estimates when $\eta < 1.0$. The noise power estimates become even more unreliable with an increase in E_b/N_J, since the jamming signal variance diminishes. Thus, if 8 pilot symbols are used under FBNJ, the sufficient-statistic chip combiner performs slightly worse than the MMSE chip combiner in the high E_b/N_J region.

Figs. 43 and 44 show the BER for different jamming fractions using eight and sixteen pilot symbols, respectively. The BER is shown for sufficient-statistic and MMSE chip combining after three EM iterations. Finally, Fig. 45 shows the E_b/N_J required to guarantee a BER $\leq 10^{-4}$. The results demonstrate that sufficient-statistic chip combining outperforms the MMSE chip combining provided that reliable parameter estimates are used (i.e., enough pilot symbols are used). The use of more pilot symbols provides for more reliable channel estimates, which in return yields more reliable AWGN-plus-PBNJ-covariance estimates.

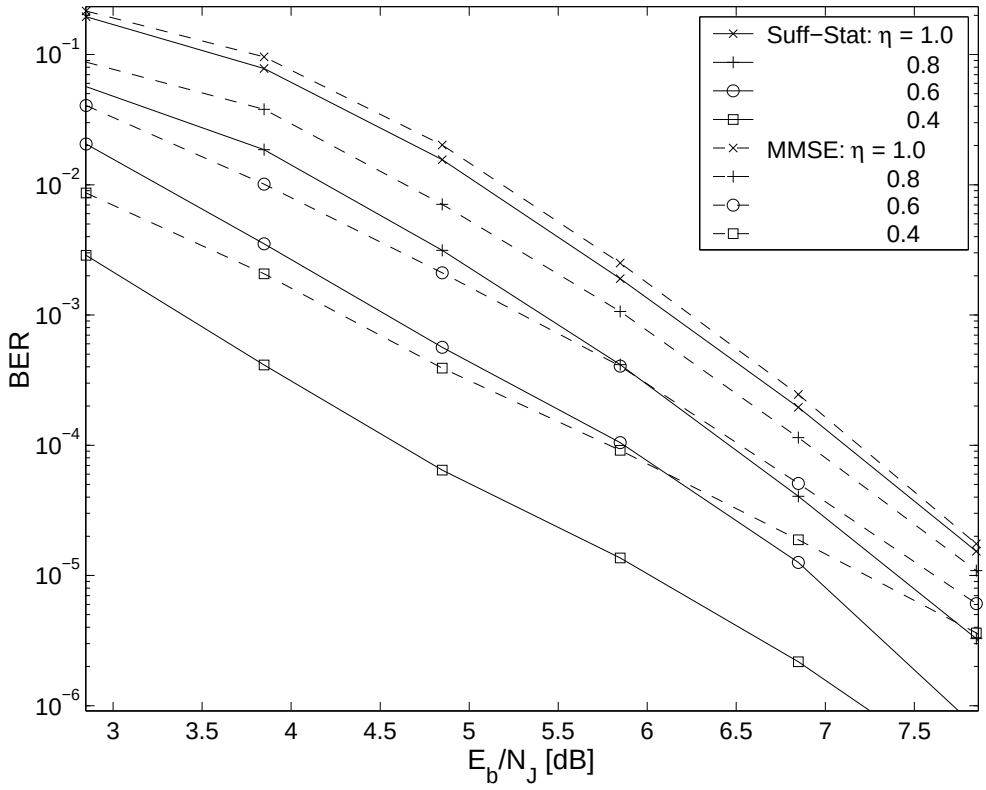

Figure 44. BER for different jamming fractions after three EM iterations when both the channel coefficients and AWGN-plus-PBNJ covariance are estimated using $N_p = 16$ pilot symbols/frame.

Hence, the E_b/N_J gain of the sufficient statistic chip combiner over the MMSE chip combiner increases as the number of pilot symbols increases.

Finally, the MMSE chip combiner minimizes the mean square error at the combiner output. In contrast, the sufficient-statistic chip combiner guarantees no loss of information in the soft output generated by the demapper, which is fed to the decoder. Therefore, the sufficient-statistic chip combiner is more pertinent to the decoder and outperforms the MMSE chip combiner in terms of BER provided that reliable parameter estimates are available.

8.7 Summary

This chapter has considered joint estimation of the channel coefficients and AWGN-plus-PBNJ covariance for an MC-CDMA system operating under PBNJ. The estimators are

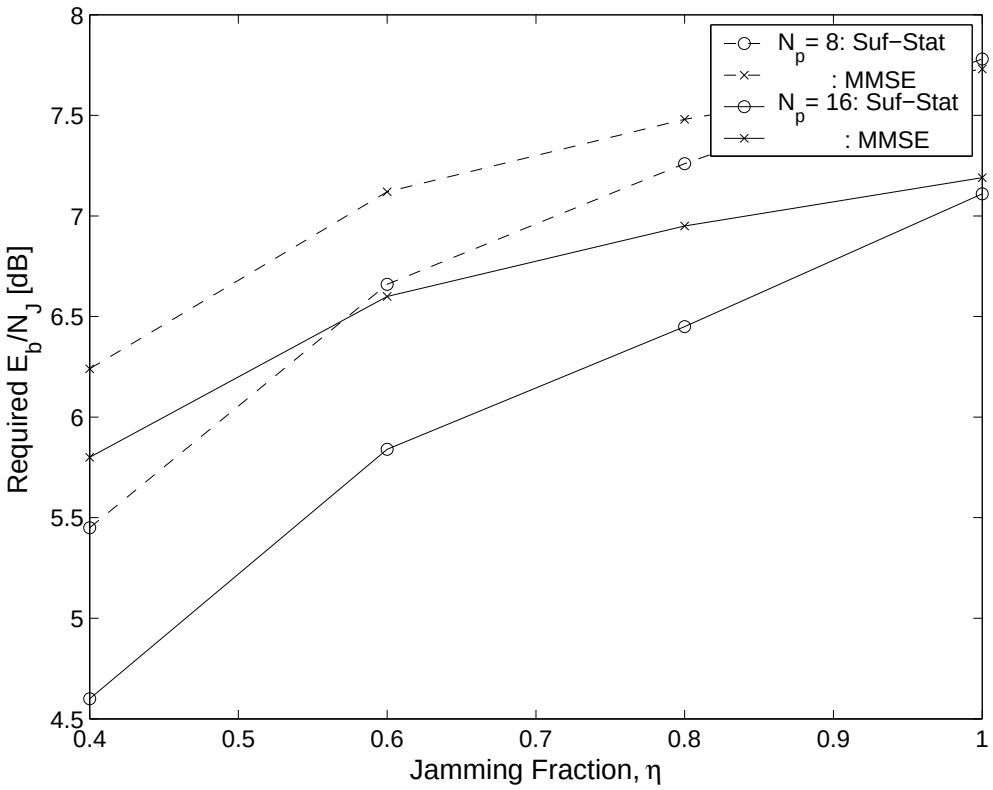

Figure 45. Required minimum E_b/N_J to guarantee BER $\leq 10^{-4}$ after three EM iterations for different jamming fractions when both the channel coefficients and AWGN-plus-PBNJ covariance are estimated using $N_p = 8$ and 16 pilot symbols/frame.

based on the EM algorithm and exploit the decoder output. The channel and covariance estimates are used along with MMSE and sufficient-statistic chip combining to suppress the adverse effect of the jamming signal. The sufficient-statistic chip combiner, which preserves mutual information, performs better than the MMSE chip combiner in most practical cases. Our proposed anti-jam receiver does not need either the subcarrier JSI or the individual powers of the AWGN and PBNJ, which reduces the complexity and power consumption of the receiver over approaches that do require these parameters. The estimation and combining techniques can be applied to any MC-CDMA system operating under jamming or interference from other systems.

CHAPTER 9

CONCLUSIONS AND FUTURE WORK

9.1 Conclusions

This thesis addressed the problem of mitigating the adverse effects of CCI and jamming by developing systems and algorithms. Many of the techniques developed in this thesis can be applied to other systems. The main contributions are summarized as follows.

In Chapter 3, we proposed two timing estimators by applying the concept of double correlation to the spatio-temporal cross-correlation matrix elements of the colored- and white-CCI-noise models. The derived timing estimator, given in (27), performs better than the correlation method of [6] and the two estimators of [86], which uses simple white- or color-CCI-noise models, respectively. It also moderately outperforms the double-correlation method [85], which is known to be robust to large frequency offsets. The derived timing estimator of (27) is robust at low SIR because the spatially colored model boosts the effective SIR by considering all the elements of the covariance matrix, while the phase offset due to frequency error that exists in the cross-correlation is diminished by double correlation.

Considering the high peak-to-average power problem of multicarrier systems and to increase the transmission reliability under fading and jamming, we introduced a constant-envelope MC-CDMA that uses cyclic delay diversity (CE-MC-CDMA-CDD) in Chapter 4. We analyzed the system's space-time coding and BER performance. A constant envelope enables the system to use very efficient nonlinear power amplifiers. We showed that full diversity is always achieved if the number of transmit antennas is less than or equal to the number of subcarriers, independent of the modulation type and alphabet size. The proposed system does not require additional error-correction coding or interleaving to guarantee full spatial diversity.

In Chapter 5, we introduced a signal-space projection-based SNR estimator for the

CE-MC-CDMA-CDD system operating under time-varying multipath-fading channel. The proposed SNR estimator does not require training symbols or data-symbol decisions. Hence, long estimation intervals can be chosen to achieve high-quality SNR estimates without any power or bandwidth constraint. The normalized bias, MSE, and variance of the estimator do not degrade even at small E_s/N_0.

In Chapter 6, we designed anti-jam receivers for the CE-MC-CDMA-CDD system that are robust against both PBNJ and PJ. The receiver is capable of iteratively estimating JSI and combining the chips in both the frequency and time domains for effective mitigation of PBNJ and PJ, respectively. A soft chip combining technique was proposed that enhances the SINR at the despreader output and outperforms the conventional hard-JSI-based chip combining under both types of jamming.

Joint iterative channel, JSI, and jamming-power estimation for the same system under PBNJ and time-varying multipath fading was studied in Chapter 7. We derived the weighted LSE and MMSE channel estimators. In addition, we identified the constraints on the cyclic delays that are essential for the LSE channel estimator to exist and minimize the channel-estimation MSE under full-band jamming. We also estimated the PBNJ power by using the signal-space projection method, which works efficiently without training sequences or data-symbol decisions. Our proposed iterative despreading, demapping, and decoding (IDDD) receiver with soft-JSI-based MMSE channel estimation and chip combining demonstrates tremendous robustness against PBNJ with various jamming fractions.

In Chapter 8, we proposed an expectation-maximization joint channel and covariance estimator [46, 47] for the generic MC-CDMA system operating under PBNJ and time-varying multipath-fading channel. Differing from the JSI-based anti-jam receivers, the channel estimator and the chip combiner proposed here only require the AWGN-plus-PBNJ covariance to mitigate jamming. Therefore, a significant complexity reduction is achieved because the receiver does not need to estimate the JSI and individual variances of the AWGN and PBNJ on each subcarrier for channel estimation and chip combining. The

proposed sufficient-statistic chip combiner enables the demapper to calculate the soft output without any information loss. Simulation results showed that the sufficient-statistic chip combiner always offers an improved BER than the MMSE chip combiner when reliable estimates of the channel and AWGN-plus-PBNJ-covariance are available at the receiver.

9.2 Future Work

The following open issues need to be addressed in future research work.

To mitigate the effects of severe CCI and frequency offsets, we have derived the frame boundary estimators by applying the concept of double correlation in the spatio-temporal cross-correlation matrix elements of the colored and white CCI-plus-AWGN models. However, the estimation metrics can be derived by using an optimal approach, where the cost function is minimized with respect to all the unknown parameters: frequency-selective channel matrix, covariance matrix, and frequency offset.

The proposed constant envelop MC-CDMA system employing cyclic delay diversity achieves full diversity on a flat-fading channel when the number of transmit antennas is less than or equal to the number of subcarriers. To maintain orthogonality among the signals transmitted from different antennas of all users operating under flat-fading channels, we have limited the number of multiusers to the ratio of the number of subcarriers and the number of transmit antennas. However, the orthogonality among these signals is lost in a multipath-fading environment. Hence, analysis of the diversity order and space-time coding gain under multiuser interference and multipath fading is desirable. This investigation may lead to the design of new spreading sequences with appropriate space-time coding schemes.

We have proposed two different anti-jam receivers that consider joint channel estimation and chip combining. To reduce the computational complexity of the JSI-based channel estimator and chip combiner, we have introduced an expectation-maximization (EM)-based joint channel and noise-covariance estimator that does not need either the subcarrier JSI or

the individual powers of the AWGN and jamming signal. Although the complexity of the expectation-maximization receiver is obviously lower than that of the former, the exact complexity of the EM-based anti-jam algorithms should be analyzed. Derivation of the Cramer-Rao bound for the unknown parameters would be valuable. The performance of these two different anti-jam receivers should also be compared.

In most literature that applies the EM algorithm to channel estimation of multicarrier systems, the channel is modeled as sample spaced, i.e., the delays of the channel taps are integer multiples of the sample duration. This assumption simplifies the derivation and makes the whole problem of channel estimation a lot tractable. However, a real channel is not sample spaced. This induces leakage, which has severe implication on the kind of channel estimation scheme that we have studied in this thesis. Therefore, derivation and performance analysis of channel estimators for non-sample-spaced channel model are of great practical interest.

REFERENCES

[1] R. W. C , "Synthesis of band-limited orthogonal signals for multi-channel data transmission," *Bell System Technical Journal*, vol. 46, pp. 1775-1796, 1966.

[2] R. C , and R. G , "A Theoretical Study of Performance of an Orthogonal Multiplexing Data Transmission Scheme," *IEEE Trans. on Commun.*, vol. 16(4), pp. 529-540, Aug. 1968.

[3] E. B , R. C , A. C , A. G , A. P , and H. V. P , *MIMO Wireless Communications*, Cambridge University Press, 2007.

[4] U. M and A N. D'A , *Synchronization Techniques for Digital Receivers*, New York: Kluwer Academic/Plenum Publishers, 1997.

[5] H. M , M. M , and S A. F , *Digital Communication Receivers*, New York: John Wiley & Sons, Inc., 1998.

[6] Y. E W and T. O , "Cell Search in W-CDMA," *IEEE J. Select. Areas Commun.*, vol.18, No.8, August 2000.

[7] K. Fazel and S. Kaiser, *Multi-Carrier and Spread Spectrum Systems*, John Wiley & Sons Ltd., 2003.

[8] S. H and R. P , "Overview of multicarrier CDMA," *IEEE Commun. Soc. Mag.*, vol. 35, pp. 126-133, Dec. 1997.

[9] S. Kondo and L. B. Milstein,"Performance of multicarrier DS CDMA systems," *IEEE Trans. Commun.*, vol. 44, no. 2, pp. 238-246, Feb. 1996.

[10] J. T and G. L. S , "Anti-jamming performance of multi-carrier spread spectrum with constant envelope," in *Proc. IEEE ICC*, 2003, pp. 743-747.

[11] D. C. C , "Polyphase codes with good periodic correlation properties," *IEEE Trans. Inform. Theory*, vol. 18, pp. 531-532, July 1972.

[12] J. G. P , *Digital Communications*, McGraw-Hill, 4th Ed., 2000.

[13] A. W , "A new bandwidth efficient transmit antenna modulation diversity scheme for linear digital modulation," in *Proc. IEEE ICC*, 1993, pp. 1630-1634.

[14] J. H. W , "The diversity gain of transmit diversity in wireless systems with Rayleigh fading," *IEEE Trans. Veh. Technol.*, vol.47, pp.119-123, Feb. 1998.

[15] S. M. A , "A simple transmit diversity technique for wireless communications," *IEEE J. Select. Areas Commun.*, vol. 16, pp. 1451-1458, Oct. 1998.

[16] V. T , H. J , and A. R. C , "Space-time block codes from orthogonal designs," *IEEE Trans. Inform. Theory,* vol. 45, pp. 1456-1467, July 1999.

[17] V. T , N. S , and A. R. C , "Space-time codes for high data rate wireless communication: Performance criterion and code construction," *IEEE Trans. Inform. Theory,* vol. 44, Mar. 1998.

[18] T. A. Summers, S. G. Wilson, "SNR mismatch and online estimation in turbo decoding," *IEEE Trans. Commun.,* vol. 46, pp. 421-423, Apr. 1998.

[19] K. K , "Enhanced maximal ratio combining scheme for RAKE receivers in WCDMA mobile terminals," *Electronics Lett.,* vol. 37, pp.522-524, Apr. 2001.

[20] N. C. B , A.S. T , and D.R. P ,"Comparison of four SNR estimators for QPSK modulations," *IEEE Commun. Lett.,* vol. 4, pp. 43-45, Feb. 2000.

[21] N. C. B and T. C , "Maximum likelihood estimation of local average SNR in Ricean fading channels," *IEEE Commun. Lett.,* vol.9, Mar. 2005.

[22] M. A , N. B. M , and R. D. Y , "Subspace based estimation of the signal to interference ratio for TDMA cellular systems," *IEEE Trans. Veh. Technol.,* vol. 2, pp. 735-739, May, 1997.

[23] M. D. A and G. L. S ü , "In-service signal quality estimation for TDMA cellular systems," *Kluwer Wirel. Personal commun.,* vol. 2, pp. 245-254, Nov. 1993.

[24] M. T and G. L. S ¨ , "An efficient algorithm for estimating the signal-to-interference ratio in TDMA cellular systems," *IEEE Trans. Commun.,* vol. 46, pp. 728-731, June 1998.

[25] L. D. G. B , "Linear Diversity Combining Techniques," in *Proc. IRE,* Vol. 47, pp. 1075-1102, June 1959.

[26] L. D. G. B , "Linear Diversity Combining Techniques," in *Proc. of the IEEE,* Vol. 91, Feb. 2003, pp. 331 - 356.

[27] L. M. K. S , L. J. K. O , L. R. A. S , and L. B. K. L , *Spread Spectrum Communications Handbook,* Rev. ed., McGraw Hill Inc., 1994.

[28] J. T and G. L. S ¨ , "Multicarrier Spread Spectrum System With Constant Envelope: Antijamming, Jamming Estimation, Multiuser Access," *IEEE Trans. Wirel. Commun.,* vol. 4, pp. 1527-1538, July, 2005.

[29] L. H. E G and L. A. R. H , "Analyzing the Turbo Decoder using the Gaussian Approximation," *IEEE Inform. Theory,* vol. 47, pp. 671-686, Feb. 2001.

[30] S. C , F. F , and G. R , "Performance comparison of multicarrier DS-SS radio access schemes for WLAN using measured channel delay profiles," in *Proc. IEEE VTC,* pp. 18771881, May 1997.

[31] U. T , D. K , and H. L , “Channel estimation for multi-carrier CDMA,” in *Proc. IEEE Int. Conf. Acoustics, Speech, and Signal Processing*, pp. 29092912, Jun. 59, 2000.

[32] X. W and Q. Y , “Uplink vector channel estimation in ISI-corrupted MC-CDMA systems with multiple antennas,” in *Proc. IEEE Int. Conf. Acoustics, Speech, and Signal Processing*, pp. 27652768, May 1317, 2002.

[33] K. D , Q. Y , M. L , and Y. Z , “Blind uplink channel and DOA estimator for space-time block coded MC-CDMA systems with uniform linear array,” in *Proc. IEEE VTC*, pp. 6973, May 1719, 2004.

[34] K. Z , G. Z , and W. W , “DFT-based uplink channel estimation for uplink MC-CDMA systems,” in *Proc. IEEE ISSSTA*, pp. 570574, Aug./Sep. 2004.

[35] P. M , A. G , and J. F , “Vectorial channel estimation for uplink MC-CDMA in beyond 3G wireless systems,” in *Proc. IEEE PIMRC*, pp. 984988, Sep. 2003.

[36] T. Z , C. F. M , J. W , and R. R. M , ”Iterative Joint Time-Variant Channel Estimation and Multi-User Detection for MC-CDMA,” *IEEE Trans. Wirel. Commun.*, vol. 5, pp. 1469-1478, June, 2006.

[37] L. S and M. M , ”Channel Acquisition and Tracking for MC-CDMA Uplink Transmissions,” *IEEE Trans. Veh. Technol.*, vol. 55, pp. 956-967, May 2006.

[38] S , C.R.C.M. and M , L.B., “The effects of narrowband interference on UWB communication systems with imperfect channel estimation,” *IEEE J. Select. Areas Commun.,*, Vol. 24, pp. 717-723, Apr. 2006.

[39] Y. (G.) L , N. S , and S. A , ”Channel estimation for OFDM systems with transmitter diversity in mobile wireless channels,” *IEEE J. Select. Areas Commun.*, vol. 17, pp. 461-471, Mar. 1999.

[40] G A. M.M. and G L. S , ”Robust Timing Estimation in the Presence of Co-Channel Interference and Frequency Offset”, in *Proc. International Symposium on Wireless Personal Multimedia Communications (WPMC)*, vol. 1, pp. 320-323, Sep. 2004.

[41] G A. M.M. and G. L. S ü , “Performance Analysis of Constant Envelope Multicarrier CDMA MIMO Systems with Cyclic Delay Diversity,” in *Proc. 10th International OFDM-Workshop*, 2005.

[42] G A. M.M. and G L. S , ”Blind Signal-to-Noise-Ratio Estimation for a Constant envelope MIMO MC-CDMA system using cyclic delay diversity,” in *Proc. European Signal Processing Conference*, Sep. 2007, pp. 459-463.

[43] G A. M.M. and G L. S ¨ , “Soft-Chip Combining MIMO Multicarrier CDMA Antijam System,” *IEEE MILCOM*, Oct. 2006.

[44] Galib Asadullah. M.M. and G. L. Stuber, "Joint Iterative Channel Estimation and Soft-Chip Combining for MIMO MC-CDMA Antijam System," in *6th Intl. Workshop on Multi-Carrier Spread Spectrum*, Springer, 2007.

[45] G A. M.M. and G L. S , "Joint Iterative Channel Estimation and Soft-Chip Combining for a MIMO MC-CDMA Antijam System," under revision for publication in *IEEE Trans. Commun.*.

[46] G A. M.M. and G L. S , "Joint EM Channel and Covariance Estimation with Sufficient Statistic Chip Combining for a SIMO MC-CDMA Antijam System," Submitted to *IEEE WCNC*, 2008.

[47] G A. M.M. and G L. S , "Joint EM Channel and Covariance Estimation with Sufficient Statistic Chip Combining for a SIMO MC-CDMA Antijam System," Submitted to *IEEE Trans. Commun.*.

[48] G. L. S , *Principles of Mobile Communications*, Boston: Kluwer Academic Publishers, 2001.

[49] W. C. J , *Microwave Mobile Communications*, IEEE Press, 1994.

[50] P. D , G. E. B , and T. C , "Jakes fading model revisited," *Electronics Letters*, Vol. pp. 1162-1163, June 1993.

[51] A. G. Z , G. L. S , "Efficient simulation of rayleigh fading with enhanced de-correlation properties," *IEEE Trans. Wirel. Commun.*, Vol. 5, pp. 1866-1875, July 2006.

[52] N. C. B , A. A. A -D , "Bandwidth efficient QPSK in cochannel interference and fading," *IEEE Trans. Commun.*, Vol. 43, Issue 9, pp. 2464-2474, Sep. 1995.

[53] A. S , and R. Prasad, "Effects of correlated shadowing signals on channel reuse in mobile radio systems," *IEEE Trans. Veh. Technol.*, Vol. 40, pp. 708-713, Nov. 1991.

[54] X. Z , A. N. A , and S. T , "Cochannel interference computation and asymptotic performance analysis in TDMA/FDMA systems with interference adaptive dynamic channel allocation," *IEEE Trans. Veh. Technol.*, Vol. 49, pp. 711-723, May 2000.

[55] A. L. B , L. B. L , and D. C. M L , "Method for timing recovery in presence of multipath delay and cochannel interference," *Electronics Lett.*, Vol. 30, pp. 1028-1029, June 1994.

[56] R. M , W. H. G , R. S , and J. B. H , "A single antenna interference cancellation algorithm for increased gsm capacity," *IEEE Trans. Wirel. Commun.*, Vol. 5, pp. 1616-1621, July 2006.

[57] J. A. C. B , "In-band digital audio radio: An update on AT&T Amati PAC/DMT solution," in *Proc. International Symposium on Digital Audio Broadcasting*, pp. 270277, Mar. 1994.

[58] N. S. J , E. Y. C , J. D. J , S. R. Q , S. M. D , K. T , R. L. C , J.-D. W , C.-E. W. S , and N. S , "The AT&T in-band adjacent channel system for digital audio broadcasting," in *Proc. International Symposium on Digital Audio Broadcasting*, pp. 254267, Mar. 1994.

[59] C.-E. W. S , "Digital audio broadcasting in the FM band," in *ISIE97 Conference Record*, pp. SS37SS41, July 1997.

[60] M. K. S , J. K. O , R. A. S , and B. K. L , *Spread Spectrum Communications: Vol. I*, Computer Science Press, Inc., 1985.

[61] M. B. P and W. E. S , "Performance of ReedSolomon coded frequency-hop spread-spectrum communications in partial-band interference," *IEEE Trans. Commun.*, vol. COM-33, pp. 767774, Aug. 1985.

[62] C. D. F and M. B. P , "Concatenated coding for frequency- hop spread-spectrum with partial-band interference," *IEEE Trans. Commun.*, vol. 44, no. 3, pp. 377387, Mar. 1996.

[63] A. A. A ,"Worst-case partial-band noise jamming of Rician fading channels," *IEEE Trans. Commun.*, vol. 44, no. 6, pp. 660662, Jun. 1996.

[64] J. H. K and W. E. S ,"Turbo codes for coherent FH-SS with partial band interference," *IEEE Trans. Commun.*, vol. 46, no. 11, pp. 14511458, Nov. 1998.

[65] H. E G and E. G , "Turbo codes with channel estimation and dynamic power allocation for anti-jam FH/SSMA," in P . IEEE M . C . C ., vol. 1, pp. 170175, Oct. 1998.

[66] H. E G and E. G , "Iterative channel estimation and decoding for convolutionally coded anti-jamming FH signals," *IEEE Trans. Commun.*, vol. 50, no. 2, pp. 321331, Feb. 2002.

[67] J. H. K , W. E. S , "Iterative estimation and decoding for FH-SS with slow Rayleigh fading," *IEEE Trans. Commun.*, vol. 48, pp. 2014-2023, Dec. 2000.

[68] G. K. K , "Frequency-Diversity Spread Spectrum Communication System to Counter Bandlimited Gaussian Interference," *IEEE Trans. Commun.*, vol. 44, pp. 886-893, July 1996.

[69] S. Z , G. B. G , and A. S , "Digital Multi-Carrier Spread Spectrum Versus Direct Sequence Spread Spectrum for Resistance to Jamming and Multipath," *IEEE Trans. Commun.*, vol. 50, pp. 643-655, Apr. 2002.

[70] S. B , *Multiantenna Wireless Communication Systems*, Artech House Inc., 2005.

[71] J. U and A. R , "Cellular Digital Mobile Radio System and Method of Transmitting Informaiton in a Digital Cellular Mobile Radio System," *US Patent no. 5088108*, 1992.

[72] Y L , F , M.P., and T , O.Y., "Space-time codes performance criteria and design for frequency selective fading channels," *IEEE ICC 2001*, Vol. 9, pp. 2800-2804, June 2001.

[73] A. F. N , and V. T , N. S , and A. R. C , "A space-time coding modem for high-data-rate wireless communications," *IEEE J. Select. Areas Commun.*, Vol. 16, pp. 1459-1478, Oct. 1998.

[74] V. T ; A. N ; N. S ,; and A. R. C ,; "Space-time codes for high data rate wireless communication: performance criteria in the presence of channel estimation errors, mobility, and multiple paths'" *IEEE Trans. Commun.*, Vol. 47, pp. 199-207, Feb. 1999.

[75] GSM 05.02 version 8.5.1, "Multiplexing and multiple access on the radio path," Release 1999.

[76] GSM 05.04 version 8.1.2, "Modulation," Release 1999.

[77] J.J. S J ., *Digital Communication by Satellite*, Englewood Cliffs, NJ: Prentice Hall, 1997.

[78] R. A. S , "Frame Synchronization Techniques," *IEEE Trans. Commun.*, vol. COM-28, pp. 1204-1212, Aug. 1980.

[79] P. T. N , "Some optimum and suboptimum frame synchronizers for binary data in Gaussian Noise," *IEEE Trans. Commun.*, vol.COM-21, pp. 770-772, June 1973.

[80] B. S , *Digital Communications*, Englewood Cliffs, NJ: Prentice Hall, 1988.

[81] U. L , J. H , and H. M ,"Techniques for frame synchronization for unknown frequency selective channel," in *Proc. IEEE VTC*, pp.1059-1063, 1997.

[82] J.L. M , "Optimum Frame Synchronization," *IEEE Trans. Commun.*, vol. COM-20, pp. 115-119, Apr. 1972.

[83] G.L. L and H.H. T , "Frame synchronization for Gaussian channels," *IEEE Trans. Commun.*, vol. 30, pp. 1327-1337, Oct. 1997.

[84] J. A. G , M. P. F , and J. V. K , "Optimum and sub-optimum frame synchronization for pilot-symbol-assisted modulation," *IEEE Trans. Commun.*, vol. 45, pp.1327-1337, Oct. 1997.

[85] Z Y C and Y . H. L , “Frame Synchronization in the Presence of Frequency Offset,” *IEEE Trans. on Commun.*, vol.50, no.7, July 2002.

[86] D. A , A. J and A.L. S , “Burst Synchronization on Unknown Frequency Selective Channels with Co-channel Interference using an Antenna Array,” in Proc. IEEE 49th VTC, Volume: 3, 16-20 May 1999, p.2363-2367, 1999.

[87] ETSI, ”Radio broadcasting systems; digital audio broadcasting (DAB) to mobile, portable and fixed receivers.,” Tech. Rep. ETS 300 401, *European Telecommunications Standards Institute (ETSI)*, May 1997.

[88] ETSI, ”Digital video broadcasting (DVB); framing structure, channel coding and modulation for digital terrestrial television (DVB-T).,” Tech. Rep. ETS 300 744, *European Telecommunications Standards Institute (ETSI)*, Nov. 1996.

[89] J. Z , “Performance of optimum transmitter power control in cellular radio systems,” *IEEE Trans. Veh. Technol.*, vol. 41, pp. 57-62, Feb. 1992.

[90] K. B , S. R. K , and S. N , “Channel quality estimation and rate adaptation for cellular mobile radio,” *IEEE J. Sel. Areas Commun.*, vol. 17, pp. 1244-1256, July 1999.

[91] R. M. G and C. M. T , “PCM data reliability monitoring through estimation of signal-to-noise ratio,” *IEEE Trans. Commun.*, vol. 16, pp. 479-486, June 1968.

[92] D. R. P and N. C. B , “A comparison of SNR estimation techniques for the AWGN channel,” *IEEE Trans. Commun.*, vol. 48, pp. 1681-1691, Oct. 2000.

[93] M. C. R and J. A , “A novel variance estimator for turbocode decoding,” in *Proc. Int. Conf. Telecommunications*, pp. 173178, Apr. 1997.

[94] S. K and P. H , “Performance of multi-carrier CDMA systems with channel estimation in two dimensions,” in *Proc. IEEE PIMRC*, pp. 115119, Sep. 1997.

[95] M , V. and M , A., “CD3-OFDM: A Novel Demodulation Scheme for Fixed and Mobile Receivers,” *IEEE Trans. Commun.*, vol. 44, pp. 11441151, Sept. 1996.

[96] L , Y. G., S , N., and A , S., “Channel Estimation for OFDM Systems with Diversity in Mobile Wireless Channels,” *IEEE J. Select. Areas Commun.*, pp. 461471, Mar. 1999.

[97] E , O., S , M., B , J.-J., W , S. K., and B , P. O., “OFDM Channel Estimation by Singular Value Decomposition,” *IEEE Trans. Commun.*, vol. 46, pp. 931939, July 1998.

[98] Y , B., C , Z., and L , K. B., Analysis of Low-Complexity Windowed DFT-Based MMSE Estimator for OFDM Systems,” *IEEE J. Select. Areas Commun.*, vol. 49, pp. 19771987, Nov. 2001.

[99] R , G. G. and J , V. K., “Channel Estimation for Wireless OFDM Systems,” in *Proc. IEEE GLOBECOM 1998*, vol. 2, pp. 980985, Nov. 1998.

[100] Y. (G.) L , L. J. C , and N. R. S , ”Robust channel estimation for ofdm systems with rapid dispersive fading channels,” *IEEE Trans. Commun.*, vol. 46, pp. 902-915, July 1998.

[101] Y. (G.) L , ”Simplified channel estimation for OFDM systems with multiple transmit antennas,” IEEE Trans. Wirel. Commun., vol. 1, pp. 67-75, Jan. 2002.

[102] D. S , ”Porlate Spheroidal Wave Functions, Fourier Analysis and Uncertainty - V: The discrete case,” The Bell System Technical Journal, vol. 57, pp.1371-1430, May-June, 1978.

[103] K. M and G. B , “Adaptive Array Processing MLSE Receivers for TDMA digital cellular/PCS communications,” *IEEE J. Select. Areas Commun.*, vol.16, pp.1340-1351, Oct. 1998.

[104] COST 207 TD(86)51-REV 3 (WG1):, “Proposal on channel transfer functions to be used in GSM tests late 1986,” September 1986.

[105] J. T and G. L. S , “Multicarrier delay diversity modulation for MIMO Systems,” *IEEE Trans. Wirel. Commun.*, vol. 3, Sept. 2004.

[106] S. K , “Spatial transmit diversity techniques for broadband OFDM systems,” in *Proc. IEEE GLOBECOM*, 2000, pp. 1824-1828.

[107] A. D and S. K , “Standard conformable antenna diversity techniques for OFDM and its application to the DVB-T system,” in *Proc. IEEE GLOBECOM*, 2001, pp.3100-3105.

[108] A. D and S. K , “On the equivalence of space-time block coding with multipath propagation and/or cyclic delay diversity in OFDM,” in *Proc Eur. Wirel.*, 2002, pp. 847-851.

[109] J. R. B , E. A. L , and D. G. Messerschmitt, *Digital Communicaiton*, 3rd ed., Kluwer Academic Publishers, 2003, pp. 537-552.

[110] H. K and F. A , “Tight error bounds for nonuniform signalling over AWGN channels,” *IEEE Trans. Inform. Theory*, vol. 46, Nov. 2000.

[111] L. J. S. L and L. M. B. P , “Error Probabilities for Binary Direct-Sequence Spread Spectrum Communications with Random Signature Sequences,” *IEEE Trans. Commun.*, vol. COM-35, pp. 87-98, Jan. 1987.

[112] L. S. T B , L. J. S , and L. Y. R -H , “Iterative demapping and decoding for multilevel modulation,” in *Proc. GLOBECOM*, 1998, pp. 579 - 584.

[113] L. C. B , and L. A. G , “Near optimum error correcting coding and decoding: turbo-codes,” *IEEE Trans. Commun.*, vol. 44, pp. 1261-1271, Oct. 1996.

[114] S S. P , "Implementation and Performance of a Turbo/MAP Decoder," http://www.itr.unisa.edu.au/ steven/turbo.

[115] L. S. T , L. A. U. H. S , and L. M. Z. Z , "Combining schemes in rake receiver for low spreading factor long-code W-CDMA systems," in *IEE Electronics Letters*, vol. 36, no. 22, Oct. 2000.

[116] L. J. M. L and L. C. W. S , "Soft Selection Combining for Terrestrial Digital Audio Broadcasting in the FM Band," *IEEE Trans. Broadcast.*, vol. 47, pp. 103-114, June 2001.

[117] S. M. K , *Fundamentals of Statistical Signal Processing, Volume 1: Estimation Theory*, Prentice Hall, 1993.

[118] T. L. T , K. Y , and R.E. H , "Channel estimation and adaptive power allocation for performance and capacity improvement of multiple antenna OFDM systems," in *Proc. IEEE Workshop on Signal Process. Advances in Wirel. Commun.*, 2001, pp. 82-85.

[119] P. J. B and K. A. D , *Mathematical Statistics, 2nd Edition*, Prentice Hall, 2006.

[120] T. M. C and J. A. T , *Elements of Information Theory*, John Wiley Inc., 1991.

[121] L. R. B , J. C , F. J , and J. R , "Optimal decoding of linear codes for minimizing symbol error rate," *IEEE Trans. Inform. Theory*, vol. 20, pp. 284-287, Mar. 1974.

[122] A. P. Dempster, N. M. Laird, and D. B. Rubin,"Maximum likelihood from incomplete data via the EM algorithm," *J. Royal Statist. Soc.*, ser. B, vol. 39, no. 1, pp. 138, 1977.

[123] A. Dogandzic, W. Mo, and Z. Wang. "Semi-blind SIMO flat-fading channel estimation in unknown spatially correlated noise using the EM algorithm," *IEEE Trans. Signal Processing*, vol. 52, pp. 17911797, June 2004.

VITA

Galib Asadullah M.M. was born in Pabna, Bangladesh in 1972. He received B.E. and M.E. degrees in electronics engineering from Nagoya University, Nagoya, Japan in 1997 and 1999, respectively. In spring, 2002, he joined the wireless systems laboratory (WSL) at Georgia Institute of Technology, Atlanta, GA, USA and received his M.S. degree in electrical and computer engineering in 2003. He is currently working toward Ph.D. degree in electrical and computer engineering at Georgia Tech. Prior to coming to USA, he worked as a R&D engineer in the mobile phones division at ERICSSON, Tokyo, Japan, where he was actively involved with the research and development of baseband platform for the wideband code division multiple access (WCDMA) system. During the summer of 2007, he worked at Qualcomm Inc. developing MIMO receivers for the WCDMA and long term evolution (LTE) systems. His current research interests are physical layer of wireless communication and communication signal processing including multicarrier modulation, MIMO communications, iterative-receiver design, interference/jamming suppression, synchronization, SNR and channel estimation, and peak-to-average-power ratio suppression.